AFML-TR-73-145
Volume II

A SYNTHESIS PROCEDURE FOR MECHANICALLY FASTENED JOINTS IN ADVANCED COMPOSITE MATERIALS

J. P. WASZCZAK
T. A. CRUSE

DTIC QUALITY INSPECTED 4

TECHNICAL REPORT AFML-TR-73-145 Volume II

SEPTEMBER 1973

Approved for public release: distribution unlimited

19960328 107

AIR FORCE MATERIALS LABORATORY
AIR FORCE SYSTEMS COMMAND
WRIGHT PATTERSON AIR FORCE BASE, OHIO

UNCLASSIFIED 19659

NOTICE

When Government drawings, specifications, or other data are used for any purpose other than in connection with a definitely related Government procurement operation, the United States Government thereby incurs no responsibility nor any obligation whatsoever; and the fact that the government may have formulated, furnished, or in any way supplied the said drawings, specifications, or other data, is not to be regarded by implication or otherwise as in any manner licensing the holder or any other person or corporation, or conveying any rights or permission to manufacture, use, or sell any patented invention that may in any way be related thereto.

Copies of this report should not be returned unless return is required by security considerations, contractual obligations, or notice on a specific document.

AFML-TR-73-145
Volume II

A SYNTHESIS PROCEDURE FOR MECHANICALLY FASTENED JOINTS IN ADVANCED COMPOSITE MATERIALS

J. P. WASZCZAK
T. A. CRUSE

TECHNICAL REPORT AFML-TR-73-145 Volume II

SEPTEMBER 1973

Approved for public release: distribution unlimited

AIR FORCE MATERIALS LABORATORY
AIR FORCE SYSTEMS COMMAND
WRIGHT PATTERSON AIR FORCE BASE, OHIO

FOREWARD

This report describes work performed in the Department of Mechanical Engineering, Carnegie-Mellon University, Pittsburgh, Pennsylvania, 15213, under Air Force Contract F33615-72-C-1214, Project 6169 CW; Subject: "Development of Design and Analytical Techniques for Advanced Composite Aircraft Structures." This work was accomplished between 1 November 1971 and 31 August 1973. The Project Engineers for the Air Force Materials Laboratory were Mr. George E. Husman and Mr. Robert M. Neff, AFML/LC. The research projects in this report were undertaken by several graduate students under the direction of Dr. T. A. Cruse, the Principal Investigator. Chapters II-IV in Volume I were prepared by Messers. David Gamret, Mark Emerson, and Warren Bamford, respectively. Volume II is the Ph.D. Dissertation of Dr. J. P. Waszczak; Volume III is the Ph.D. Dissertation of Dr. H. J. Konish, Jr.

The authors wish to acknowledge the active support of various engineers in industry; particularly the support of Messers. M. E. Waddoups, C. W. Rogers, J. E. Eisenman, B. E. Kaminski, and Dr. D. J. Wilkins of General Dynamics, Fort Worth, Texas. We also wish to acknowledge the assistance of the Project Engineers and Dr. J. C. Halpin of the Air Force Materials Laboratory.

This report was submitted on 31 May (Volumes II, III) and 31 August (Volume I), 1973.

This technical report has been reviewed and is approved.

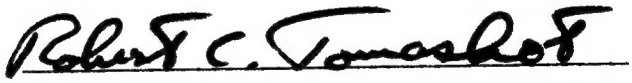

Robert C. Tomashot
Technical Area Manager
Advanced Composites Division

ABSTRACT

The Carnegie-Mellon University team has completed the second two year program in advanced composites technology. The program has had significant impact in several areas as the CMU team, working closely with the engineers at General Dynamics, Convair Aerospace Division, Fort Worth, has continued work on several projects. The work reported herein included: continuing development of university-industry interaction; development of educational material including reports on manufacturing methods, Weibull statistics, and stresses due to an elliptical hole in an anisotropic plate; and, advanced research into synthesis procedures for mechanically fastened joints and elastic fracture mechanics for laminated composite plates. The research projects demonstaate useful design capabilities, new analystic and numerical results, and experimental data.

TABLE OF CONTENTS

LIST OF FIGURES

LIST OF TABLES

NOMENCLATURE

Symbol	Description
a	Hole radius
A_{ij}	Laminate stiffness matrix in the x-y coordinate system
A_k, A_{km}	Complex coefficients in the stress function
A_m	Cross-sectional area of main plate
A_s	Cross-sectional area of one splice plate
B	Bearing
B/E	Boron-epoxy
C(I)	Constraint equations
C_n	Coefficients of Fourier Series representation of boundary tractions along the loaded hole
D	Bolt diameter
D_F	Draw-down factor
dS	Incremental length of a two dimensional boundary
DS	Double shear splice plates
e	Exponential function
E	Edge distance of coupon
E_{11}, E_{22}	Ply moduli in fiber and transverse fiber directions respectively
E_s	Modulus of splice plate material
F_1, F_2	Complex stress functions
F_{BRU}^{S}	Effective bearing strength of splice plate material
F_{SU}^{B}	Effective shear strength of bolt material

Symbol	Description
F_{SU}^{S}	Effective shear strength of splice plate material
F_{TU}^{S}	Effective tension strength of splice plate material
G_{12}	Ply shear modulus
G/E	Graphite-epoxy
H	Matrix of second derivatives for unconstrained objective function
h_i	Distance from laminate mid-plane to top of the i^{th} ply
HL	Half length of single fastener coupon
i	$\sqrt{-1}$
ID	Initial design
I_{MAX}	Maximum number of passes through the optimization loop
K_{tb}	Stress concentration factor for bolt loadings
K_{ts}	Stress concentration factor for tension loadings
L	Total joint length
L'	Single fastener coupon total length
M	Minimum weight design in feasible region
MP	Main plate
N	Number of bolts per column of fasteners
n_r, n_θ	Unit normals in cylindrical co-ordinates
N_x, N_y, N_{xy}	Laminate stress resultant components
p	Magnitude of cosine distribution of normal stress

Symbol	Description
p_1, p_2	Complex constants, material dependent
P_{Bi}	i^{th} bolt load
P_{IMAX}	Minimum weight design achieved after maximum number of allowable passes through the optimization loop
P_k	k^{th} bolt load
P_{MAX}	Magnitude of cosine distribution of normal stress
P_{Si}	i^{th} skin load
P_{ULT}	Ultimate load to be carried by a column of fasteners
P_z	Percentage of zero degree plies present
q_1, q_2	Complex constants, material dependent
QI	Quasi-isotropic
Q_{ij}	Ply stiffness matrix in the ply principal directions
$\overline{Q}_{ij}$	Ply stiffness matrix in the x-y coordinate system
R	Radius
r, θ	Cylindrical coordinates
S	Side distance or coupon width
S	Direction in design space along which linear minimizations are performed
S_H	Shear
SO	Shear-out
SP	Splice plate
S_p	Splitting

Symbol	Description
SS	Single shear splice plates
t	Total laminate thickness
T	Tension
t_0, $t_{\pm\alpha}$, t_{90}	Thickness of 0°, $\pm\alpha$ and 90° plies respectively
THC	Magnitude of quadratic expression representing the Tsai-Hill Criterion
t_i	Thickness of i^{th} ply
T_i	Titanium
T_{ij}	Transformation matrix
T_r, T_θ	Boundary tractions, cylindical coordinates
t_s	Thickness of splice plate
T_x, T_y	Boundary tractions, cartesian coordinates
u	Displacement in x direction
v	Displacement in y direction
W	Total joint weight
W_B	Total weight of bolts
W_F	Weighting factor
W_m	Width of main plate
W_M	Weight of main plate
W_s	Width of splice plate
W_S	Total weight of splice plates
X(I)	Position of I^{th} bolt along the joint
x, y	Cartesian coordinates
z	Complex physical coordinates

Symbol	Description
z_1, z_2	Complex characteristic coordinates
α	Angle ply value; scalar defining a distance along a vector in design space
α'	That value of α which corresponds to the minimum value of the objective function along direction vector
β_{ij}	Material compliances
γ	Engineering shear stress; percentage used as the convergence criterion in the series stress analysis
ε_i	Strain components
ζ_k	Complex mapping function
λ	Ratio of a finite size coupon stress concentration factor to its corresponding infinite plate value
λ_b	λ value for single fastener coupons
λ_h	λ value for plates containing three collinear cut-outs loaded in tension
λ_s	λ value for plates containing a single cut-out loaded in tension
μ_1, μ_2	Roots of the characteristic equation
ν	Poisson's ratio for an isotropic material
ν_{12}, ν_{21}	Poisson's ratios for a given ply
σ_1, σ_2, τ_{12}	Principal stress components for a given ply
σ_r, σ_θ, $\tau_{r\theta}$	Stress components in cylindrical coordinates

Symbol	Description
τ	Shear stress on a bolt cross-section
Φ_1, Φ_2	First derivative of the complex stress function F_1 and F_2 respectively
∂	Partial derivative
∇	Gradient
$\|_\theta$	Evaluated at theta

Subscripts and Superscripts

1, 2	Fiber and transverse fiber directions
0, $\pm\alpha$, 90	Ply of interest
B	Bearing loading
c	Compression
m, M	Main plate
s, S	Splice plate
S	Skin loading
t	Tension
u	Ultimate
x, y	Directions parallel and perpendicular to the applied load

CHAPTER I

INTRODUCTION

Currently much emphasis is being directed toward replacing metal components in weight sensitive structures, such as aircraft, with composite materials, due to their superior specific strength and stiffness properties. The potential weight savings which could result from such replacements, however, have not as yet been fully realized.

Significant weight savings can be achieved throughout the bulk of a replacement component by tailoring the composite material to efficiently carry the loads which are known to occur in the existing metal component. The weight savings which result, however, are often eliminated due to the use of inefficient joint* designs in all areas of structural attachments. The measure of joint efficiency used here is simply load carried per pound of material. Thus, if a given load is to be carried by a structural member the load carrying efficiency of that member will increase as its weight is decreased.

The composite material systems being considered consist of parallel, high strength fibers supported in a relatively ductile matrix material. The fibers act as load carriers while the matrix serves principally as a load transfer medium between fibers. The two most commonly used material systems consist of either graphite or boron fibers in an epoxy matrix.

*The term joint will imply a mechanically fastened joint throughout the report.

Plies, which are single layers of parallel fibers surrounded by the matrix material, are stacked at various orientations relative to one another to form a laminate. This is the procedure which enables the designer to achieve the desired strength and stiffness properties and to increase the structural efficiency of a given amount of material.

The strength and stiffness properties, however, are highly directional; panels fabricated out of layers of unidirectional composite tape are anisotropic. The designer therefore has the difficulty of including the effects of this anisotropy in his calculations.

The design of an efficient bolted joint in a composite material is much more complex than it is in a metal, for three major reasons: Laminated composites exhibit unique failure modes not found in metals; the material properties of composites can be allowed to vary along the length of the joint; and the material is generally quasi-brittle. The price of the additional flexibility of material tailorability is a significant increase in the number of possible design variables, making hand design methods impractical, if not impossible.

The purpose of the current study is to provide the designer with an efficient, automated preliminary design capability which can account for the effects of material anisotropy. The synthesis procedure reported automates the tedious analysis-resizing cycle.

The computer program which evolved from the study is not intended to serve as a "black box", however, into which the designer feeds design constraints and receives in return valid optimum designs. Rather, the designer must interact with the program to take full advantage of its capabilities.

A critical feature of the computer program is an efficient stress analysis package which allows for many redesigns in a reasonable amount of computer time. A series solution based on the theory of anisotropic elasticity for infinite plates is employed, using anisotropic correction factors to account for the effects of finite dimensions in the joint. Computer run times using this analysis package are some 600 times faster than finite element solutions of comparable accuracy. Since the analysis package is called hundreds of times in a typical joint synthesis, the availability of an efficient analysis package is essential to this work.

The specific goal of the reported study is the development of a synthesis procedure for minimum weight bolted joints in which load is transferred from a composite main plate to double shear metal splice plates by means of a single column of fasteners. A typical joint is illustrated in Figure 1. Individual items of interest include the determination of the most efficient families of laminates, the influence of material tailorability, the effects of various constraint combinations, the most efficient combinations of failure modes and the selection of initial valid designs. The

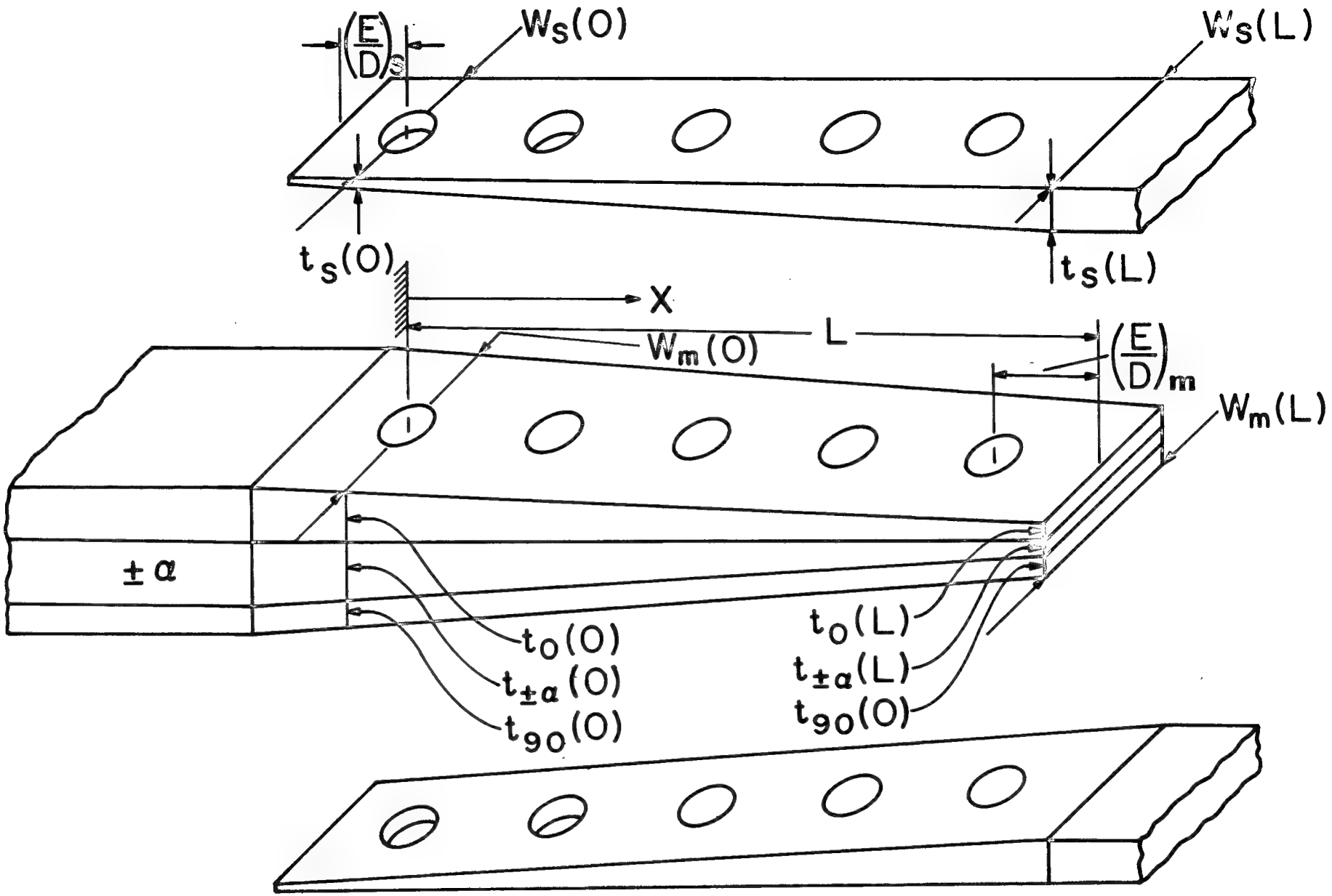

Figure 1. Schematic of a Typical Joint Design Showing the Possible Design Variables

limited results of the current study contain some surprises, a few unrealistic designs, but a gratifying number of simple, intuitive conclusions.

The class of possible designs considered is rather broad in that independent linear variations in plate widths and thicknesses are admissible. It is assumed that the bolts act as rigid pins which fit snugly into the joint. The number of bolts used and the bolt diameter are specified by the designer. Proposed main plate designs are restricted to the $[0/\pm\alpha/90]$* class of laminates. The joint stress analyses are performed assuming that the laminate is mid-plane symmetric and that it can be modeled as an anisotropic, but homogeneous material using lamination theory [1].** Main plate strength analyses are performed based on a maximum stress failure criterion, although a more complex failure criterion could be used at little additional expense. Main plate failures are predicted on a ply-by-ply basis with first failure at any bolt location governing the strength of the main plate at that location. Standard techniques involving nominal strength allowables [2] are used to predict failures in the bolt and metal splice plates.

*Square brackets used in a laminate description denote a general class or family of laminates. Information regarding laminate composition is not implied. Parentheses, on the other hand, indicate that a specific laminate is being referenced; the various ply orientation values are subscripted to denote the relative number of plies of each orientation present.

**Single numbers enclosed in square brackets indicate reference numbers.

CHAPTER II

PROBLEM FORMULATION

2.1 General Description of the Synthesis Procedure

A detailed flow diagram of the synthesis procedure is shown in Figure 2. Given an initial design, a design ultimate load, P_{ULT}, and the remaining required input data, a complete stress analysis of the initial joint design is performed. The applied load used for this initial analysis is the design ultimate load. Various failure criteria, expressed in the form of behavioral constraint equations, are then checked for possible failures at each hole along the joint in the composite main plate, the metal splice plates and the bolts. If all the behavioral constraints are satisfied by the proposed initial design, the minimization algorithm is given control of the program and a minimum weight design is sought, subject to the imposed design constraints.

If, on the other hand, the proposed initial design does not satisfy all the behavioral constraints, then the applied load is reduced to a level which the proposed design can support. A reasonable effort should be made to propose a valid initial design since difficulties with run time and convergence can occur for syntheses which must move great distances in design space. If scaling of the applied load is required, the program automatically begins to treat the applied load as an additional design variable. The objective function is in turn redefined such that the total joint weight is

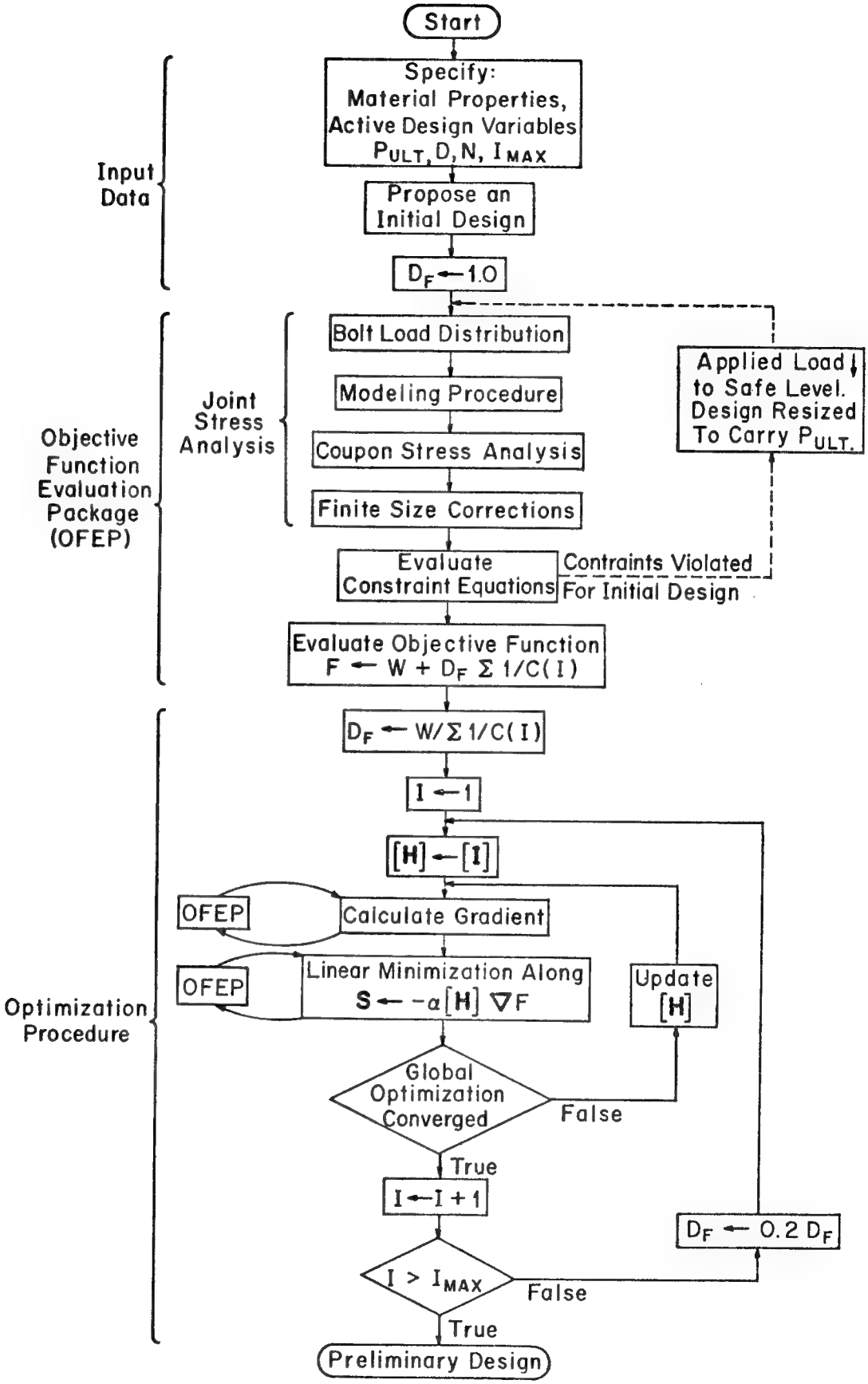

Figure 2. Flow Diagram for the Synthesis Procedure

minimized while the applied load is driven back toward the desired design ultimate load. It is possible that constraints placed on the design would eliminate the possibility of any design in design space carrying the desired design ultimate load. In such a case the program seeks that minimum weight design which can support the largest load possible. Linear scaling based on the values of the exceeded constraints is used to determine an initial acceptable reduced applied load since the stress analysis is linear.

It is assumed in both the above cases that all the side constraints built into the program logic are satisfied for the proposed initial design. The side constraints enforce maximum and minimum values for the various geometric design variables. If a side constraint is accidentally violated due to a user error, program execution automatically terminates.

There are several possible methods available to perform the required joint stress analyses. An obvious analysis method is to perform a finite element stress analysis of the entire joint. Such procedures require large core capacities for complex joints and extremely large run times, which are not tolerable as far as a general purpose synthesis procedure is concerned.

In the current study the multiple fastener joint is modeled as a series of single fastener coupons, which are analyzed individually. It is assumed that the effects of adjacent fasteners can be accounted for separately. The loading on each fastener is derivable from a

bolt load partitioning analysis. The load distribution is calculated by matching total elongations between pairs of adjacent fasteners in the main plate to those in the splice plates.

Finite element analyses of single fastener coupons present little difficulty as far as core limitations are concerned (e.g., see Appendix A and [3]). Run times, however, even though they are typically less than one minute on the UNIVAC 1108, are still much too large, since in this synthesis procedure single coupon stress analyses must be performed many hundreds of times if the synthesis procedure is to be effective.

The stress analysis procedure used herein performs analyses of these same single fastener coupons using a series solution based on the theory of anisotropic elasticity for infinite plates. The infinite plate stress analyses are corrected for the effects of finite size using anisotropic correction factors. The time required on the UNIVAC 1108 using this method to perform a single fastener stress analysis is less than a tenth of a second, making the procedure some 600 times faster than comparably accurate finite element analyses.

2.2 Material Model

A laminated composite plate is made up of oriented plies of parallel brittle fibers embedded in a ductile matrix material. A single ply has two principal directions as illustrated in Figure 3a.

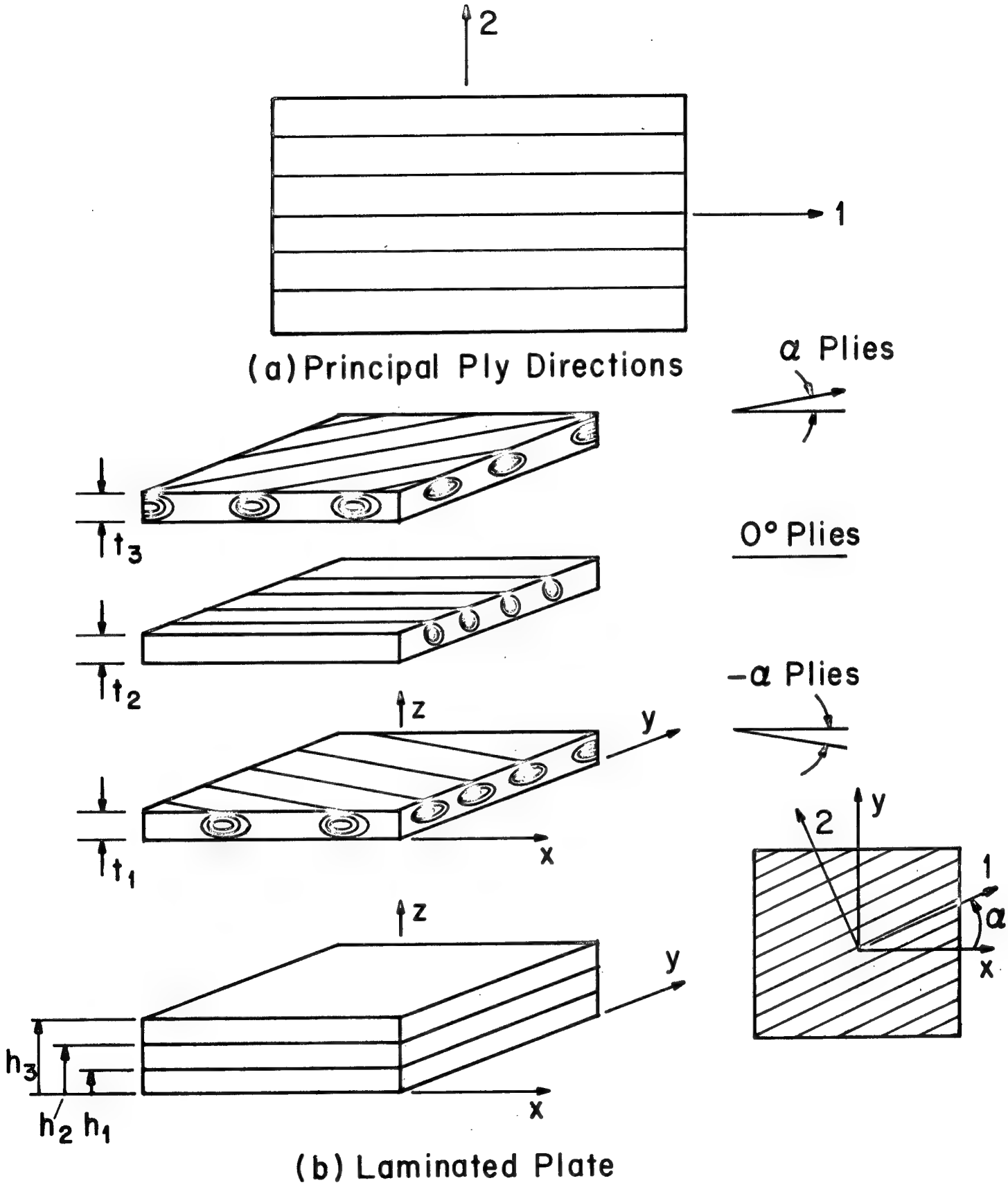

Figure 3. Schematic of a Laminated Composite

Each ply is assumed to be a homogeneous orthotropic material which can be defined by four independent elastic constants: the elastic moduli in the 1 and 2 directions (i.e., the fiber direction and transverse fiber direction respectively), E_{11} and E_{22}, the shear modulus, G_{12}, and the material's major Poisson's ratio, ν_{12}. The materials minor Poisson's ratio, ν_{21}, is given by

$$\nu_{21} = \nu_{12} E_{22}/E_{11} \tag{1}$$

The ply properties for the graphite-epoxy and boron-epoxy material systems used in this study are listed in Table 1. The respective ply ultimate stress and strain allowables are listed in Table 2 for later use.

The various plies which make up a laminated composite plate are each assumed to be in a state of plane stress. The interlaminar shear stresses present between plies are neglected, although estimates of their magnitude can be made based on equilibrium considerations [4]. Analytical studies [4, 5] have shown that lamination theory gives very good approximations to the average stresses and strains throughout the laminate at points further than a few ply thicknesses away from free edges. The effects of interlaminar stresses for loaded holes has yet to be reported.

The constitutive relationship for a single orthotropic layer in a state of plane stress is

$$\begin{Bmatrix} \sigma_1 \\ \sigma_2 \\ \tau_{12} \end{Bmatrix} = \begin{bmatrix} Q_{11} & Q_{12} & 0 \\ Q_{12} & Q_{22} & 0 \\ 0 & 0 & 2Q_{66} \end{bmatrix} \begin{Bmatrix} \varepsilon_1 \\ \varepsilon_2 \\ \frac{1}{2}\gamma_{12} \end{Bmatrix} \tag{2}$$

Table 1. Ply Properties for Graphite-Epoxy and Boron-Epoxy

Material Properties	Graphite-Epoxy	Boron- Epoxy
E_{11}	21.0×10^6 psi	30.0×10^6 psi
E_{22}	1.7×10^6 psi	2.7×10^6 psi
G_{12}	1.4×10^6 psi	0.65×10^6 psi
ν_{12}	0.21	0.21

Table 2. Ply Ultimate Allowables for Graphite-Epoxy and Boron-Epoxy

Ultimate Allowables	Graphite-Epoxy	Boron-Epoxy
σ_{1ut}	151,000 psi	194,000 psi
σ_{2ut}	7,700 psi	12,200 psi
σ_{1uc}	205,000 psi	416,500 psi
σ_{2uc}	15,400 psi	37,500 psi
τ_{12u}	21,000 psi	18,500 psi
ε_{1ut}	0.0072 in/in	0.0071 in/in
ε_{2ut}	0.0045 in/in	0.0045 in/in
ε_{1uc}	0.00975 in/in	0.0128 in/in
ε_{2uc}	0.0090 in/in	0.0125 in/in
ε_{12u}	0.0075 in/in	0.0275 in/in

where

$$Q_{11} = E_{11}/(1-\nu_{12}\nu_{21})$$
$$Q_{22} = E_{22}/(1-\nu_{12}\nu_{21})$$
$$Q_{12} = \nu_{21}E_{11}/(1-\nu_{12}\nu_{21}) \qquad (3)$$
$$Q_{66} = G_{12}$$

Individual plies are stacked at various orientations relative to the laminate's x axis as shown in Figure 3b. In a 0° ply the fibers are parallel to the x axis; in an α ply the fibers are oriented at an angle α relative to the x axis.

In this study only mid-plane symmetric, angle-plied laminates are considered subject to in-plane loading. Therefore, plate bending and in-plane warping will not occur and, as a result, the laminate strains through the thickness are assumed constant. The individual ply stress components, which are symmetric about the mid-plane of the laminate, induce laminate stress resultants but no laminate moment resultants.

To determine the laminate's constitutive relationship, which relates the laminate stress resultants to laminate strains, the principal stresses and strains for each ply must first be transformed to the x-y axes system. Both stresses and strains transform as second order tensors. Therefore for the k^{th} ply

$$\begin{Bmatrix} \sigma_1 \\ \sigma_2 \\ \tau_{12} \end{Bmatrix}_k = \begin{bmatrix} T_{ij} \end{bmatrix}_k \begin{Bmatrix} \sigma_x \\ \sigma_y \\ \tau_{xy} \end{Bmatrix}_k \qquad (4)$$

and

$$\begin{Bmatrix} \varepsilon_1 \\ \varepsilon_2 \\ \frac{1}{2}\gamma_{12} \end{Bmatrix}_k = \begin{bmatrix} \\ T_{ij} \\ \\ \end{bmatrix}_k \begin{Bmatrix} \varepsilon_x \\ \varepsilon_y \\ \frac{1}{2}\gamma_{xy} \end{Bmatrix}_k \tag{5}$$

where $[T_{ij}]_k = \begin{bmatrix} m^2 & n^2 & 2mn \\ n^2 & m^2 & -2mn \\ -mn & mn & m^2-n^2 \end{bmatrix}$ (6)

$$m = \cos\alpha_k$$

$$n = \sin\alpha_k$$

Substituting (4) and (5) into (2) results in the ply's constitutive relationship in the x-y coordinate system

$$\begin{Bmatrix} \sigma_x \\ \sigma_y \\ \tau_{xy} \end{Bmatrix}_k = \begin{bmatrix} \\ \overline{Q}_{ij} \\ \\ \end{bmatrix}_k \begin{Bmatrix} \varepsilon_x \\ \varepsilon_y \\ \frac{1}{2}\gamma_{xy} \end{Bmatrix} \tag{7}$$

where $[\overline{Q}_{ij}]_{k=} = [T_{ij}]_k^{-1} [Q_{ij}]_k [T_{ij}]_k$

By integrating the ply stress components through the thickness, t, three stress resultants are obtained

$$\begin{Bmatrix} N_x \\ N_y \\ N_{xy} \end{Bmatrix} = \int_{-t/2}^{t/2} \begin{Bmatrix} \sigma_x \\ \sigma_y \\ \tau_{xy} \end{Bmatrix} dz = \sum_{k=1}^{n} \int_{h_{k-1}}^{h_k} \begin{Bmatrix} \sigma_x \\ \sigma_y \\ \tau_{xy} \end{Bmatrix}_k dz \tag{8}$$

where n is the total number of individual plies present. Substituting (7) into (8) results in the laminate constitutive relationship

$$\begin{Bmatrix} N_x \\ N_y \\ N_{xy} \end{Bmatrix} = \left(\sum_{k=1}^{n} [\bar{Q}_{ij}]_k \; t_k \right) \begin{Bmatrix} \varepsilon_x \\ \varepsilon_y \\ \frac{1}{2}\gamma_{xy} \end{Bmatrix} = \begin{bmatrix} A_{ij} \end{bmatrix} \begin{Bmatrix} \varepsilon_x \\ \varepsilon_y \\ \frac{1}{2}\gamma_{xy} \end{Bmatrix} \qquad (9)$$

where $[A_{ij}]$ is the laminate stiffness matrix for the x-y axes system and t_k is the thickness of the k^{th} ply (i.e., $t_k = h_k - h_{k-1}$).

Using lamination theory a laminate stiffness matrix for the assumed homogeneous anisotropic material has been developed. As a result problems involving laminated composite plates can be solved using available numerical and analytical techniques for homogeneous anisotropic materials. In this study three such methods are used: the theory of anisotropic elasticity [6], which is an analytical method, and two numerical methods; finite elements [7] and boundary-integral equations [8]. Given a well-defined problem the laminate strains at any point can be determined by one of these methods. Principal ply strains can, in turn, be determined directly from (5). The principal ply stresses are then given directly by (2). In the laminate strength analyses performed herein these principal ply stress components are compared to their respective tensile and compressive ultimate allowables to check for possible failure initiation.

2.3 Bolt Load Partitioning Analysis

Given a design ultimate load the designer must first specify the number of bolts, N, which the column of fasteners will contain.

The optimization algorithm is not designed to admit integer variables and as a result N must be preassigned. A conservative estimate of N can be made based on the effective shear strength of the bolt material and a preselected bolt diameter. It may prove worthwhile in practice to run the synthesis program for more than one set of N and bolt diameter values to achieve a lower weight preliminary design.

The technique used herein to predict bolt load distributions in a given joint is based on an elongation matching technique. It is assumed that all bolts act as snugly fitting rigid pins and that the effects of plate bending are negligible. The change in length of the section of main plate between any two adjacent bolts is assumed equal to the change in length of the corresponding section of splice plates between the same two bolts. That is

$$\Delta\ell_m(i \rightarrow i+1) = \Delta\ell_s(i \rightarrow i+1) \tag{10}$$

Referring to Figure 4 we may express the strain in the composite main plate and metal splice plates at some point x between the bolts labeled i and i+1 as

$$\varepsilon_m(x_i \leq x \leq x_{i+1}) = \frac{d\ell_m}{dx} = \frac{F - \sum_{k=1}^{i} P_k}{E_m(x)\, A_m(x)} \tag{11}$$

$$\varepsilon_s(x_i \leq x \leq x_{i+1}) = \frac{d\ell_s}{dx} = \frac{\frac{1}{2}\sum_{k=1}^{i} P_k}{E_s(x)\, A_s(x)} \tag{12}$$

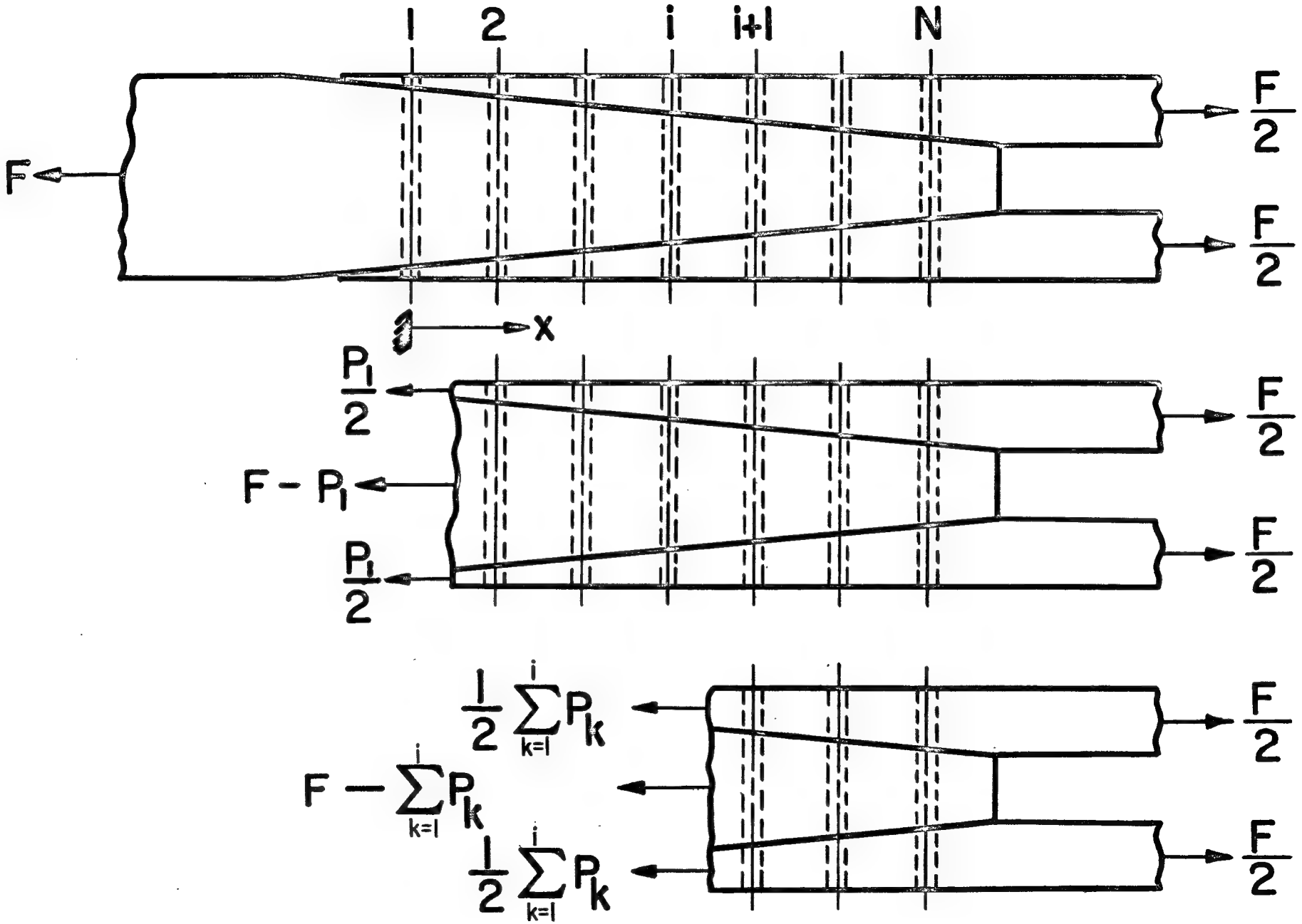

Figure 4. Load Transfer in a Multiple Fastener Joint Loaded in Double Shear

where x_i represents the location of the i^{th} bolt. By integrating (11) and (12) with respect to x from x_i to x_{i+1} and substituting into (10), it follows that

$$\sum_{k=1}^{i} P_k = \frac{m}{m+s/2} \times F \tag{13}$$

$$\text{where } m = \int_{x_i}^{x_{i+1}} \frac{dx}{E_m(x)\, A_m(x)} \quad \text{and } s = \int_{x_i}^{x_{i+1}} \frac{dx}{E_s(x)\, A_s(x)} \tag{14}$$

For a given joint design the modulus of the main plate and cross sectional areas of both the main plate and splice plates can be expressed as polynomials in x. In fact, for joints which have linear variations in joint width and ply thicknesses, the expressions for $E_m(x)$, $A_m(x)$ and $A_s(x)$ can all be represented by quadratic functions in x.

Note that (13) and (14) can only be evaluated for i=1, N-1, which results in (N-1) equations in terms of the N unknown bolt loads. The necessary additional equation which relates the various bolt loads is, of course, the overall joint equilibrium equation

$$F = \sum_{k=1}^{N} P_k \tag{15}$$

Equations (13) and (15) represent N equations in N unknowns which may be solved directly for P_1 thru P_N.

The main plate and splice plate cross sectional areas are readily

defined as functions of x. Referring to Figure 1 it is apparent

$$A_m(x) = [(t_m(L)-t_m(0))\ (x/L) + t_m(0)]\ [(W_m(L)-W_m(0))\ (x/L) + W_m(0)] \quad (16)$$

$$A_s(x) = [(t_s(L)-t_s(0))\ (x/L) + t_s(0)]\ [(W_s(L)-W_s(0))\ (x/L) + W_s(0)] \quad (17)$$

where $A_s(x)$ represents the cross sectional area of one of the two double shear splice plates.

It has been found that a quadratic polynomial in x can be used to represent the modulus of the main plate to within a few percent when linear variations in ply thicknesses are employed. Thus, the modulus of the main plate may be determined at several locations along the joint using lamination theory and a second order curve of the form

$$E_m(x) = Ax^2 + Bx + C \quad (18)$$

may be fit to the resulting modulus values. The values of A, B and C for a given design are determined automatically by an internal curve fitting subroutine which uses modulus information from three bolt locations.

The only remaining unknowns which are needed to calculate the bolt load distribution are the coordinate locations of the N bolts. Since the bolts are evenly spaced along the joint, the N bolt locations can be expressed as

$$X(I) = \frac{I-1}{N-1} \left[L - \left(\frac{E}{D}\right)_m\right] \quad , \quad I = 1, N \quad (19)$$

where L is the total joint length and $(E/D)_m$ is the ratio of the main plate leading edge distance to bolt diameter (See Figure 1).

2.4 Joint Modeling Procedure

As described above, the joint is modeled as a series of single fastener coupons to make the joint stress analysis feasible. The modeling procedure is illustrated in Figure 5. The cross sectional properties and dimensions of the i^{th} coupon are assumed uniform and equal to those of the joint at the i^{th} cut-out, cross section A-A in Figure 5.

In the bolt load distribution analysis the various bolt loads are defined explicitly in terms of the variable laminate properties. As a result, the bolt load on the i^{th} fastener, P_{Bi}, is known. The skin load induced by the forward fasteners, P_{Si}, is derivable from equilibrium considerations and is given by

$$P_{Si} = \sum_{k=i+1}^{N} P_{Bk} \tag{20}$$

It is assumed that P_{Bi} and P_{Si} can be imposed through appropriate stress boundary conditions on the i^{th} coupon. Thus a well-posed problem has been formulated in that the coupon geometry, lamination and loading have been specified.

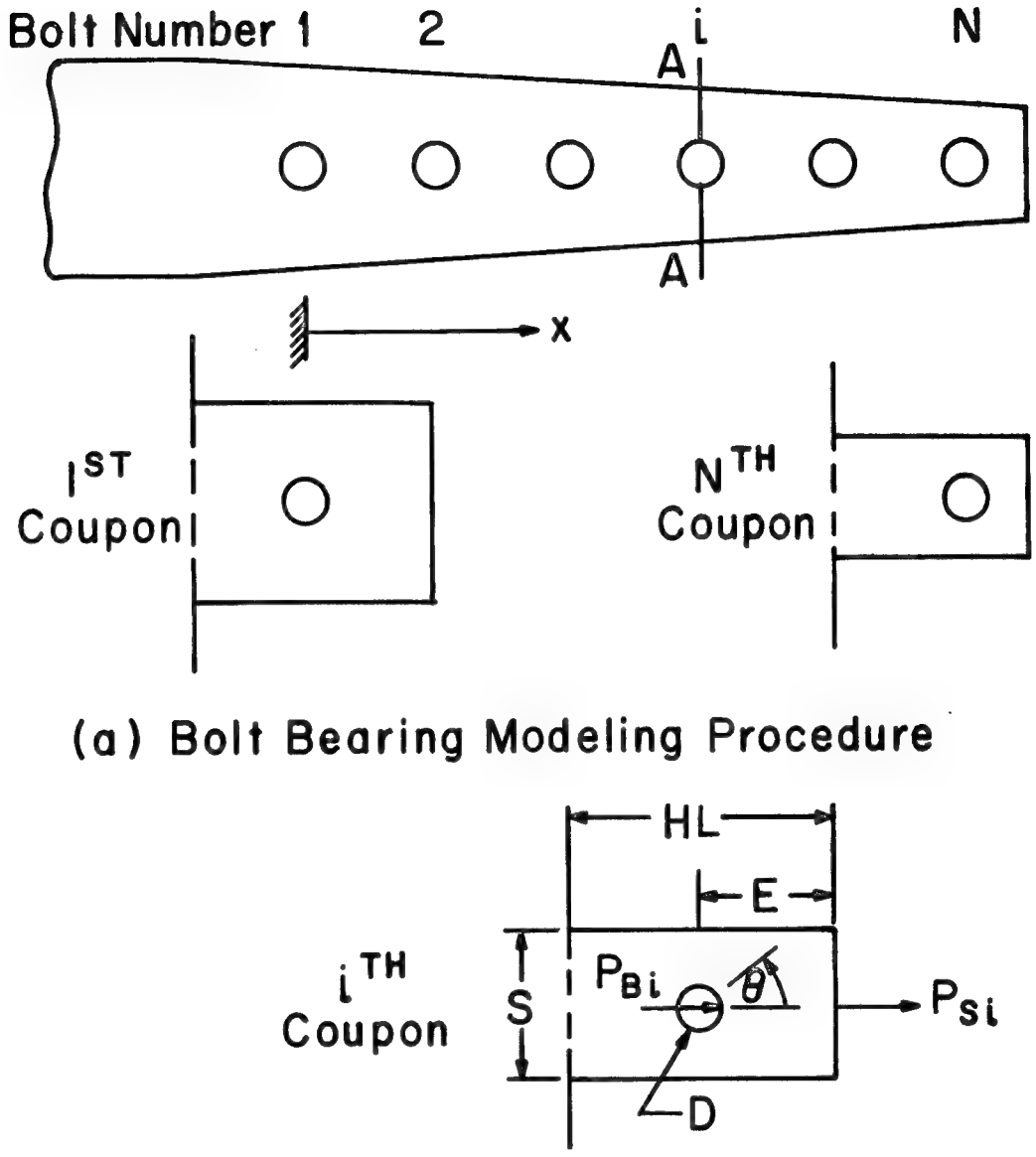

Figure 5. Modeling Procedure for Single Column Fasteners

2.5 Joint Strength Analysis

The objective of this section is to propose and verify a simple strength theory for metal-to-composite multiple fastener joints. Since it is to be used in an automated design procedure it should be as operationally simple as possible. The development of a strength theory for these joints required two analytical studies. The first involved the prediction of failure loads and modes for a number of single fastener bolt bearing coupons to evaluate several proposed failure criteria for composites. The failure criterion selected from this study was then used in the second analytical study to predict failure loads and modes, and failure locations for a number of multiple fastener joints. The major goal of the second study was to verify the joint modeling procedures and the method for partitioning loads among the various fasteners, as described above.

Due to the tailorability of composite materials it is impossible to specify laminate strength allowables for the entire range of laminates which are available to the designer. As a result strength criteria are usually applied on a ply-by-ply basis in the ply principal directions. Currently the three most popular ply failure criteria are the maximum ply stress, the maximum ply strain and a quadratic stress failure surface, sometimes called the Tsai-Hill criterion. The maximum ply stress (strain) criterion predicts failure to occur when any one of the ply principal stresses (strains) exceeds its ultimate allowable.

The Tsai-Hill criterion is a quadratic failure criterion in the ply principal stresses. By using both tension and compression allowables as required in the quadratic formula, a closed surface in design space results which is composed of four quarter ellipses. All three of these ply failure criteria are illustrated in Figure 6 (for $\tau_{12} = 0$ in the case of Tsai-Hill criterion). A more detailed discussion of these criteria is presented in [1].

The option exists in laminated composites of predicting laminate failure using a successive ply failure analysis, or by defining first ply failure to be total laminate failure. Local ply failures may occur which do not significantly degrade the laminate's strength. In such a case a first failure analysis would predict laminate failure to occur prematurely since the laminate would still possess a great deal of additional load carrying capacity. A successive failure analysis, on the other hand, models local load redistribution and results in less conservative predictions for failure loads. Bolted joints in composites are often observed [9] to be linear to failure, which tends to justify the use of a first failure analysis.

To get good correlation with experimental data successive failure analyses are used herein. In the synthesis procedure, however, it is desirable to design away from premature localized ply failures which may or may not significantly degrade the laminate strength. Designs which are weak at certain positions will not be efficient load carriers

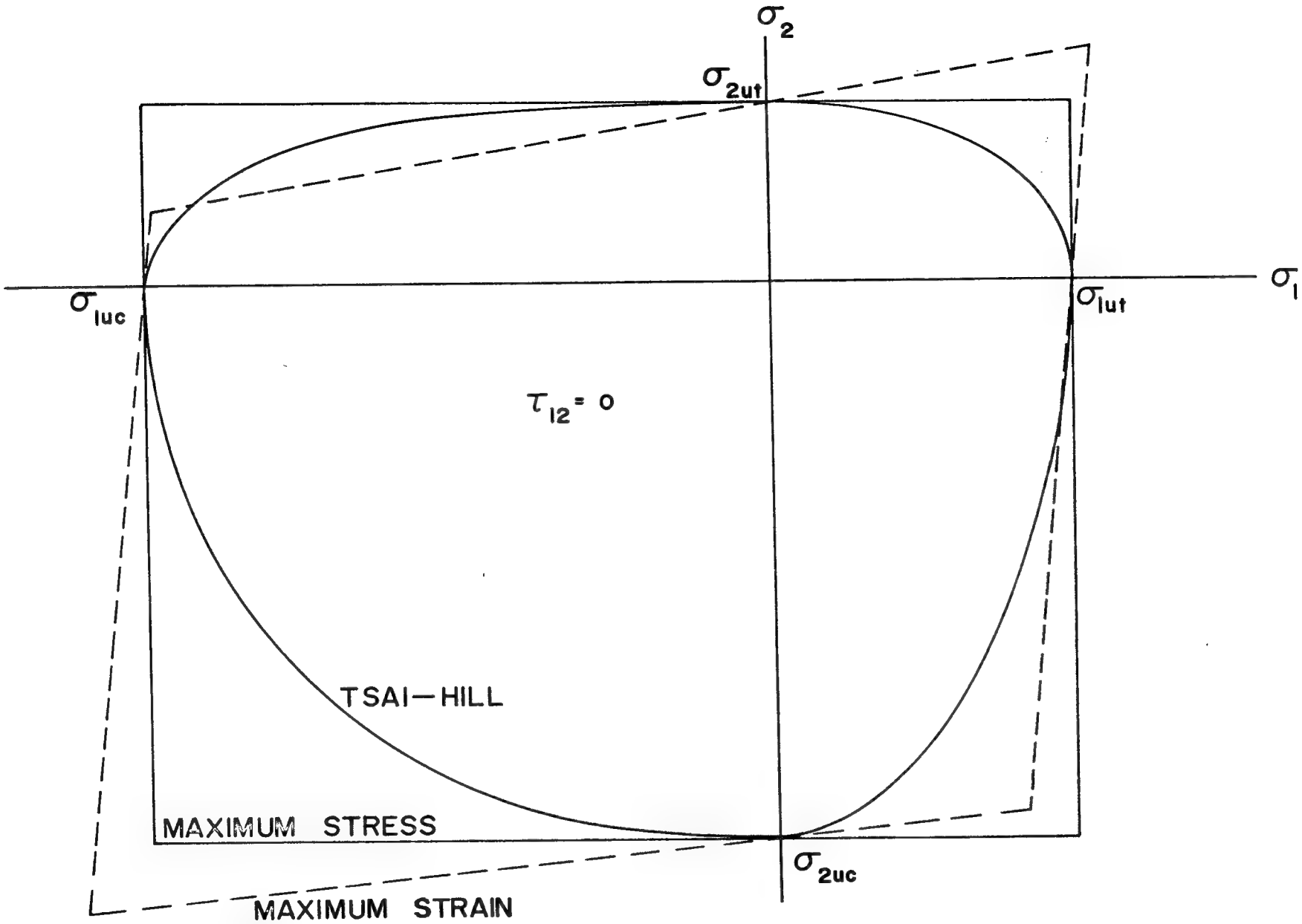

Figure 6. Comparison of Predicted Failure Surfaces in Stress Space

when viewed from a first failure analysis and an optimization algorithm will drive the design away from these weak designs toward more efficient ones. Optimum designs are usually critical at several locations simultaneously which increases the likelihood that the first ply failure for an optimized design will result in significant laminate damage and a resulting complete joint failure.

In the first numerical study to be discussed a number of experimentally failed single fastener coupons were analyzed using a constant strain finite element program. The stress analysis results were evaluated using the three proposed ply failure criteria to see how accurately each could predict the failure characteristics of the coupons. The laminates were modeled as anisotropic, homogeneous materials using lamination theory [1]. The analysis assumed that the bolt-specimen interaction was frictionless and could be represented by a cosine distribution of normal stress acting over the front half of the circular boundary. A successive failure analysis was used in an attempt to make the strength analysis as accurate as possible. In all but one case, however, first ply failure resulted in total laminate failure, which agrees with the experimentally observed linear load-displacement behavior of the coupons. The one exception involved a premature matrix splitting failure which did not significantly degrade the laminate's strength. The details of this study are discussed in Appendix A.

Of the three criteria the Tsai-Hill criterion proved to be the most convenient in terms of being able to readily predict failure initiation sites and accompanying failure modes. Contour plots constructed from the Tsai-Hill criterion and illustrated in Appendix A indicate very clearly those regions where failure initiation occurs and give a clear indication of the direction of crack propagation. As far as predicting failure loads the Tsai-Hill criterion was always conservative. The degree of conservatism was a function of specimen anisotropy, varying from 2% for a $(0_6/\pm45_5)$ boron-epoxy laminate to 53% for a (±45) boron-epoxy laminate. The error encountered in predicting failure loads for laminates which did not exhibit large shear deformations, which do occur in the (±45) laminate, was always less than 24%. To take advantage of this smaller error band it was decided that all proposed designs in the synthesis would be required to have a finite number of 0° plies present at all times. The synthesis results presented later show that this restriction is not really necessary since all minimum weight designs have significant amounts of both 0° and ±45° plies present.

The maximum stress and maximum strain criteria were both non-conservative in predicting failure of one of the six specimens analyzed. The maximum stress criterion predictions, however, were all within 12% of the Tsai-Hill criterion predictions for the laminates which did not exhibit large matrix shear stresses. Since the maximum stress criterion is operationally much simpler to apply than the Tsai-Hill criterion, it

was selected as the preferred method of strength analysis for the synthesis procedure.

In the second analytical study the same finite element program was used to perform the required single coupon stress analyses. The modeling procedure discussed in section 2.4 was used to model each of the six multiple fastener joints included in this study as a series of single fastener coupons. A bolt load partitioning analysis based on a point strain matching technique was used to determine the bolt load distribution for each joint. By equating the longitudinal strains in the main plate to those in the splice plates at the mid-points between adjacent fasteners and writing an overall joint equilibrium equation, N equations in terms of the N unknown bolt loads are obtained. All but one of the specimens was experimentally loaded in single shear. The assumption was made, however, that the effects of bending could be neglected and the problems were solved as if equivalent double shear splice plates were used. The details of this study are discussed in Appendix B.

In the reported results the successive failure analysis predicted a bearing failure to take place in one of the joints. Additional load applied to the joint, after the bearing failure was predicted to occur, was assumed to be distributed among the remaining fasteners in proportion to their relative existing load levels at bearing failure initiation. For this graphite-epoxy specimen (which failed in net tension) the

predicted failure load was conservative by just 3%. The correct experimental failure mode was predicted but the predicted location was off by one fastener location.

The remaining joints discussed in Appendix B were all made of boron-epoxy and were *designed* to fail in net tension at the innermost fastener. Four of the five joints experimentally failed in a splitting mode ahead of the last bolt at a much lower load level than anticipated based on the designer's prediction of a net tension failure. The other joint failed in net tension at the innermost fastener as desired. In all five cases the successive failure analysis using the maximum ply stress failure criterion was conservative in predicting failure load and correct in predicting failure mode and location. The predicted failure load for the net tension failure was conservative by 22%; predictions for the splitting failures were conservative by 30 to 40%. These results are very similar to the single fastener data; the failure load predictions are far less conservative for net tension failures than for any of the other modes. This is encouraging since the synthesis results discussed later show that a common characteristic of efficiently designed joints is that they are all critical in net tension.

One other very important fact was clear. In every case failure initiation occurred at positions on the circular boundary where fibers were either tangent to the hole surface or perpendicular to it. This enables us to be very selective in choosing locations at which checks

are to be made to insure against main plate failures in the synthesis. In a [0/±α/90] laminate checks for fiber failures are made at points where fibers are tangent to the hole surface; θ=90°, 90°-α and 0° for the 0°, -α and 90° plies respectively (Refer to Figure 7). Checks for matrix failures are made at points where fibers are perpendicular to the hole surface θ=0°, α and 90° for the 0°, +α and 90° plies respectively. At θ=0° in the 0° plies a fiber compressive failure must also be insured against to eliminate the possibility of a bearing failure. Predicting premature bearing failures which result from matrix splitting, as discussed in Appendices A and B, is not a consideration in the synthesis since matrix splitting is not permitted to occur in a first failure strength analysis. Matrix shear and compressive failures are assumed not to be a problem.

2.6 Summary

A method for performing analyses of multiple fastener joints in composites has been formulated and verified. A strength theory for joints based on a first failure analysis using the maximum ply stress failure criterion has been selected for use in the synthesis. Since it was observed that failure initiation always occurs at points on the circular boundary where fibers are either tangent or perpendicular to the cut-out, the strength analysis need only be applied at these critical locations. The success of both of the analytical studies in conservatively predicting failure loads and correctly predicting failure modes and locations indicates that both the modeling procedure

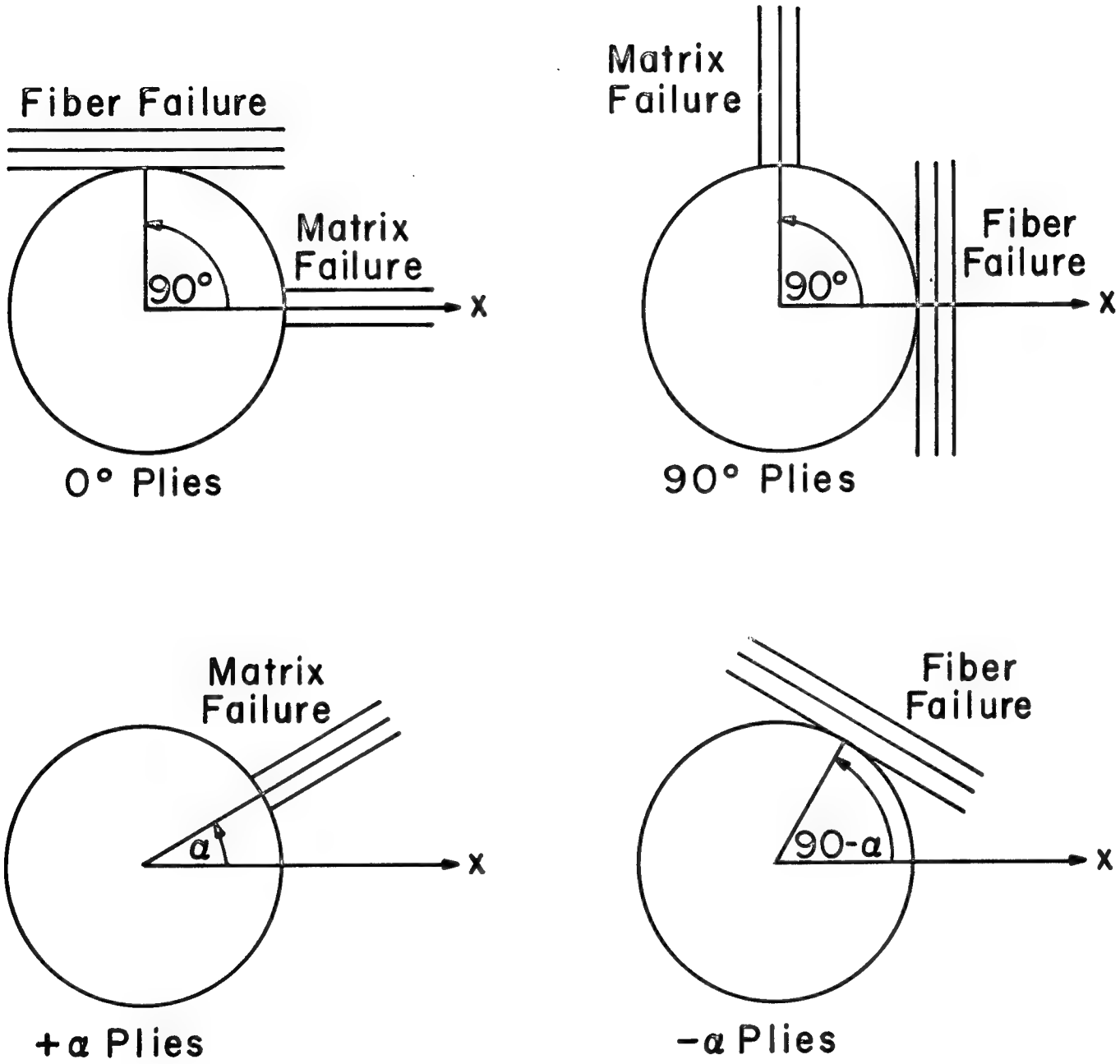

Figure 7. Points of Application of the Main Plate Failure Criterion

and the method of determining bolt load distributions are adequate for the current study.

Recently a somewhat different failure theory [10] has been proposed for laminated composites which helps explain the consistent conservatism exhibited by the maximum ply stress failure criterion in the joint studies reported in Appendix B. Experimental data [10, 11] indicates that there is a hole size effect exhibited by laminated composites which cannot be accounted for using simple elastic stress analysis procedures. A series of geometrically similar graphite-epoxy bolt bearing specimens, shown in Figure 8, were designed and tested to failure. The specimens all failed in net tension. If the material is truly stress critical (i.e., failure occurs when some stress allowable is exceeded) the failure load of all the specimens should be predictable from the failure load of any one of the specimens by a simple scaling procedure. Such scaling was not possible for the smaller coupons. The observed [11] size effect could be explained, however, via a fracture mechanics model: Two symmetric radial cracks of some given length were assumed at θ=90° and 270° in each specimen prior to failure. Given the mode I critical stress intensity factor for the laminate, K_{Ic}, and the "correct value" of the crack length, the fracture mechanics model was used to fit the experimental data. The "correct value" of the crack length was not known *a priori* for the laminate analyzed but was back calculated from the known failure load

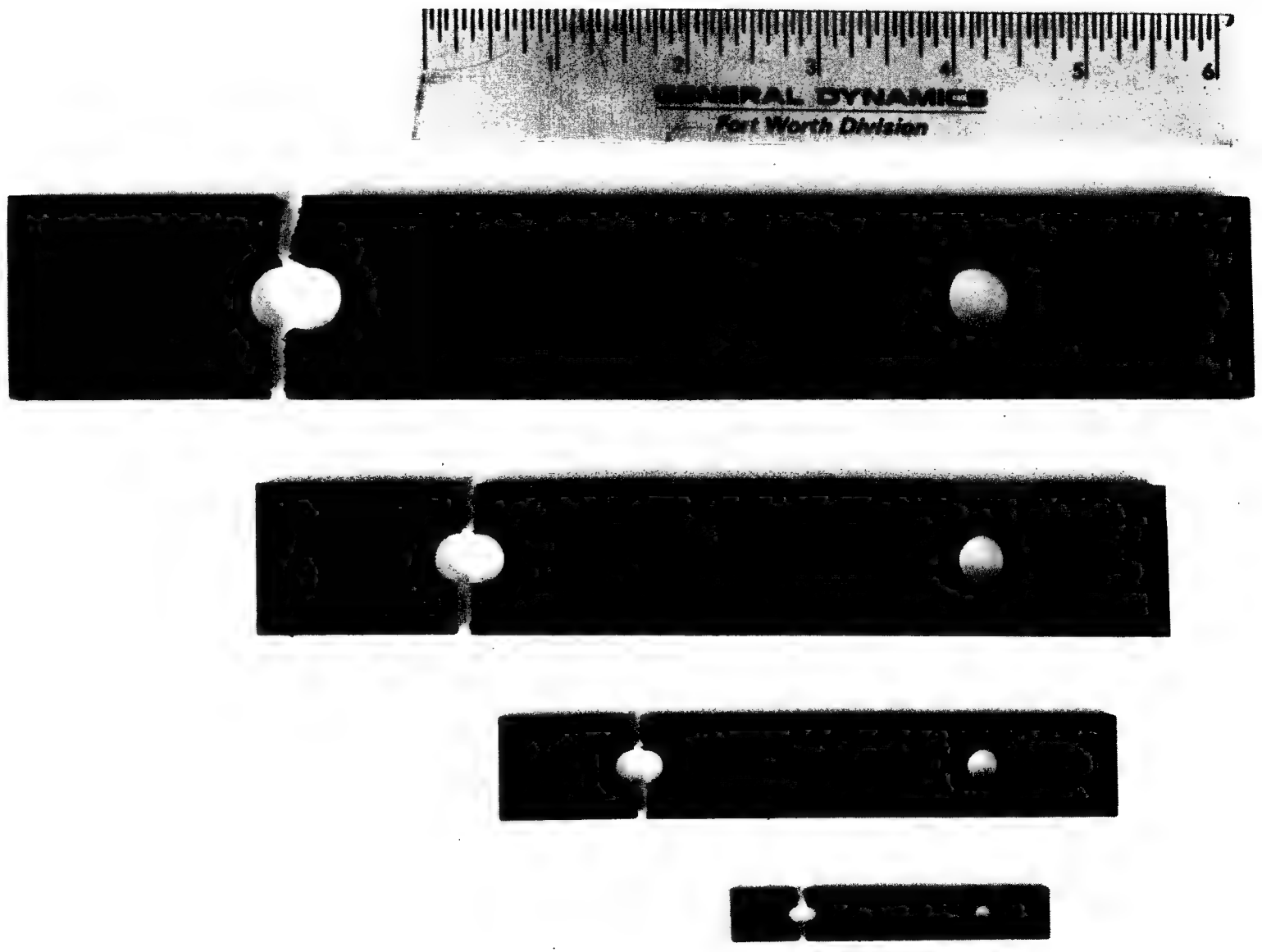

Figure 8. Geometrically Similar Bolt Bearing Specimens

of one of the specimens. Similar success of the fracture mechanics model to predict size effects has been reported [10] in fitting failure data of a number of graphite-epoxy open hole tension coupons. Unfortunately the very limited data available does not permit the use of this failure theory in the current study.

CHAPTER III

EFFICIENT STRESS ANALYSIS PACKAGE

3.1 Introduction

It was demonstrated in the previous chapter that the proposed joint failure theory, used in conjunction with the described joint modeling procedure and bolt load partitioning analysis, can be used to predict the failure characteristics of multiple fastener joints in composites. The task now is to devise an *efficient* stress analysis procedure for the single fastener coupons which can be used to automate the tedious analysis – resizing cycle to achieve minimum weight designs. Using the finite element method to perform the required single fastener coupon stress analyses in such an automated design procedure is not practical since the analysis package is called many hundreds of times in a given synthesis. As a result an approximate method has been developed to perform the analyses and is shown to be some 600 times faster than comparably accurate finite element solutions.

Consider the stress analysis of the i^{th} coupon in a given joint design. The problem of an infinite anisotropic plate containing a circular cut-out, having the same material properties as the i^{th} coupon is analyzed first. The infinite plate is loaded as shown in Figure 9. The bolt load, P_{Bi}, is represented by cosine distribution of normal stress, σ_{Bi}, acting over the front half of the hole surface; the net load of this distribution in the x direction being equal to P_{Bi}. The

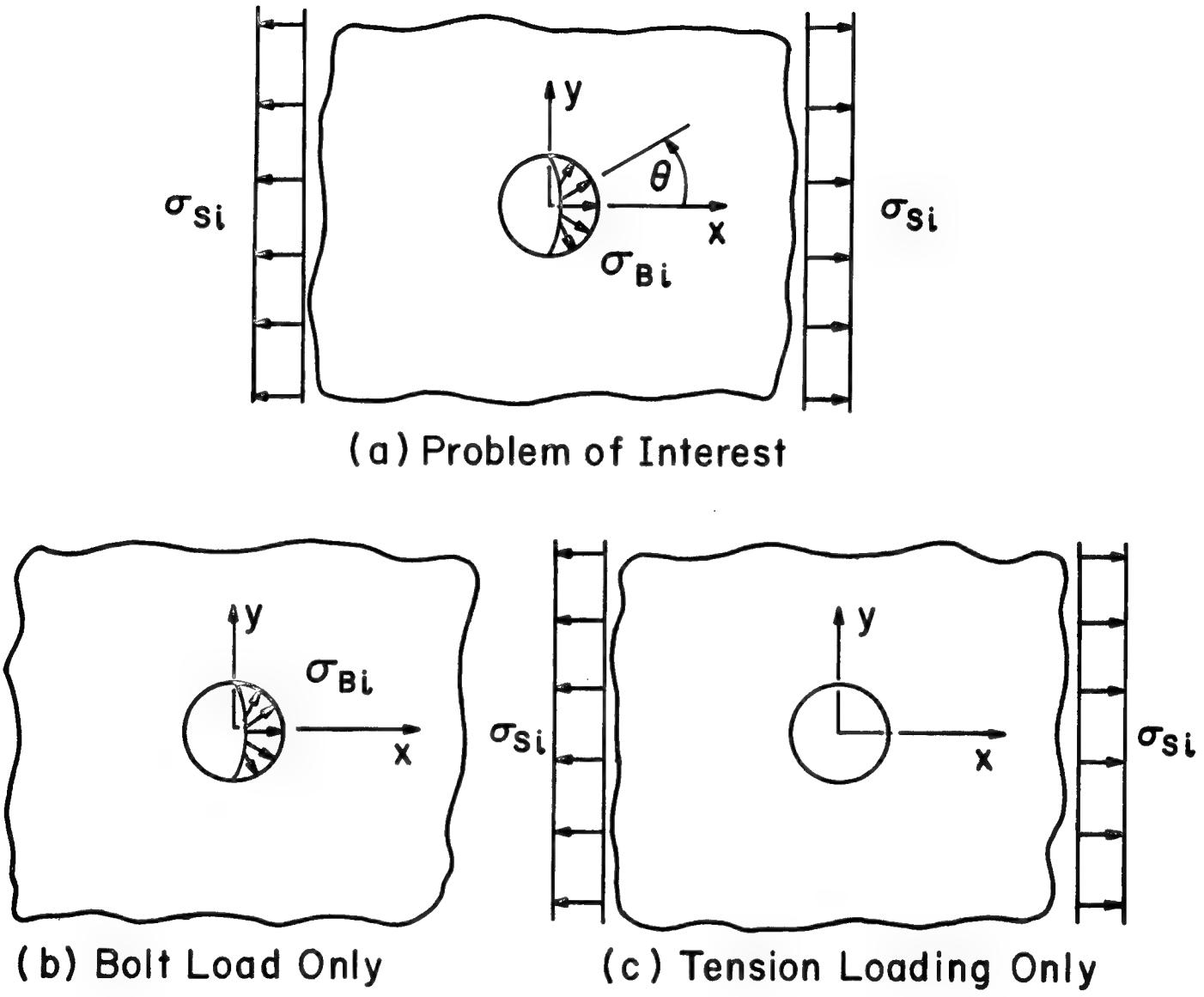

Figure 9. Method of Superposition for the Infinite Plate Solution

interaction is assumed frictionless. It was shown in Appendix A that such a distribution can be used to adequately represent the bolt-specimen interaction. A uniform stress, $\sigma_{Si} = P_{Si}/St$, was used to represent the loading from preceding bolts.

Solutions to the two infinite plate problems above are based on the theory of anisotropic elasticity [6]. The series solution to the loaded hole problem, Figure 9b, is derived in section 3.2.2; the solution to the problem of a plate under tension, Figure 9c, is presented in [6] and the results are summarized in section 3.2.3. Each of the infinite plate solutions are corrected for the effects of finite specimen size using anisotropic correction factors prior to their superposition. The tension loaded results are then corrected for the effects of adjacent cut-outs. These various correction factors are discussed in detail in section 3.3.

The use of correction factors to modify the infinite plate solutions produces a stress field which no longer strictly satisfies overall equilibrium requirements. A comparison of this approximate solution with a finite element solution is made in section 3.4 which shows that the predicted stresses are somewhat higher, and therefore more conservative, than those predicted using finite elements. A development of the two infinite anisotropic plate solutions is

presented in the next section followed by a detailed discussion of the anisotropic correction factors.

3.2 Infinite Plate Stress Analyses

3.2.1 Summary of Pertinent Equations

The basic equations and notation from the mathematical theory of anisotropic elasticity as presented in [6] are summarized below. The stress components for the state of generalized plane stress in the absence of body forces in an anisotropic material can be expressed in terms of a complex stress function of the form

$$F(x,y) = 2Re[F_1(z_1) + F_2(z_2)]^* \tag{21}$$

where

$$\begin{aligned} \sigma_x &= \partial^2 F/\partial y^2 \\ \sigma_y &= \partial^2 F/\partial x^2 \\ \tau_{xy} &= -\partial^2 F/\partial x \partial y \end{aligned} \tag{22}$$

The complex stress functions $F_1(z_1)$ and $F_2(z_2)$ are analytic functions of the complex characteristic coordinates z_1 and z_2 respectively, where

$$\begin{aligned} z_1 &= x + \mu_1 y \\ z_2 &= x + \mu_2 y \end{aligned} \tag{23}$$

*The notation $Re[\ ]$ represents the real part of the complex expression enclosed by the brackets.

The complex characteristic coordinates z_k should not be confused with the complex physical coordinates z given by

$$z = x + i\,y \tag{24}$$

In order to satisfy compatibility the following characteristic equation must be satisfied by the μ_k values.

$$\beta_{11}\mu^4 - 2\beta_{16}\mu^3 + (2\beta_{12}+\beta_{66})\mu^2 - 2\beta_{26}\,\mu + \beta_{22} = 0 \tag{25}$$

The μ_k values are seen to be functions only of the material compliances β_{ij}. Pairs of equal roots ($\mu_1=\mu_2$, $\bar{\mu}_1=\bar{\mu}_2$) result for isotropic materials. For an anisotropic material four distinct roots (μ_1, μ_2, $\bar{\mu}_1$ and $\bar{\mu}_2$) are obtained.

To simplify notation the following two functions are introduced:

$$\begin{aligned}\Phi_1(z_1) &= dF_1(z_1)/dz_1 \\ \Phi_2(z_2) &= dF_2(z_2)/dz_2\end{aligned} \tag{26}$$

The stress and displacement components, written in terms of these new functions, are given by

$$\begin{aligned}\sigma_x &= 2Re[\mu_1^2\,\Phi_1'(z_1) + \mu_2^2\,\Phi_2'(z_2)] \\ \sigma_y &= 2Re[\Phi_1'(z_1) + \Phi_2'(z_2)] \\ \tau_{xy} &= -2Re[\mu_1\,\Phi_1'(z_1) + \mu_2\,\Phi_2'(z_2)]\end{aligned} \tag{27}$$

$$\begin{aligned}u &= 2Re[p_1\,\Phi_1(z_1) + p_2\,\Phi_2(z_2)] \\ v &= 2Re[q_1\,\Phi_1(z_1) + q_2\,\Phi_2(z_2)]\end{aligned} \tag{28}$$

where

$$
\begin{aligned}
p_1 &= \beta_{11}\,\mu_1^2 + \beta_{12}-\beta_{16}\,\mu_1 \\
p_2 &= \beta_{11}\,\mu_2^2 + \beta_{12}-\beta_{16}\,\mu_2 \\
q_1 &= \beta_{12}\,\mu_1 + \beta_{22}/\mu_1-\beta_{26} \\
q_2 &= \beta_{12}\,\mu_2 + \beta_{22}/\mu_2-\beta_{26}
\end{aligned}
\tag{29}
$$

Rigid body displacements have been omitted from (28).

A mapping function is used to map the characteristic coordinates z_k into a transformed coordinate system ζ_k, where k = 1,2 as before. The mapping function is constructed such that the physical internal circular boundary of radius "a" is mapped onto a unit circle in the ζ_k plane. This reduces the dimensionality of the problem by one and allows us to expand the boundary conditions along the unit circle using a complex Fourier series in terms of the single variable, θ. The mapping function is given by

$$
\zeta_k = \frac{z_k \pm \sqrt{z^2 - a^2 - \mu_k^2 a^2}}{a(1-i\mu_k)} \tag{30}
$$

For a given value of z_k two values of ζ_k result. One value maps the point z_k to a point ζ_k which is inside the unit circle; the other maps z_k to a point outside the unit circle. The latter mapping is the one of interest and represents the criterion for selecting the correct sign in (30).

By requiring that all the stress components be real and single valued for a problem containing a single loaded circular cavity with

stress free boundaries at infinity, it can be shown that Φ_k should have the following general form:

$$\Phi_k(\zeta_k) = A_k \ln \zeta_k + \sum_{m=1}^{\infty} A_{km} \zeta_k^{-m} \qquad , \quad k = 1, 2 \tag{31}$$

Since

$$\Phi_k'(z_k) = \frac{d\,\Phi(z_k)}{d\,z_k} = \frac{d\Phi(\zeta_k)}{d\,\zeta_k} \frac{d\,\zeta_k}{d\,z_k} \tag{32}$$

it follows that

$$\Phi_k'(z_k) = \frac{A_k - \sum_{m=1}^{\infty} m\, A_{km}\, \zeta_k^{-m}}{\sqrt{z_k^2 - a^2 - a^2\,\mu_k^2}} \tag{33}$$

By further requiring that the displacements be single-valued it can be shown that equations (34) must be satisfied.

$$\begin{aligned}
A_1 - \bar{A}_1 + A_2 - \bar{A}_2 &= P_{yi}/2\pi i \\
\mu_1 A_1 - \bar{\mu}_1 \bar{A}_1 + \mu_2 A_2 - \bar{\mu}_2 \bar{A}_2 &= -P_{xi}/2\pi i \\
\mu_1^2 A_1 - \bar{\mu}_1^2 \bar{A}_1 + \mu_2^2 A_2 - \bar{\mu}_2^2 \bar{A}_2 &= \frac{-\beta_{12} P_{yi}}{2\pi i \beta_{11}} - \frac{\beta_{16} P_{xi}}{2\pi i \beta_{11}} \\
\frac{A_1}{\mu_1} - \frac{\bar{A}_1}{\bar{\mu}_1} + \frac{A_2}{\mu_2} - \frac{\bar{A}_2}{\bar{\mu}_2} &= \frac{\beta_{12} P_{xi}}{2\pi i \beta_{22}} + \frac{\beta_{26} P_{yi}}{2\pi i \beta_{22}}
\end{aligned} \tag{34}$$

The terms P_{xi} and P_{yi} represent the net load resultants (per unit thickness) applied to the i^{th} internal circular boundary in the x and y directions respectively. The values of P_{xi} and P_{yi} are derivable

from the boundary conditions. Equations (34) represent four equations in terms of four unknowns, the real and imaginary parts of A_1 and A_2. Thus the values of A_1 and A_2 can be determined once the boundary conditions are specified. Note that if the net loads on the internal circular boundary are both zero, then $A_1 = A_2 \equiv 0$.

The coefficients A_{km} are also derivable from the boundary conditions. Assume that a complete description of the stress boundary conditions are given for the internal circular boundary (i.e., $\sigma_r(\sigma)$,* $\sigma_\theta(\sigma)$ and $\tau_{r\theta}(\sigma)$). The boundary tractions $T_r(\sigma)$ and $T_\theta(\sigma)$ written in terms of the known boundary stresses are

$$\begin{aligned} T_r(\sigma) &= \sigma_r(\sigma)\ n_r + \tau_{r\theta}(\sigma)\ n_\theta \\ T_\theta(\sigma) &= \sigma_\theta(\sigma)\ n_\theta + \tau_{r\theta}(\sigma)\ n_r \end{aligned} \tag{35}$$

By integrating the tractions $T_x(\sigma)$ and $T_y(\sigma)$ around the circular boundary and utilizing equations (27) and (33) it can be shown that

$$\begin{aligned} i\int (T_x(\sigma) + i\ T_y(\sigma))\ dS &= i\int (T_r(\sigma) + i\ T_\theta(\sigma))\ e^{i\theta} dS = \\ -i(P_{xi}+i\ P_{yi})\theta/2\pi &+ \sum_{m=1}^{\infty} \Big\{[(1+i\mu_1)A_{1m}+(1+i\mu_2)A_{2m}]e^{-im\theta} \\ &+ [(1+i\bar{\mu}_1)\bar{A}_{1m}+(1+i\bar{\mu}_2)\bar{A}_{2m}]e^{\ im\theta}\Big\} \end{aligned} \tag{36}$$

Now consider expanding the boundary tractions on the unit circle in a general complex Fourier series of the form

$$T_r(\sigma) + i\ T_\theta(\sigma) = \sum_{n=-\infty}^{\infty} C_n\ e^{in\theta} \tag{37}$$

*A point on the boundary of the circular hole of radius "a" is denoted by $\sigma = a\ e^{\ i\theta}$.

The coefficients C_n can be evaluated by multiplying both sides of (37) by $e^{-im\theta}$ and integrating with respect to θ from 0 to 2π.

$$\int_0^{2\pi} [T_r(\sigma)+i\ T_\theta(\sigma)]e^{-im\theta}d\theta = \sum_{n=-\infty}^{\infty} C_n \int_0^{2\pi} e^{-i(m-n)\theta}\ d\theta \tag{38}$$

Since

$$\int_0^{2\pi} e^{-i(m-n)\theta}\ d\theta = \begin{cases} 0 & \text{for } m \neq n \\ 2\pi & \text{for } m = n \end{cases} \tag{39}$$

it follows that

$$C_m = \frac{1}{2\pi}\int_0^{2\pi} [T_r(\sigma)+i\ T_\theta(\sigma)]\ e^{-im\theta}\ d\theta \tag{40}$$

Substituting (37), the known Fourier series representation for the boundary tractions, into (36) and equating the series coefficients, the solution of the unknown A_{km} coefficients is obtained. At this point the known coefficients A_k and A_{km} can be substituted into (31) and (33) and the expressions for Φ_k and Φ_k' substituted back into (27) and (28). Stresses and displacements at any point (x,y) can then be determined by evaluating the appropriate series representation.

3.2.2 Solution to the Loaded Hole Problem

In order to perform a stress analysis for the problem of a bolt loaded circular hole in an anisotropic plate the boundary conditions must first be specified. Consider first the interaction between the bolt and the circular cut-out. Work by this investigator [3], which is

discussed in Appendix A, has shown that a distribution of normal stress varying as the cosine of theta over the front half of the hole can be used to adequately represent the interaction of a snugly fitting pin in an anisotropic plate (See Figure 10). It is assumed in this analysis that the interaction is frictionless. Thus the stress boundary conditions on the circular boundary are

$$\begin{aligned} &\sigma_r(\sigma) = -p\cos\theta\ , \quad \tau_{r\theta}(\sigma) = 0 \quad \text{for } -\pi/2 \le \theta \le \pi/2 \\ &\sigma_r(\sigma) = 0\ , \quad \tau_{r\theta}(\sigma) = 0 \quad \text{for } \pi/2 \le \theta \le 3\pi/2 \end{aligned} \tag{41}$$

Next consider the loading at infinity which is required to satisfy equilibrium. A finite force resultant, F_x, equal in magnitude and opposite in direction to the net applied bolt load in the x direction, must be applied at $x = -\infty$. Applying a finite force to an infinite boundary results in a uniform stress resultant of zero magnitude. Thus, all the boundaries at infinity are stress free and the equations from section 3.2.1 can be used directly.

The boundary conditions represented by (41) can be substituted into (35) to determine the boundary tractions

$$\begin{aligned} &T_r(\sigma) = p\cos\theta\ , \quad T_\theta(\sigma) = 0 \quad \text{for } -\pi/2 \le \theta \le \pi/2 \\ &T_r(\sigma) = 0\ , \quad T_\theta(\sigma) = 0 \quad \text{for } \pi/2 \le \theta \le 3\pi/2 \end{aligned} \tag{42}$$

Since $T_r(\sigma)$ is not a continuous function of theta the integral in (40) must be broken into two parts.

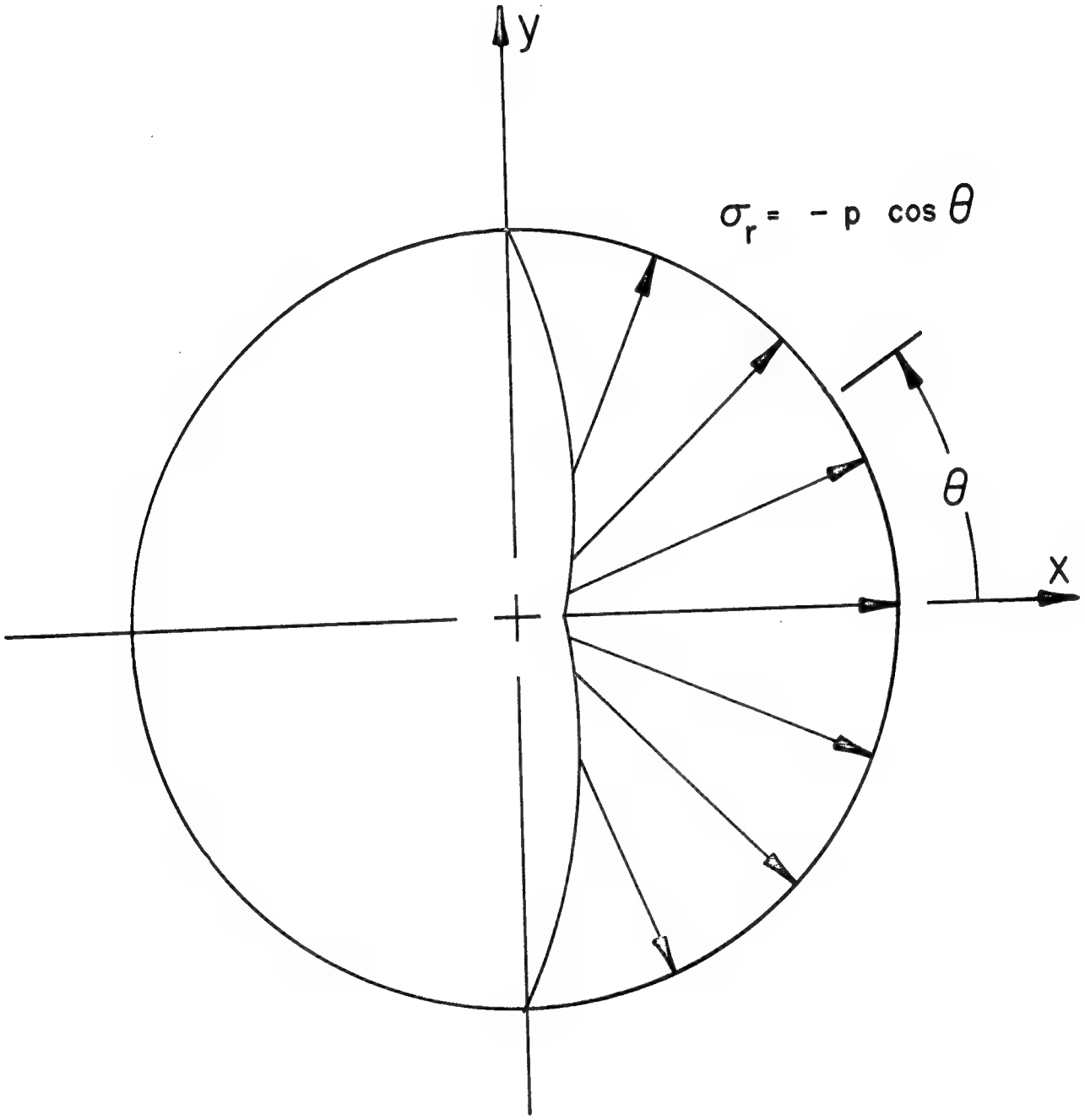

Figure 10. Cosine Distribution of Normal Stress

$$2\pi C_m = \int_{-\pi/2}^{\pi/2} p \cos\theta \; e^{-im\theta} \, d\theta + \int_{\pi/2}^{3\pi/2} 0 \cdot e^{-im\theta} \, d\theta \tag{43}$$

Substituting ($\cos m\theta - i \sin m\theta$) for $e^{-im\theta}$ and integrating the values of C_m can be determined.

$$\begin{aligned} C_1 &= C_{-1} = p/4 \\ C_m &= 0 \qquad\qquad \text{for } m = \pm 3, \pm 5, \pm 7, \ldots \\ C_m &= -p(-1)^{m/2}/\pi(m^2-1) \quad \text{for } m = 0, \pm 2, \pm 4, \ldots \end{aligned} \tag{44}$$

Now that the values of the constants C_m are known we can combine (36) and (37) which results in

$$\begin{aligned} i\int \left(\sum_{m=-\infty}^{\infty} C_m e^{im\theta} \right) e^{i\theta} \, dS \;\; &= \;\; -i(P_x + i P_y)\, \theta/2\pi \\ + \;\; \sum_{m=1}^{\infty} \Big\{ &[(1+i\mu_1)A_{1m} + (1+i\mu_2)A_{2m}] \, e^{-im\theta} \\ + \;\; &[(1+i\bar{\mu}_1)\bar{A}_{1m} + (1+i\bar{\mu}_2)\bar{A}_{2m}] \, e^{im\theta} \Big\} \end{aligned} \tag{45}$$

All integrations along boundaries, by convention, are performed such that the material is always to the left, which means

$$dS = -a \, d\theta \tag{46}$$

By substituting (46) into (45), performing the required integration and equating coefficients of $e^{im\theta}$, $e^{-im\theta}$ and θ, the unknown constants

A_{1n} and A_{2n} can be determined. The resulting expressions are:

$$
\begin{aligned}
A_{12} &= a\ p\ i\ (1+i\mu_2) \,/\, [16(\mu_2-\mu_1)] \\
A_{22} &= -a\ p\ i\ (1+i\mu_1) \,/\, [16(\mu_2-\mu_1)] \\
A_{1n} &= A_{2n} = 0 \qquad\qquad n=4,6,8\ldots \\
A_{1n} &= -a\ p\ i\ (-1)^{(n-1)/2}(2+i\ n\mu_2) \,/\, [\pi n^2(n^2-4)(\mu_2-\mu_1)] \qquad n=1,3,5\ldots \\
A_{2n} &= a\ p\ i\ (-1)^{(n-1)/2}(2+i\ n\mu_1) \,/\, [\pi n^2(n^2-4)(\mu_2-\mu_1)]
\end{aligned}
\tag{47}
$$

The series solution for the stresses throughout the laminate has thus been obtained. Prior to programming these results they were simplified by restricting the analysis to points along the circular boundary since this is where the joint failure criterion is applied. This simplification resulted in less complex expressions for the boundary stresses and reduced computer run time.

As a check on the theoretical development the expressions for the stress boundary solution were reduced to the case of an isotropic material (i.e., $\mu_1 = \mu_2 = i$), since the complete boundary solution to this problem is available. The values of $\sigma_r(\sigma)$ and $\tau_{r\theta}(\sigma)$ are known from the boundary conditions, equations (41). The values of $\sigma_\theta(\sigma)$ have been reported by Bickley [12]. In [12] the problem of a bolt loaded hole in an infinite isotropic plate was solved analytically using the same bolt load representation used herein: A cosine distribution of normal stress acting over the front half of a frictionless circular cut-out.

Only two locations were selected for comparison to the isotropic results; $\theta=0°$ and $90°$. At these two locations the solution for the boundary tractions $\sigma_r(\sigma)$ and $\tau_{r\theta}(\sigma)$ reduce to

$$\sigma_r(\sigma)\big|_{\theta=0} = -p$$

$$\sigma_r(\sigma)\big|_{\theta=90} = \tau_{r\theta}(\sigma)\big|_{\theta=0} = \tau_{r\theta}(\sigma)\big|_{\theta=90} = 0 \tag{48}$$

which agrees with the imposed boundary conditions, equations (41).

An intermediate step in a similar reduction of the hoop stresses is also of interest. For an anisotropic material

$$\sigma_\theta(\sigma)\big|_{\theta=0} = \frac{\beta_{12}}{\beta_{22}}\frac{p}{4} + \frac{p}{4}\,Re\left[\frac{1 + i(\mu_1+\mu_2)}{\mu_1\mu_2}\right] + \frac{2p}{\pi}\,Re\left[\sum_{n=1,3,5,\ldots}\frac{-(-1)^{(n-1)/2}}{n(n^2-4)}\,\frac{2 + in(\mu_1+\mu_2)}{\mu_1\mu_2}\right] \tag{49}$$

$$\sigma_\theta(\sigma)\big|_{\theta=90} = \frac{\beta_{16}}{\beta_{11}}\frac{p}{4} - \frac{p}{4}\,Re\,[\mu_1+\mu_2+i\mu_1\mu_2] + \frac{2p}{\pi}\,Re\left[\sum_{n=1,3,5,\ldots}\frac{i(2\mu_1+2\mu_2+in\mu_1\mu_2)}{n(n-2)(n+2)}\right] \tag{50}$$

The criterion used to define convergence of the series stress analysis in (49) and (50) is very simple. The last term added to the accumulated sum can be no larger than some specified percentage, γ, of the accumulated sum. The number of terms required to satisfy this criterion is, obviously, a function of γ but results show that the number does not change significantly from laminate to laminate for a given value of γ. For example for γ equal to 1.0% the number of terms required is typically ten; for γ equal to 0.1% nearly fifty terms are required. Since the majority of run time for a stress analysis is spent evaluating these series, it is desirable to evaluate the fewest number of terms possible. Methods for performing efficient stress analyses, based on careful selection of values for γ, are discussed in section 4.6.

The hoop stress at both θ=0° and 90° is seen to be material dependent for anisotropic materials. These expressions, reduced to the case of an isotropic material, become

$$\sigma_\theta(\sigma)\Big|_{\theta=0} = p[(1-\nu)/4 + 0.1367] \tag{51}$$

$$\sigma_\theta(\sigma)\Big|_{\theta=90} = 2p/\pi \tag{52}$$

Note that the hoop stress is material dependent ahead of the bolt but not at θ=90°. In fact, the value of $\sigma_\theta(\sigma)$ is material dependent at every location on the circular boundary except at θ=90°. Since $\sigma_\theta(\sigma)\Big|_{\theta=90}$ is independent of material properties for

isotropic materials, it is possible to represent the effect of finite specimen size on $\sigma_\theta(\sigma)|_{\theta=90}$ by a single set of curves for all isotropic materials. In Peterson [13] a single curve is presented which represents the dependence of $\sigma_\theta(\sigma)|_{\theta=90}$ for an edge distance to hole diameter ratio of approximately 2.5. The infinite series which resulted from equations (49) and (50) for these isotropic calculations ($\mu_1 = \mu_2 = i$) were evaluated using the computer since closed form equivalent expressions could not be found.

The stress concentration factor induced by a bolt loading in an infinite plate is herein defined as K_{tb}^{∞}, where

$$K_{tb}^{\infty} = \sigma_\theta(\sigma)/\sigma_{Bi} \tag{53}$$

and

$$\sigma_{Bi} = P_{xi}/(2at) \tag{54}$$

Furthermore, it is easily verified from equilibrium considerations that

$$P_{xi} = \frac{\pi a t}{2} p \tag{55}$$

Therefore, for an isotropic material

$$K_{tb}^{\infty}|_{\theta=0} = (1.5468-\nu)/\pi \tag{56}$$

$$K_{tb}^{\infty}|_{\theta=90} = 8/\pi^2 \doteq 0.81 \tag{57}$$

which agrees exactly with the results presented in [12]. These same numerical results were used as check cases for verifying the subroutine developed to perform stress analyses along bolt loaded circular boundaries in infinite plates.

3.2.3 Solution to the Open Hole Problem

The problem of an infinite anisotropic plate with an internal circular cut-out subject to a unidirectional tension loading in the x direction has been solved and is presented in [6]. The hoop stress solution, referring to Figure 9, is given by

$$\sigma_\theta(\sigma) = \sigma_{Si} E_\theta \beta_{11} [\mu_1\mu_2 \cos^2\theta + (1-i(\mu_1+\mu_2))\sin^2\theta] \tag{58}$$

where

$$1/E_\theta = \beta_{11}\sin^4\theta + (\beta_{66}+2\beta_{12})\sin^2\theta\cos^2\theta + \beta_{22}\cos^4\theta \tag{59}$$

Since the cut-out is stress free

$$\sigma_r(\sigma) = \tau_{r\theta}(\sigma) \equiv 0 \tag{60}$$

Evaluating $\sigma_\theta(\sigma)$ at θ=0° and 90° results in

$$\sigma_\theta(\sigma)\big|_{\theta=0} = \sigma_{Si}\ \mu_1\mu_2\beta_{11}/\beta_{22} \tag{61}$$

$$\sigma_\theta(\sigma)\big|_{\theta=90} = \sigma_{Si}\ (1-i(\mu_1+\mu_2)) \tag{62}$$

For an isotropic material $\beta_{11} = \beta_{22}$ and $\mu_1 = \mu_2 = i$. Therefore

$$\sigma_\theta(\sigma)\big|_{\theta=0} = -\sigma_{Si} \tag{63}$$

$$\sigma_\theta(\sigma)\big|_{\theta=90} = 3\sigma_{Si} \tag{64}$$

Representing the stress concentration factor induced by a tension

loading on an infinite plate containing a circular cut-out by K_{ts}^{∞}, where

$$K_{ts}^{\infty} = \sigma_{\theta}(\sigma)/\sigma_{Si} \tag{65}$$

it follows that

$$K_{ts}^{\infty}\big|_{\theta=0} = -1.0 \tag{66}$$

$$K_{ts}^{\infty}\big|_{\theta=90} = 3.0 \tag{67}$$

These results agree, of course, with results reported in the literature [14]. They were also used in verifying the tensile stress analysis subroutine.

3.2.4 Laminate Infinite Plate Results

The general anisotropic equations for the boundary stresses induced by both bolt and tension loadings in infinite plates have been programmed and results for the seven [0/±45] boron-epoxy laminates listed in Table 3 have been generated. In Figure 11 K_{tb}^{∞} has been plotted as a function of the percentage of 0° plies at the three different boundary locations of interest; θ=0°, 45° and 90°. Figure 12 represents a similar plot for K_{ts}^{∞}. In each figure three additional solid data points are plotted on the vertical axis. They represent corresponding stress concentration factors for isotropic materials having a Poisson's ratio of 0.3.

Table 3. Seven [0/±45] Boron-Epoxy Laminates of Interest

Laminate	% 0° Plies	% ±45° Plies
(±45)	0.0	100.0
$(0_2/\pm 45_5)$	16.6	83.4
(0/±45)	33.3	66.7
$(0_2/\pm 45)$	50.0	50.0
$(0_4/\pm 45)$	66.7	33.3
$(0_{10}/\pm 45)$	83.4	16.6
(0)	100.0	0.0

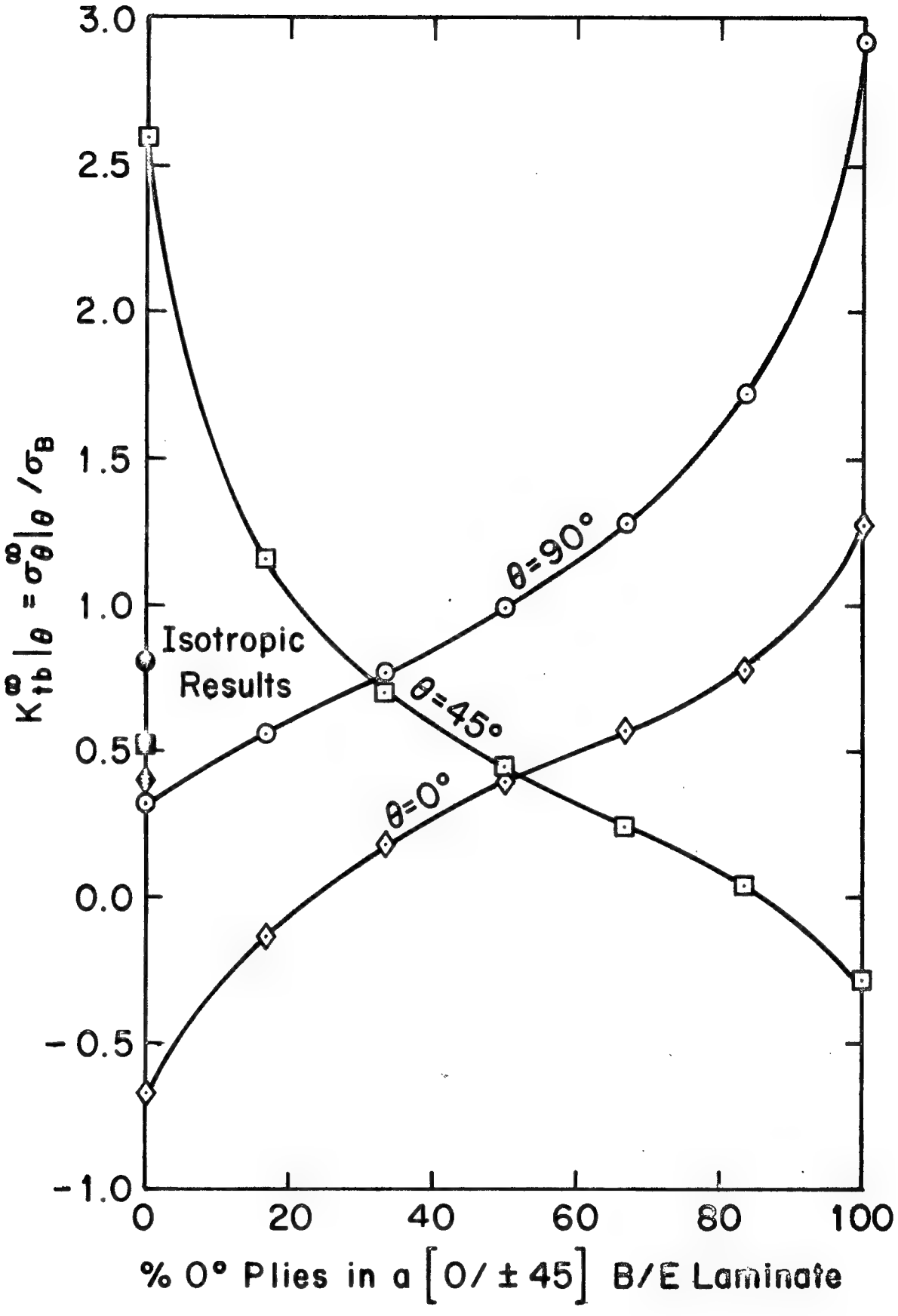

Figure 11. Infinite Plate Stress Concentration Factors, K^{∞}_{tb}, for a Loaded Hole in [0/±45] Boron-Epoxy Laminates

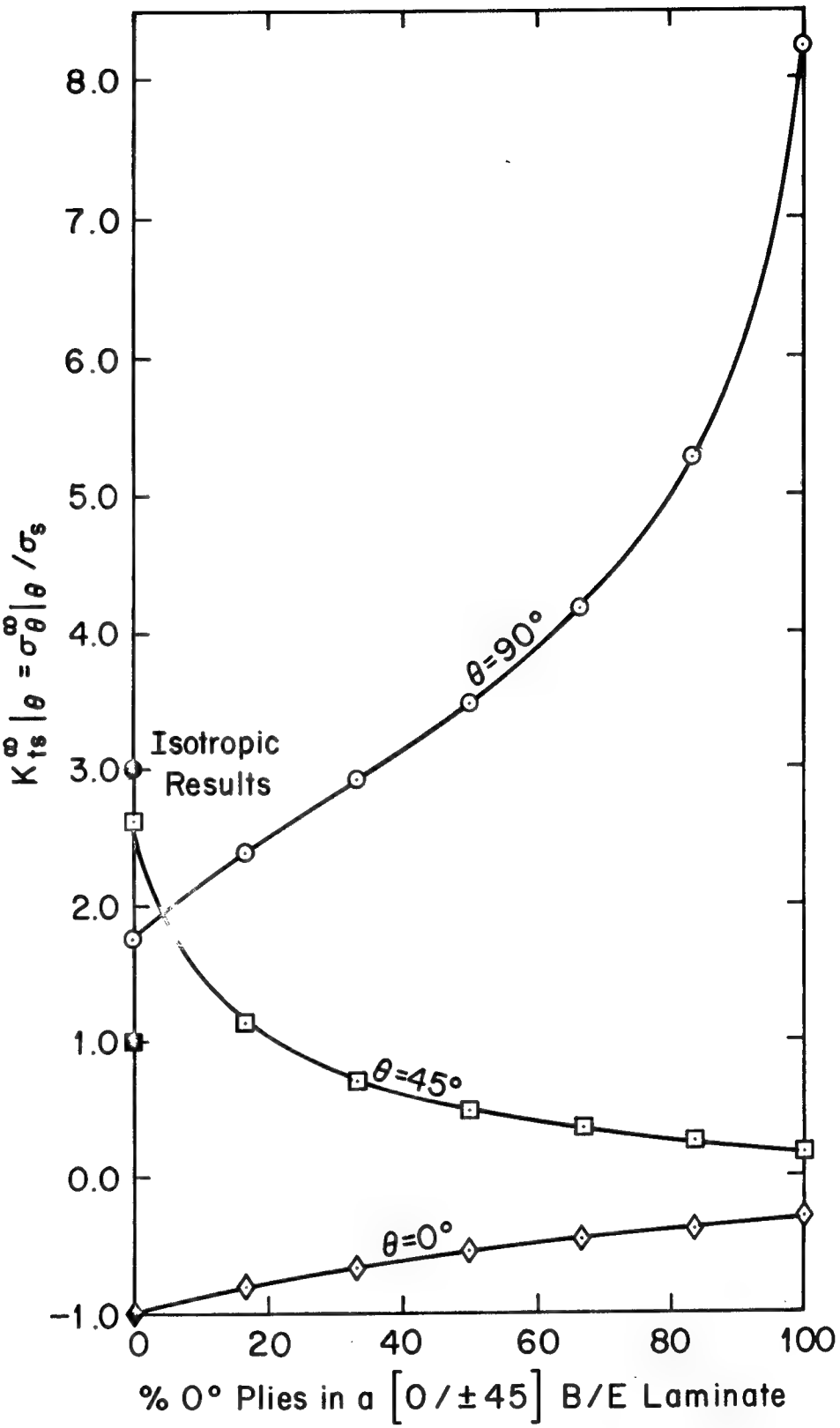

Figure 12. Infinite Plate Stress Concentration Factors, K_{ts}^{∞}, for an Open Hole in [0/±45] Boron-Epoxy Laminates

Several interesting observations can be made from this data. The magnitude of a stress concentration induced in anisotropic materials can be much larger than that observed in isotropic materials. For example, the stress concentration factor for a bolt loaded hole at $\theta=90°$ in a (0) laminate is nearly four times greater than that in isotropic materials; in a tension loaded hole the ratio is nearly three. Thus, much of the composite material's specific strength advantage over metals is lost in the joint due to these large stress concentrations and the brittle nature of the material. It is also interesting to note that the stress field for a laminate made up of about 40% 0° plies is nearly the same as that for an isotropic material for both the bolt loaded hole and the tension loaded hole.

A further significant result is that the hoop stress at both $\theta=0°$ and 45° goes through a stress reversal for the bolt loaded hole results (but not for the tension loaded hole results) as the percentage of 0° plies is varied. This phenomenon is important since it could affect the mechanism which governs failure at each bolt location. Tensile hoop stresses ahead of the bolt can induce matrix splitting failures in the 0° plies whereas a compressive hoop stress inhibits such failures. Matrix splitting in the 0° plies can also lead to premature bearing failures. Therefore, it is expected that laminates which exhibit compressive hoop stresses or relatively small tensile hoop stresses will be preferred over those which exhibit large tensile hoop stresses in the design of minimum weight bolted joints.

3.3 Anisotropic Correction Curves

3.3.1 Introduction

It was decided early in this investigation that the [0/±α/90] family of laminates was to be used for the main plate construction. Due to computer budget limitations, however, it was apparent that it would not be possible to generate boundary correction data for this entire family of laminates. It was decided, therefore, to generate correction data for the popular [0/±45] family of laminates. The plan here was to reduce the data in such a way that it would be possible to predict the stress concentration factors for any anisotropic finite size coupon from known isotropic infinite plate results. It was felt that a material dependent correction factor and a geometric correction factor of the form

$$K_t(\text{laminate})\big|_\theta = f(\text{material}) \times g(\text{geometry}) \times K_t^{\infty}(\text{isotropic})\big|_\theta \qquad (68)$$

could be developed using the [0/±45] data. Such a relationship would greatly simplify the procedures required to correct the infinite plate stress analyses for the effects of finite size and adjacent fasteners in the synthesis. All attempts at fitting the data using equation (68) were unsuccessful, however. As a result it was decided that an interpolation method based on a limited amount of data for the [0/±45] family of laminates would be used in the synthesis procedure.

The computer budget limitations in conjunction with the need to use an interpolation method for correcting the infinite plate stress analyses forced the narrowing of the laminate families which could be considered. Rather than just consider the [0/±45] family of laminates the assumption was made that the available data was applicable to a limited range of the [0/±α/90] family. It was assumed that the data was valid as long as α did not differ from 45° by more than 15° and the percentage of 90° plies present did not exceed 25%. In using the data it was assumed that both laminate families could be categorized on the basis of the percentage of 0° plies present. For example, the correction factors used for a (0/±45/90) quasi-isotropic laminate were those corresponding to a $(0_2/\pm 45_3)$ laminate since both laminates consist of 25% 0° plies.

To perform a strength analysis on a [0/±α/90] laminate the stresses must be calculated at four points along the circular boundary; θ=0°, α, 90°-α and 90°. These four locations represent the only points of possible failure initiation. Due to the limited amount of numerical correction factor data available, the correction factor data derived for θ =45° in the [0/±45] laminates is applied at both θ=α and θ=90°-α in the various [0/±α/90] laminates analyzed. This should result in fairly accurate corrections to the various hoop stresses at these two locations since α has been restricted to the

range $30° \leq \alpha \leq 60°$. It is also worthwhile noting that the failure predictions at $\theta=45°$ were always much more conservative than at $\theta=90°$ in the two analytical studies discussed earlier.

Although the above restrictions appear to be very limiting, they are not. Results of the syntheses discussed in chapter V show that of all the possible laminates which satisfy the above restrictions, the [0/±45] family is preferred. This tends to satisfy one's intuition that an angle-ply of 45° for a rather arbitrary combination of biaxial states of stress is probably the most efficient possible. Thus, through hindsight, the apparent restrictive assumptions did not penalize the results but in fact saved significant amounts of computer run time.

All of the correction data which is presented below was generated for boron-epoxy laminates. It was not necessary to run a separate set of results for graphite-epoxy since the stress concentration factors for both material systems, when normalized on their respective infinite plate values, agree, to within just a few percent, over almost the entire range of laminates analyzed. The only exceptions occur for laminates which are composed of nearly 100% 0° plies or 100% ±45° plies. This presents no real problem since restrictions imposed above exclude these two cases from consideration in the synthesis.

A description of how the correction data is used in the synthesis

and a description of the numerical method used to generate the data is presented in the next two sections followed by a detailed discussion of the resulting numerical data. All of the data which is used in the synthesis procedure is presented in the following sections in either tabular or graphical form.

3.3.2 Finite Geometry Problems Considered

As mentioned above three different sets of correction factors are used to account for the effects of finite size and adjacent fasteners. The various correction factors are derived by comparing numerical results for a variety of finite size coupons to their respective infinite plate results. The required infinite plate data was generated in section 3.2.4 using the anisotropic infinite plate series solutions developed in section 3.2. The assumption is made that the various corrections can be applied independently.

The required finite size correction factors have been developed using the boundary integral equation (BIE) method [8] for the entire [0/±45] boron-epoxy family of laminates. In generating the finite size correction factors for both the loaded hole and unloaded hole, a total of thirty different coupon geometries was analyzed for each of the seven laminates. Thirty different geometries were required since five E/D values and six S/D values were selected for study. The values selected covered the range $2.0 \leq E/D \leq 10.0$ and $2.0 \leq S/D \leq 20.0$ as shown in Table 4. This broad range of values was selected to insure

Table 4. Various Finite Size Fastener Geometries Considered

S/D / E/D	2.0	2.5	3.33	5.0	10.0	20.0
2.0	X	X	X	X	X	X
2.5	X	X	X	X	X	X
3.33	X	X	X	X	X	X
5.0	X	X	X	X	X	X
10.0	X	X	X	X	X	X

that problems would not arise in the synthesis for which interpolation could not be used. When correcting the open hole results for the effects of adjacent cut-outs the only important parameter is the ratio of hole separation distance to bolt diameter, E/D. As a result it was only necessary to run five problems per laminate to generate this correction data. The range of E/D values was the same as before. In all cases the various stress concentration factors were generated for the hoop stresses at $\theta = 0°$, 45° and 90°. Corrections are obviously never made to $\sigma_r(\sigma)$ or $\tau_{r\theta}(\sigma)$ since they are applied boundary conditions.

The following notation is used to describe these various correction factors. The symbol $\lambda_{b|\theta}$ denotes the finite size correction factor for a bolt loaded hole. That is, for a given laminate and bolt load the hoop stress at a position θ on the circular boundary of the finite plate is given by

$$\sigma_{\theta b}(\sigma)_{|\theta} = \lambda_{b|\theta} \quad \sigma^{\infty}_{\theta b}(\sigma)_{|\theta} \tag{69}$$

where $\sigma^{\infty}_{\theta b}(\sigma)_{|\theta}$ is the value of the infinite plate hoop stress at that same location, θ. The value of $\lambda_{b|\theta}$ is a function of specimen geometry, defined by the ratios E/D and S/D, and of lamination, defined herein by the percentage of 0° plies present in the laminate, P_z. Equation (69) can be rewritten in terms of the stress concentration at θ, $K_{tb|\theta}$, by dividing both sides of (69) by σ_B

$$K_{tb|\theta} = \lambda_{b|\theta} \; K^{\infty}_{tb|\theta} \tag{70}$$

The remainder of the results are presented in terms of stress concentrations rather than stresses. In a similar manner $\lambda_{s|\theta}$ denotes the finite size correction for the case of a uniform skin loading.

The final correction factor involves correcting the open hole stress concentrations for the effects of adjacent fasteners. In both the infinite plate stress analyses and the development of the correction curves for the effects of finite specimen size, the skin load was modeled as a uniform stress. In the actual problem, however, the material surrounding a given bolt does not see a uniform skin stress in the vicinity of the preceding cut-out unless the holes are separated by a sufficient distance. Compare the actual stress distribution at the leading edge of the imaginary coupon, Figure 13a, with the uniform stress distribution imposed at that boundary in the BIE analysis, Figure 13b. The amount of load which must flow around the cut-out in Figure 13b is significantly greater than that in Figure 13a. Thus the finite size correction factors are too large and as a result conservative. A series of problems involving three equally spaced collinear holes in an infinite anisotropic plate subjected to a tension field are solved using the BIE method. The two outer holes are used to create the desired incoming stress field on the inner cut-out. This final correction factor, $\lambda_{h|\theta}$, is used to correct for this geometric condition.

Consider the procedures involved in correcting the infinite plate

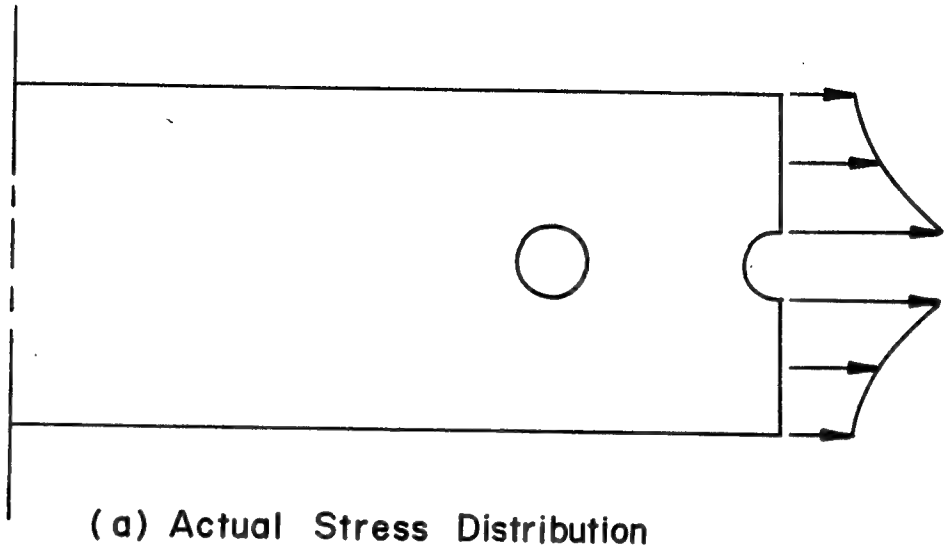

(a) Actual Stress Distribution

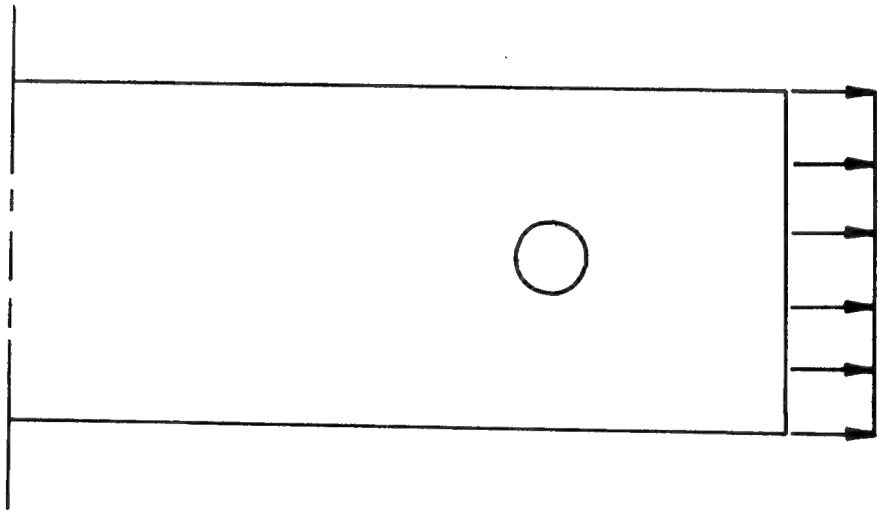

(b) Finite Element Stress Distribution

Figure 13. Skin Stress Boundary Conditions at the Leading Edge of a Finite Size, Single Fastener Coupon

stress analysis of a single coupon during the synthesis. Values for E/D, S/D and P_z are known from the modeling procedure results. Estimates for $\lambda_{b|\theta}$, $\lambda_{s|\theta}$ and $\lambda_{h|\theta}$ are determined from the correction data by interpolation. The hoop stresses on the circular boundary of an infinite plate having the same material properties as the finite plate of interest, are calculated for two separate loading conditions: An applied bolt load, P_B, and then an applied skin load, P_S. These two solutions are individually corrected for the effects of finite size.

To correct for the effects of finite size for the bolt loaded problem the individual infinite plate stress concentrations, $K^{\infty}_{tb|\theta}$, are multiplied by $\lambda_{b|\theta}$ as shown in equation (70). The infinite plate stress analysis for the skin loaded hole is corrected for the effects of finite size in a similar manner. To correct for modeling the skin load as a uniform distribution in deriving $\lambda_{s|\theta}$, $K^{\infty}_{ts|\theta}$ must also be multiplied by the correction factor $\lambda_{h|\theta}$. Therefore,

$$K_{ts|\theta} = \lambda_{h|\theta}\, \lambda_{s|\theta}\, K^{\infty}_{ts|\theta} \tag{71}$$

The hoop stress due to the combined loading is gotten by a direct superposition of the two solutions

$$K_{t|\theta} = K_{tb|\theta} + K_{ts|\theta}$$

or

$$K_{t|\theta} = \lambda_{b|\theta} K^{\infty}_{tb|\theta} + \lambda_{h|\theta}\, \lambda_{s|\theta}\, K^{\infty}_{ts|\theta} \tag{72}$$

This procedure is followed in each coupon stress analysis throughout the entire synthesis.

3.3.3 Numerical Modeling Procedure

The BIE method was selected over the finite element (FE) method to perform the many numerical analyses required to generate the correction data for several reasons. In the BIE method numerical approximations are made only along the boundaries of a two dimensional problem, not over the entire volume as done in the FE method. Since only the boundary need be discretized run times are decreased significantly, solution accuracy is increased and data preparation is reduced when compared to similar FE solutions.

The BIE method involves the solution of the boundary constraint equation [8] which relates surface displacements to surface tractions. Given a well defined set of boundary data (tractions and/or displacements) the method first solves for the unknown displacements and/or tractions along the boundaries. The boundary stresses can then be determined from the boundary data in a straightforward manner.

A typical grid used to represent a single fastener coupon is shown in Figure 14. Only half of the coupon defined by the modeling procedure (refer back to Figure 5) need be considered since the x axis represents a line of specimen and loading symmetry. In the BIE method lines of symmetry need not be discretized since they are not physical external boundaries. The grid used to model the semi-circle contains 29 segments which are defined by 30 nodes. The grid used to model the outer rectangular boundary contains 30 segments and 31

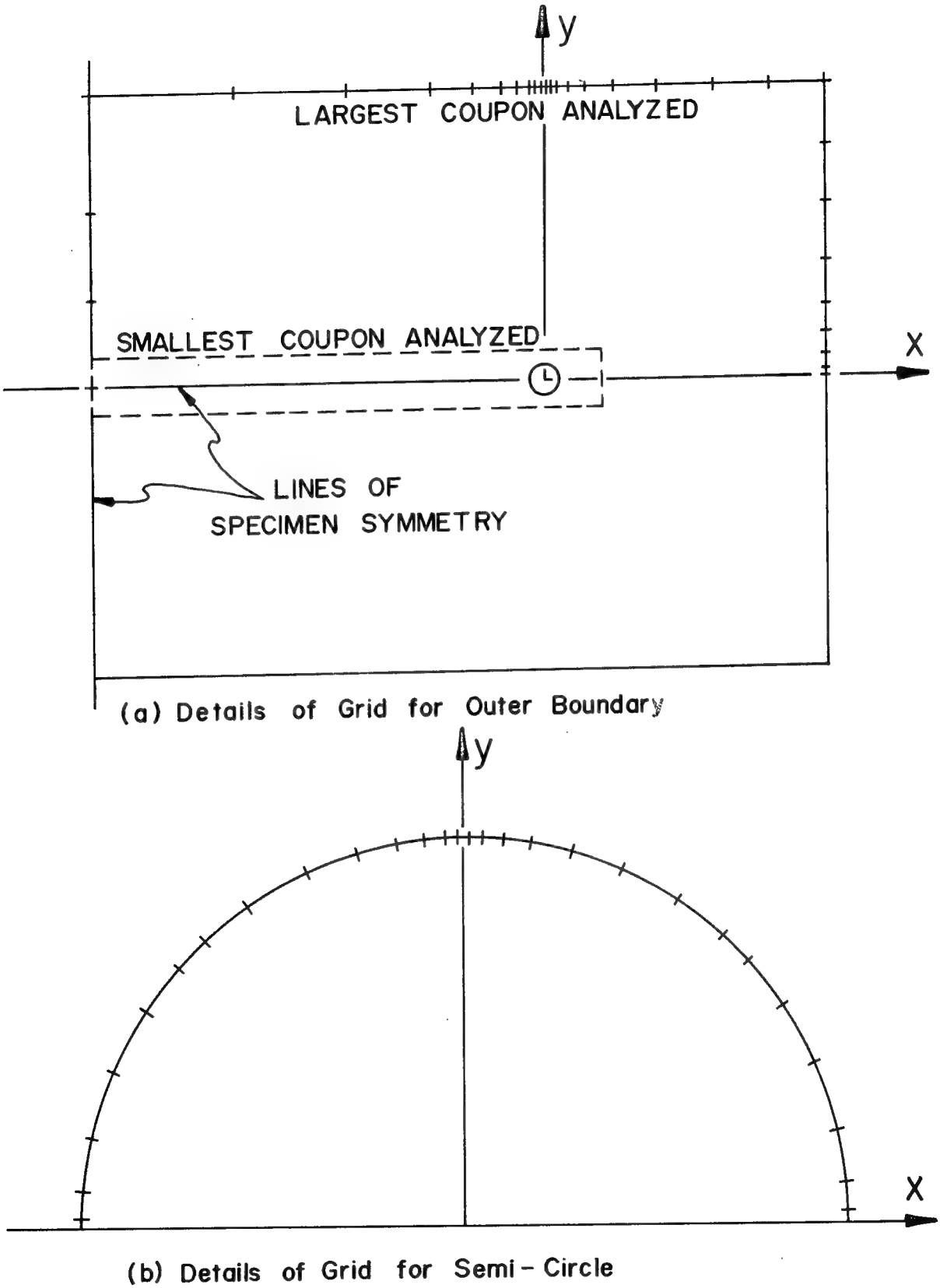

Figure 14. Boundary Grid Used to Model a Finite Size Coupon

nodes. A typical run time for this grid is 20 seconds on a UNIVAC 1108 as compared to approximately 40 seconds for a FE solution of comparable accuracy.

As in the FE method the boundary discretization is refined at points of expected peak stress concentration and at points where boundary solutions are of special interest. The grid used to model the semi-circle is refined at θ=0°, 45° and 90° since these points are of special interest in this stress analysis. The grid used to model the outer rectangular boundary is also refined at θ=0° and 90° for a slightly different reason. It has been shown [8] that numerical errors can be significant within one boundary segment length of a given boundary. To avoid inducing such errors on the semi-circle it is necessary to refine the outer grid at the two points closest to the semi-circle. The grid shown in Figure 14 is automatically scaled to size for specified values of E/D, S/D and HL/D; the number of nodes and segments is fixed, however. The largest and smallest coupons analyzed are drawn to scale in the figure. In the solutions involving three collinear holes subject to a tension field, the grid for the semi-circle is used one and a half times to model only the quarter specimen shown in Figure 15. These solutions are run for infinite plates which, as mentioned, is a capability of the BIE method not available with finite elements. In these runs only the ratio of hole spacing to hole diameter is important since the idea here is to account for the effects of adjacent cut-outs, not finite size.

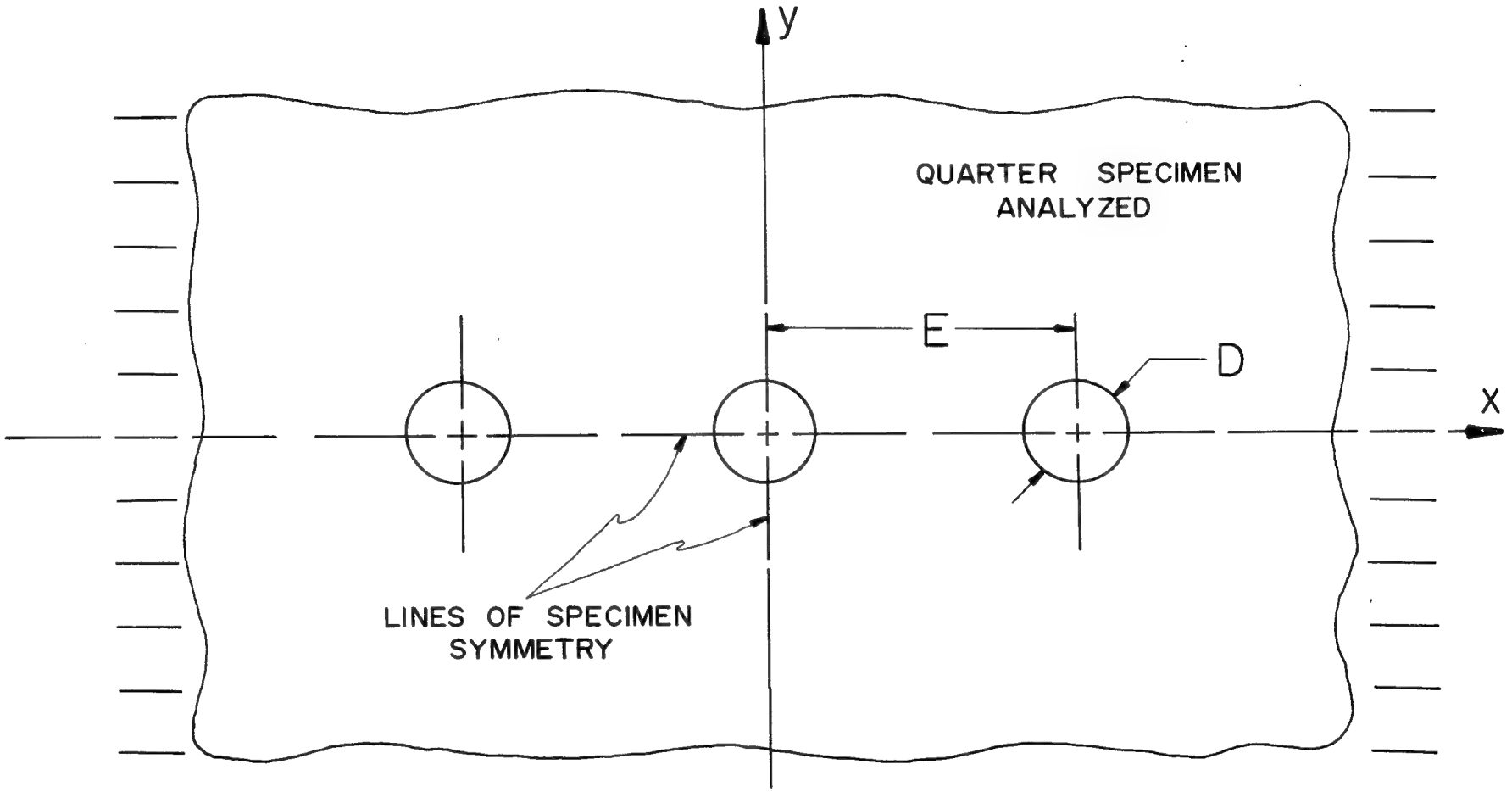

Figure 15. Tension Loading of Three Equally Spaced Collinear Holes in an Infinite Plate

To verify that the grid used for the semi-circle was sufficiently refined the exact solution for an infinite isotropic plate subjected to a tension load was compared to the corresponding BIE solution. In Table 5 a comparison of the exact solution to the BIE results is made. The exact solution results were obtained using the stress analysis program developed in section 3.2.3. The maximum error is seen to be well within the range of acceptability.

3.3.4 Correction Data for a Loaded Hole

The anisotropic single fastener coupons were the first to be analyzed. For each of the coupons the values of $K_{tb|\theta}$ were generated at θ=0°, 45° and 90°. The individual $K_{tb|\theta}$ values were then divided by their respective infinite plate stress concentration values, $K^{\infty}_{tb|\theta}$, which resulted in $\lambda_{b|\theta}$. For example, for an isotropic material

$$K^{\infty}_{tb|\theta=90} = 0.81 \tag{73}$$

and

$$K_{tb|\theta=90} \quad (D/E=0.3,\ D/S=0.3) = 1.45 \tag{74}$$

Therefore

$$\lambda_{b|\theta=90} \quad (D/E=0.3,\ D/S=0.3) = 1.79 \tag{75}$$

A complete set of results for an isotropic material having ν=0.3 is given in Table 6. The results for θ=90° are also plotted in Figure 16 since other data is available in graphical form of θ=90°.

Table 5. Comparison of Approximate Solution and Boundary-Integral Equation Results to Verify the Grid Used to Model the Semi-Circle: Infinite Plate Solution

Position on Circular Boundary, θ	$K^{\infty}_{ts\|\theta}$ for a (0/±45/90) B/E Laminate	
	Numerical Results from Section 3.2.3	BIE Results, 29 Segment Grid
1°	0.39	0.42
10°	0.39	0.40
29°	0.44	0.45
45°	0.51	0.54
61°	0.61	0.61
77°	0.72	0.72
90°	0.81	0.82
135°	0.21	0.22
180°	-0.04	-0.03

Table 6. Loaded Hole Finite Finite Size Correction Factors, $\lambda_{b|\theta}$, for an Isotropic Material (ν=0.3): θ=0°, 45°, 90°

E/D	S/D	$\lambda_{b\|\theta=0}$	$\lambda_{b\|\theta=45}$	$\lambda_{b\|\theta=90}$
2.0	2.0	0.60	1.44	2.85
"	2.5	0.55	1.44	2.25
"	3.33	0.50	1.44	1.89
"	5.0	0.58	1.44	1.69
"	10.0	0.83	1.48	1.54
"	20.0	0.98	1.50	1.50
2.5	2.0	0.68	1.44	2.84
"	2.5	0.68	1.40	2.22
"	3.33	0.68	1.37	1.82
"	5.0	0.68	1.33	1.58
"	10.0	0.85	1.35	1.43
"	20.0	0.98	1.37	1.38
3.33	2.0	0.68	1.44	2.84
"	2.5	0.73	1.40	2.21
"	3.33	0.78	1.33	1.79
"	5.0	0.80	1.27	1.51
"	10.0	0.88	1.23	1.35
"	20.0	0.98	1.25	1.29
5.0	2.0	0.70	1.42	2.83
"	2.5	0.73	1.40	2.21
"	3.33	0.80	1.33	1.78
"	5.0	0.88	1.25	1.47
"	10.0	0.93	1.15	1.26
"	20.0	0.98	1.15	1.21
10.0	2.0	0.70	1.42	2.82
"	2.5	0.73	1.40	2.20
"	3.33	0.80	1.33	1.78
"	5.0	0.90	1.23	1.47
"	10.0	0.98	1.13	1.22
"	20.0	1.00	1.10	1.14
∞	∞	1.00	1.00	1.00
$K^{\infty}_{tb\|\theta}$		0.40	0.52	0.81

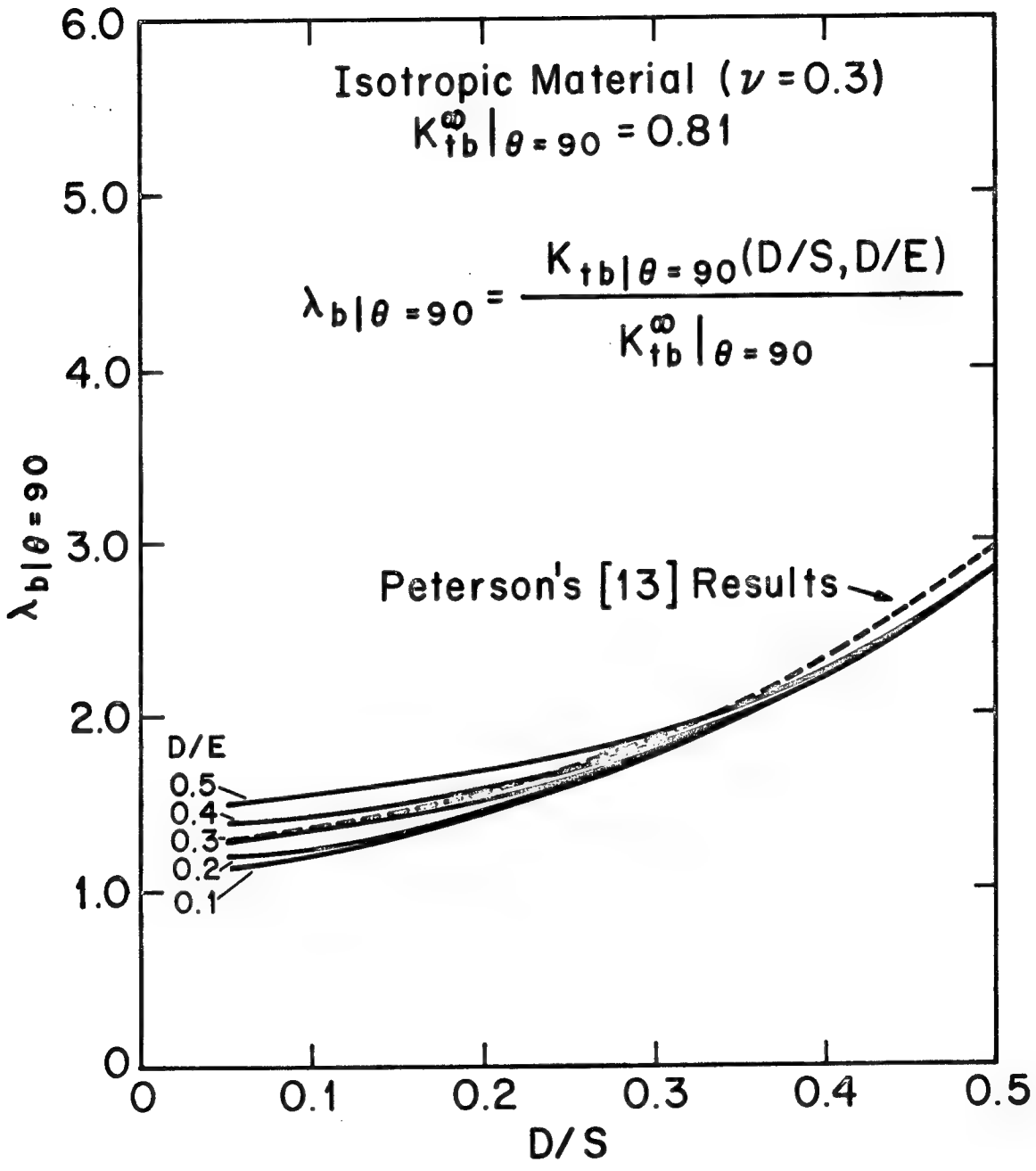

Figure 16. Loaded Hole Finite Size Correction Factors, $\lambda_{b|\theta=90}$, for an Isotropic Material (ν=0.3)

These curves are also of special interest to the designer since $\theta=90°$ is the location of failure initiation of net tension failures, probably the most common failure mode in joints.

The data available for comparison [13] is a combination of theoretical and experimental data for isotropic finite size, single fastener coupons. In Peterson [13] a single curve is drawn which is intended to represent the effect of variations in D/S on the stress concentration at $\theta=90°$. The influence of variations of D/E is not considered in that the data is reported for values of D/E in the neighborhood of 0.4. The data from [13] appears to indicate that the stress concentration factor, $\lambda^{\infty}_{b|\theta=90}$, for an infinitely wide plate, is approximately 1.0. If the curve presented in [13] is drawn for values of D/E in the neighborhood of 0.4, decreasing D/E to zero, as is the case for truly infinite plates, would decrease the induced stress concentration factor $\lambda^{\infty}_{b|\theta=90}$ to a value less than 1.0. A value of 0.81 therefore seems reasonable. Normalizing Peterson's data on an infinite plate stress concentration factor of 0.81 results in the dashed curve shown in Figure 16. The numerical results agree reasonably well with the data presented by Peterson, considering the unknown nature of the D/E values represented by his data.

Similar results are presented in tabular form for $\lambda_{b|\theta=0}$ and $\lambda_{b|\theta=45}$ for the seven boron-epoxy laminates of interest; Tables 7

and 8 respectively. The data for $\lambda_{b|\theta=90}$ is presented in graphical form in Figure 17. In the case of a (0) laminate the effect of variations in specimen width is seen to be much less that it is for some of the angle-ply laminates. The reason for this is that the laminate can only carry load away from the line of specimen symmetry, which is parallel to the direction of applied load, by shear transfer between fibers. In the case of angle-ply laminates the load is transferred away from the line of symmetry by the fibers themselves which act as direct load paths. As a result the effects of specimen width are more significant for angle-ply laminates. In fact in a (±45) coupon the fibers are so efficient at carrying load away from the hole that the maximum stress concentration occurs at a position off of the boundary at $\theta=90°$ where the first continuous fibers which pass the hole intersect. Of all the [0/±45] laminates studied only the (±45) laminate exhibited this behavior.

The common practice of correcting analyses involving composite materials using the isotropic correction data presented in Peterson [13] is seen to be accurate only for certain laminates. The isotropic correction factors for bolt loaded holes in finite plates most resemble those for boron-epoxy laminates composed of between 33% and 50% 0° plies. In most other cases the error involved in using the isotropic results for anisotropic plates is significant. The error is conservative in some cases and nonconservative in others. In an extreme case the

Table 7. Loaded Hole Finite Size Correction Factors, $\lambda_{b|\theta=0}$, for [0/±45] Boron-Epoxy Laminates

E/D	S/D	100% 0	83.4% 0	66.7% 0	50% 0	33.3% 0	16.6% 0	0% 0
2.0	2.0	0.91	0.89	0.86	0.80	0.56	1.54	1.00
"	2.5	0.86	0.84	0.79	0.72	0.39	1.69	1.04
"	3.33	0.83	0.84	0.79	0.69	0.33	1.92	1.12
"	5.0	0.82	0.86	0.84	0.80	0.56	1.54	1.09
"	10.0	0.83	0.89	0.91	0.92	0.89	0.92	0.93
"	20.0	0.83	0.90	0.93	0.98	1.05	0.69	0.87
2.5	2.0	1.00	0.98	0.95	0.90	0.67	1.46	1.00
"	2.5	0.95	0.92	0.90	0.85	0.61	1.54	1.04
"	3.33	0.91	0.90	0.86	0.80	0.50	1.62	1.07
"	5.0	0.88	0.90	0.88	0.82	0.56	1.62	1.12
"	10.0	0.89	0.94	0.95	0.95	0.89	1.08	1.00
"	20.0	0.89	0.94	0.97	1.00	1.06	0.77	0.94
3.33	2.0	1.07	1.04	0.98	0.90	0.67	1.54	1.03
"	2.5	1.02	1.00	0.97	0.90	0.67	1.54	1.06
"	3.33	0.97	0.96	0.95	0.90	0.72	1.46	1.07
"	5.0	0.95	0.95	0.93	0.87	0.67	1.46	1.09
"	10.0	0.94	0.96	0.97	0.95	0.83	1.15	1.04
"	20.0	0.94	0.98	0.98	1.00	1.00	0.92	0.97
5.0	2.0	1.11	1.05	1.00	0.92	0.67	1.54	1.06
"	2.5	1.06	1.03	0.98	0.90	0.67	1.46	1.03
"	3.33	1.02	1.00	0.98	0.92	0.72	1.46	1.07
"	5.0	0.99	0.99	0.98	0.95	0.78	1.31	1.07
"	10.0	0.97	0.99	0.98	0.95	0.83	1.23	1.06
"	20.0	0.97	1.00	1.00	1.00	1.00	1.00	1.01
10.0	2.0	1.12	1.05	1.00	0.92	0.67	1.46	0.93
"	2.5	1.08	1.02	0.98	0.92	0.67	1.54	1.06
"	3.33	1.05	1.01	0.98	0.92	0.72	1.46	1.06
"	5.0	1.02	1.01	1.00	0.95	0.83	1.31	1.09
"	10.0	1.00	1.01	1.00	1.00	0.95	1.15	1.04
"	20.0	1.00	1.01	1.02	1.00	0.95	1.08	1.00
∞	∞	1.00	1.00	1.00	1.00	1.00	1.00	1.00
$K^{\infty}_{tb\|\theta=0}$		1.28	0.78	0.57	0.39	0.18	-0.13	-0.67

Table 8. Loaded Hole Finite Size Correction Factors, $\lambda_{b|\theta=45}$, for [0/±45] Boron-Epoxy Laminates

E/D	S/D	100% 0	83.4% 0	66.7% 0	50% 0	33.3% 0	16.6% 0	0% 0
2.0	2.0	0.00	5.75	1.67	1.34	1.24	1.21	1.31
"	2.5	0.07	5.75	1.71	1.36	1.27	1.25	1.37
"	3.33	0.11	5.75	1.71	1.41	1.30	1.27	1.34
"	5.0	0.11	6.00	1.83	1.45	1.34	1.30	1.36
"	10.0	0.11	6.50	1.92	1.55	1.41	1.35	1.40
"	20.0	0.18	6.25	1.92	1.57	1.44	1.37	1.39
2.5	2.0	0.21	4.75	1.54	1.29	1.23	1.21	1.33
"	2.5	0.32	4.50	1.54	1.29	1.24	1.23	1.34
"	3.33	0.39	4.25	1.50	1.29	1.23	1.22	1.30
"	5.0	0.43	4.25	1.54	1.32	1.24	1.22	1.27
"	10.0	0.43	4.50	1.63	1.36	1.28	1.26	1.30
"	20.0	0.47	4.50	1.67	1.41	1.31	1.28	1.32
3.33	2.0	0.36	4.25	1.54	1.30	1.23	1.20	1.27
"	2.5	0.50	3.75	1.46	1.27	1.23	1.23	1.35
"	3.33	0.57	3.25	1.38	1.25	1.20	1.21	1.28
"	5.0	0.64	3.00	1.33	1.20	1.17	1.17	1.22
"	10.0	0.64	3.25	1.38	1.23	1.18	1.18	1.22
"	20.0	0.68	3.25	1.42	1.27	1.21	1.20	1.23
5.0	2.0	0.47	4.25	1.54	1.30	1.23	1.20	1.27
"	2.5	o.61	3.50	1.46	1.27	1.23	1.23	1.35
"	3.33	0.72	3.00	1.38	1.23	1.20	1.20	1.27
"	5.0	0.79	2.50	1.29	1.18	1.16	1.15	1.21
"	10.0	0.82	2.25	1.25	1.13	1.13	1.12	1.15
"	20.0	0.82	2.50	1.25	1.16	1.14	1.13	1.16
10.0	2.0	0.46	4.25	1.54	1.30	1.23	1.19	1.24
"	2.5	0.64	3.50	1.46	1.27	1.23	1.23	1.30
"	3.33	0.79	2.75	1.38	1.23	1.20	1.20	1.28
"	5.0	0.86	2.25	1.25	1.18	1.16	1.16	1.20
"	10.0	0.89	1.75	1.17	1.11	1.10	1.10	1.14
"	20.0	0.93	1.75	1.17	1.09	1.09	1.08	1.10
∞	∞	1.00	1.00	1.00	1.00	1.00	1.00	1.00
$K^{\infty}_{tb\|\theta=45}$		-0.28	0.04	0.24	0.44	0.70	1.16	2.60

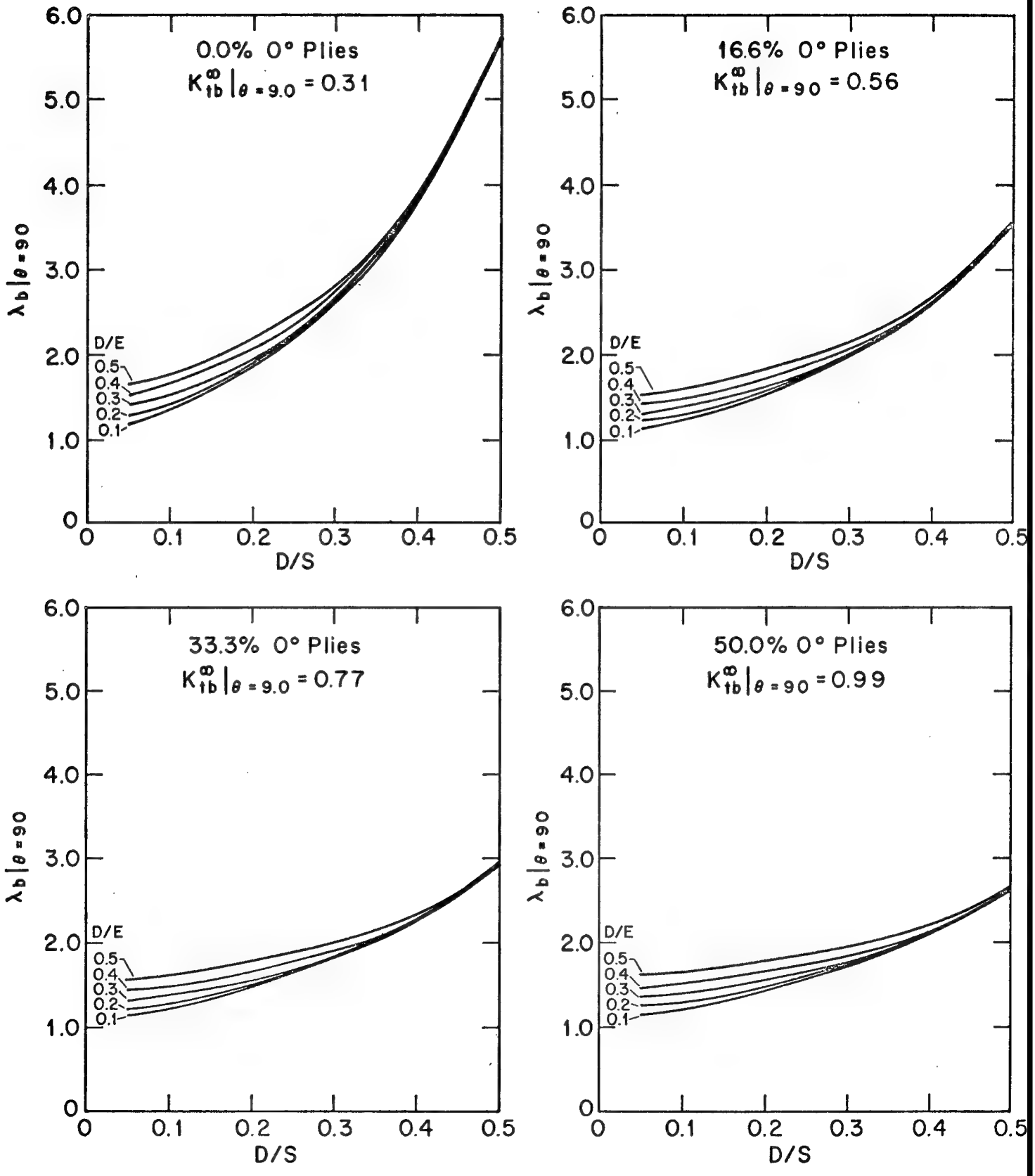

Figure 17. Loaded Hole Finite Size Correction Factors, $\lambda_{b|\theta=90}$, for [0/±45] Boron-Epoxy Laminates

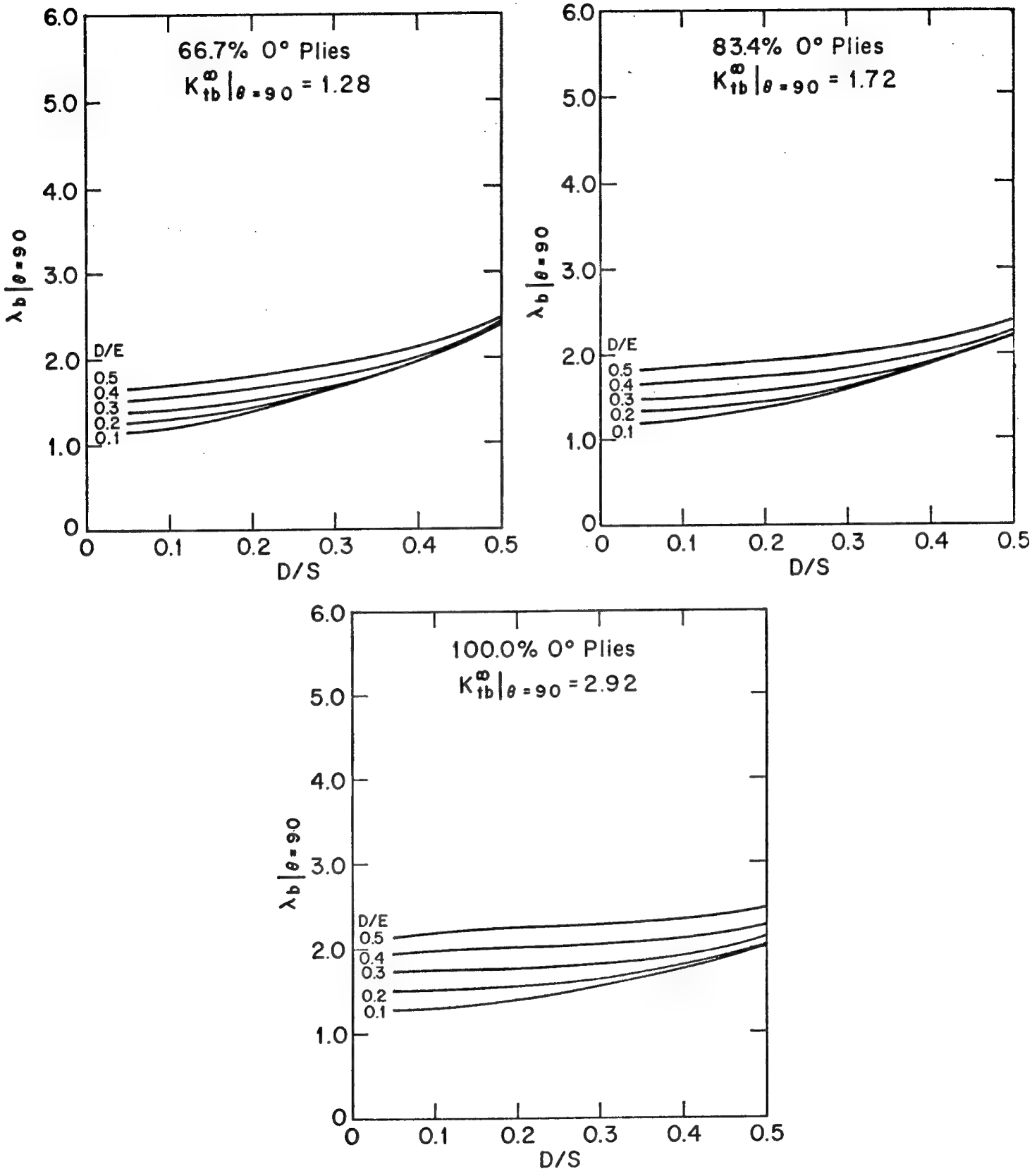

Figure 17 (Cont'd). Loaded Hold Finite Size Correction Factors, $\lambda_{b|\theta=90}$, for [0/±45] Boron-Epoxy Laminates

the error involved in using isotropic correction data for a finite size (0) laminate having D/E = 0.1 and D/S = 0.5 is conservative by 40%.

3.3.5 Correction Data for an Open Hole in a Tension Field

The method used to develop finite size correction factors for the tension loading case was identical to that used for the bolt loaded problems. Again thirty different geometries were considered for each of seven laminates and the isotropic material. The BIE method stress analysis of a given finite size coupon results in values for $K_{ts|\theta}$ for θ=0°, 45° and 90°. Values of $\lambda_{s|\theta}$ are then generated by normalizing the finite size coupon stress concentrations on their respective infinite plate values, $K^{\infty}_{ts|\theta}$ For example for an isotropic material

$$K^{\infty}_{ts|\theta=90} = 3.00 \tag{76}$$

and

$$K_{ts|\theta=90}\,(D/E=0.3,\ D/S=0.3) = 3.41 \tag{77}$$

Therefore

$$\lambda_{s|\theta=90} = (D/E=0.3,\ D/S=0.3) = 1.14 \tag{78}$$

A complete set of results for an isotropic material having ν=0.3 is shown in Table 9. The data for $\lambda_{s|\theta=90}$ is also presented in graphical form in Figure 18. These isotropic results can again be compared to graphical results presented in Peterson [15] which relate

Table 9. Open Hole Finite Size Correction Factors, $\lambda_{s|\theta}$, for an Isotropic Material (ν=0.3): θ=0°, 45°, 90°

E/D	S/D	$\lambda_{s\|\theta=0}$	$\lambda_{s\|\theta=45}$	$\lambda_{s\|\theta=90}$
2.0	2.0	1.55	0.91	1.44
"	2.5	1.47	1.03	1.27
"	3.33	1.37	1.11	1.18
"	5.0	1.22	1.14	1.12
"	10.0	1.10	1.15	1.09
"	20.0	1.09	1.15	1.08
2.5	2.0	1.48	0.89	1.43
"	2.5	1.36	1.00	1.25
"	3.33	1.27	1.06	1.15
"	5.0	1.18	1.09	1.10
"	10.0	1.06	1.10	1.07
"	20.0	1.04	1.10	1.06
3.33	2.0	1.45	0.88	1.43
"	2.5	1.31	0.99	1.25
"	3.33	1.20	1.04	1.14
"	5.0	1.12	1.06	1.08
"	10.0	1.03	1.06	1.05
"	20.0	1.01	1.06	1.04
5.0	2.0	1.43	0.89	1.43
"	2.5	1.29	0.99	1.25
"	3.33	1.16	1.03	1.13
"	5.0	1.07	1.05	1.07
"	10.0	1.01	1.05	1.04
"	20.0	1.00	1.04	1.03
10.0	2.0	1.43	0.90	1.43
"	2.5	1.28	1.00	1.25
"	3.33	1.15	1.04	1.13
"	5.0	1.04	1.05	1.06
"	10.0	0.98	1.04	1.03
"	20.0	0.99	1.03	1.02
∞	∞	1.00	1.00	1.00
$K_{ts\|\theta}^{\infty}$		-1.00	1.00	3.00

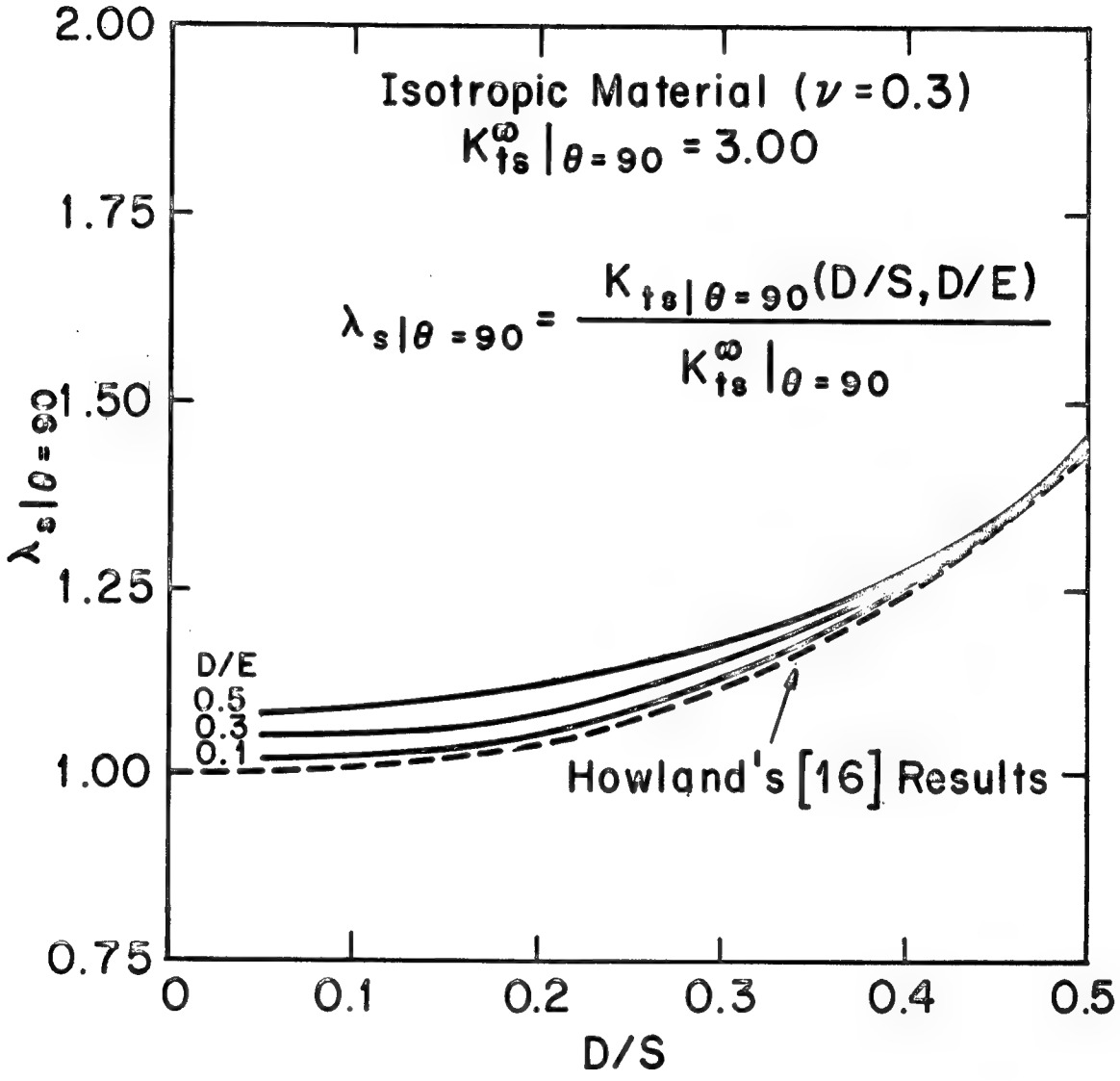

Figure 18. Open Hole Finite Size Correction Factors, $\lambda_{s|\theta=90}$, for an Isotropic Material (ν=0.3)

$\lambda_{s|\theta}$ to D/S. The data was taken from the mathematical results of Howland [16] which represent the solution to the problem of an infinitely long, finite width plate under axial loading containing a circular cut-out at its center. Howland's results represent a lower bound on the numerical results presented in Figure 18 since, as D/E goes to zero, the finite width coupons become infinitely long. The numerical results are in excellent agreement with Howland's mathematical solution which is represented by the dashed curve in Figure 18.

Similar results are presented in tabular form for $\lambda_{s|\theta=0}$ and $\lambda_{s|\theta=45}$ for the seven boron-epoxy laminates of interest; Tables 10 and 11 respectively. The data for $\lambda_{s|\theta=90}$ is presented in graphical form in Figure 19. Again in the (0) laminate the effect of specimen width is much less than it is for the majority of angle-ply laminates. A direct load path to the sides of the coupon is again necessary to enable the stress field near the hole to see the finite boundaries. The isotropic correction factors for tension loaded holes in infinite plates again closely resemble those for laminates composed of between 33% and 50% 0° plies. The error involved in applying these isotropic results to anisotropic tension loaded problems is somewhat less than that for the bolt loaded problems but can still be quite significant. In the case of a (0) laminate the conservative error involved in using isotropic correction data for a finite size coupon having D/E = 0.1 and D/S = 0.5 is 13%.

Table 10. Open Hole Finite Size Correction Factors, $\lambda_{s|\theta=0}$, for [0/±45] Boron-Epoxy Laminates

E/D	S/D	100% 0	83.4% 0	66.7% 0	50% 0	33.3% 0	16.6% 0	0% 0
2.0	2.0	2.60	1.95	1.74	1.62	1.52	1.43	1.28
"	2.5	2.40	1.79	1.63	1.53	1.45	1.38	1.26
"	3.33	2.17	1.60	1.46	1.38	1.33	1.30	1.23
"	5.0	1.97	1.45	1.30	1.24	1.18	1.14	1.11
"	10.0	1.87	1.39	1.24	1.16	1.11	1.06	0.98
"	20.0	1.83	1.37	1.24	1.16	1.11	1.06	1.04
2.5	2.0	2.10	1.63	1.52	1.45	1.41	1.35	1.25
"	2.5	1.97	1.55	1.43	1.38	1.33	1.28	1.19
"	3.33	1.80	1.42	1.35	1.31	1.26	1.24	1.18
"	5.0	1.63	1.29	1.22	1.18	1.15	1.14	1.12
"	10.0	1.53	1.24	1.15	1.09	1.06	1.03	0.99
"	20.0	1.50	1.21	1.15	1.09	1.06	1.04	1.00
3.33	2.0	1.73	1.47	1.41	1.38	1.36	1.33	1.24
"	2.5	1.60	1.37	1.30	1.27	1.26	1.23	1.12
"	3.33	1.50	1.29	1.24	1.20	1.18	1.16	1.13
"	5.0	1.37	1.18	1.15	1.13	1.12	1.11	1.11
"	10.0	1.30	1.11	1.07	1.05	1.03	1.01	0.97
"	20.0	1.27	1.11	1.07	1.05	1.03	1.01	0.99
5.0	2.0	1.53	1.39	1.37	1.36	1.35	1.31	1.20
"	2.5	1.37	1.26	1.24	1.24	1.23	1.21	1.11
"	3.33	1.27	1.16	1.15	1.15	1.14	1.13	1.11
"	5.0	1.20	1.11	1.09	1.07	1.08	1.06	1.06
"	10.0	1.13	1.05	1.04	1.02	1.02	1.01	0.99
"	20.0	1.10	1.03	1.02	1.02	1.02	1.00	0.97
10.0	2.0	1.47	1.39	1.37	1.36	1.35	1.31	1.30
"	2.5	1.30	1.24	1.24	1.24	1.23	1.21	1.14
"	3.33	1.17	1.13	1.13	1.13	1.12	1.13	1.08
"	5.0	1.07	1.03	1.04	1.04	1.03	1.04	1.02
"	10.0	1.00	1.00	1.00	1.00	1.00	0.99	0.96
"	20.0	1.00	1.00	1.02	1.02	1.02	1.00	0.99
∞	∞	1.00	1.00	1.00	1.00	1.00	1.00	1.00
$K^{\infty}_{ts\|\theta=0}$		-0.30	-0.38	-0.46	-0.55	-0.66	-0.80	-1.00

Table 11. Open Hole Finite Size Correction Factors, $\lambda_{s|\theta=45}$, for [0/±45] Boron-Epoxy Laminates

E/D	S/D	100% 0	83.4% 0	66.7% 0	50% 0	33.3% 0	16.6% 0	0% 0
2.0	2.0	1.65	1.04	0.89	0.84	0.86	0.91	1.11
"	2.5	1.88	1.32	1.14	1.06	1.06	1.09	1.27
"	3.33	2.12	1.48	1.29	1.18	1.15	1.17	1.29
"	5.0	2.18	1.60	1.37	1.27	1.21	1.19	1.28
"	10.0	2.24	1.64	1.40	1.29	1.23	1.18	1.25
"	20.0	2.12	1.56	1.37	1.27	1.20	1.18	1.20
2.5	2.0	1.18	0.84	0.77	0.78	0.82	0.89	1.13
"	2.5	1.41	1.08	0.97	0.98	0.99	1.05	1.23
"	3.33	1.59	1.20	1.11	1.08	1.08	1.11	1.23
"	5.0	1.71	1.32	1.20	1.14	1.13	1.13	1.21
"	10.0	1.76	1.36	1.23	1.16	1.14	1.13	1.21
"	20.0	1.71	1.32	1.23	1.16	1.13	1.11	1.14
3.33	2.0	0.88	0.72	0.71	0.76	0.82	0.89	1.07
"	2.5	1.12	0.92	0.91	0.94	0.97	1.04	1.26
"	3.33	1.24	1.04	1.03	1.02	1.04	1.08	1.21
"	5.0	1.35	1.12	1.09	1.06	1.07	1.10	1.16
"	10.0	1.41	1.16	1.11	1.10	1.08	1.10	1.20
"	20.0	1.35	1.16	1.11	1.08	1.07	1.07	1.07
5.0	2.0	0.71	0.68	0.71	0.76	0.82	0.91	1.13
"	2.5	0.88	0.88	0.91	0.94	0.99	1.05	1.26
"	3.33	1.00	1.00	1.00	1.02	1.04	1.09	1.25
"	5.0	1.12	1.04	1.03	1.04	1.06	1.08	1.15
"	10.0	1.18	1.08	1.06	1.06	1.06	1.08	1.16
"	20.0	1.18	1.08	1.06	1.04	1.04	1.04	1.07
10.0	2.0	0.65	0.68	0.71	0.78	0.83	0.90	1.07
"	2.5	0.82	0.88	0.91	0.94	1.00	1.07	1.31
"	3.33	0.94	0.96	1.00	1.02	1.06	1.10	1.21
"	5.0	1.00	1.04	1.03	1.06	1.07	1.10	1.19
"	10.0	1.06	1.04	1.03	1.04	1.06	1.06	1.14
"	20.0	1.06	1.04	1.03	1.02	1.03	1.04	1.07
∞	∞	1.00	1.00	1.00	1.00	1.00	1.00	1.00
$K^{\infty}_{ts\|\theta=45}$		0.17	0.25	0.35	0.49	0.71	1.14	2.61

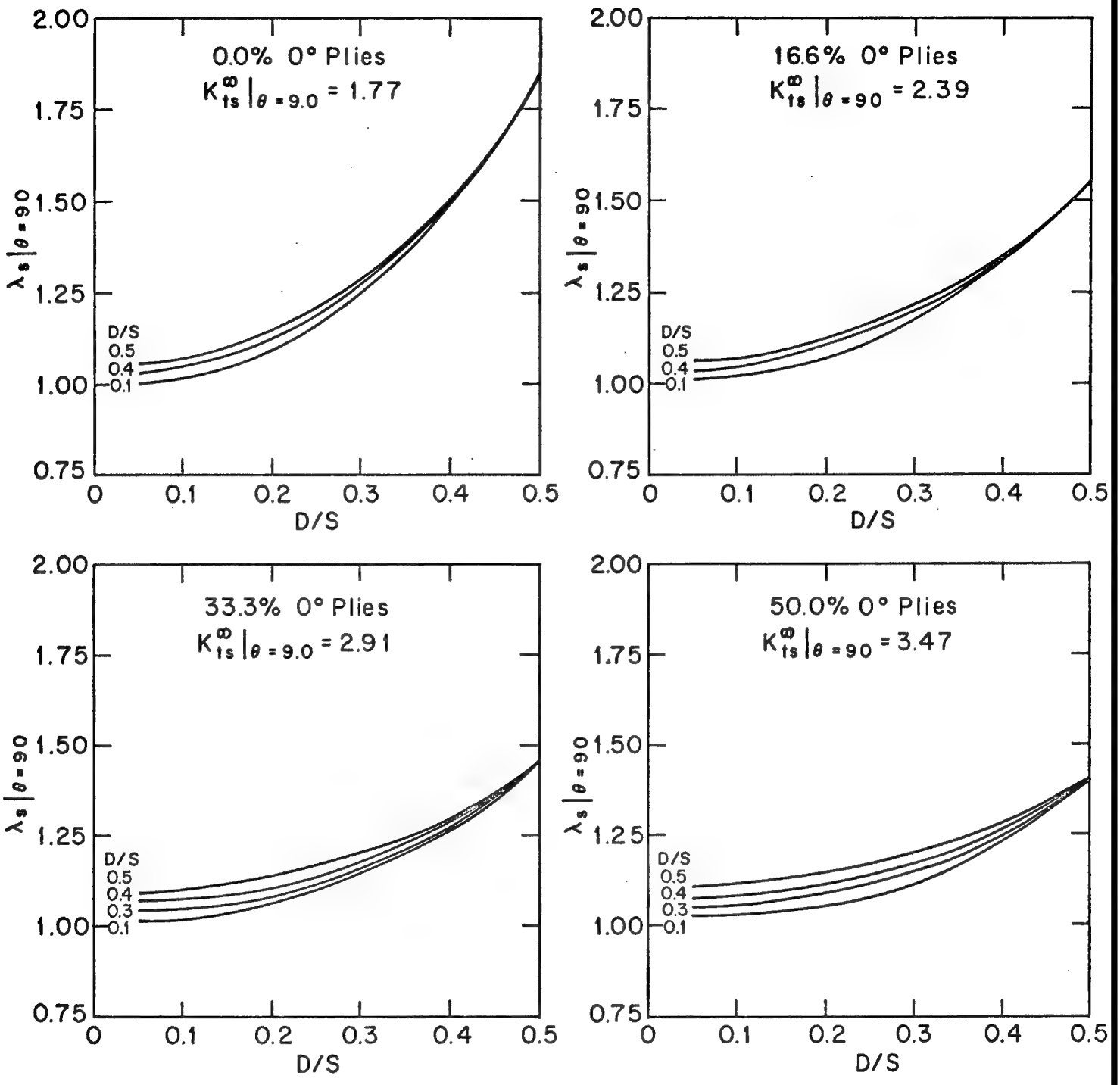

Figure 19. Open Hole Finite Size Correction Factors, $\lambda_{s|\theta=90}$, for [0/±45] Boron-Epoxy Laminates

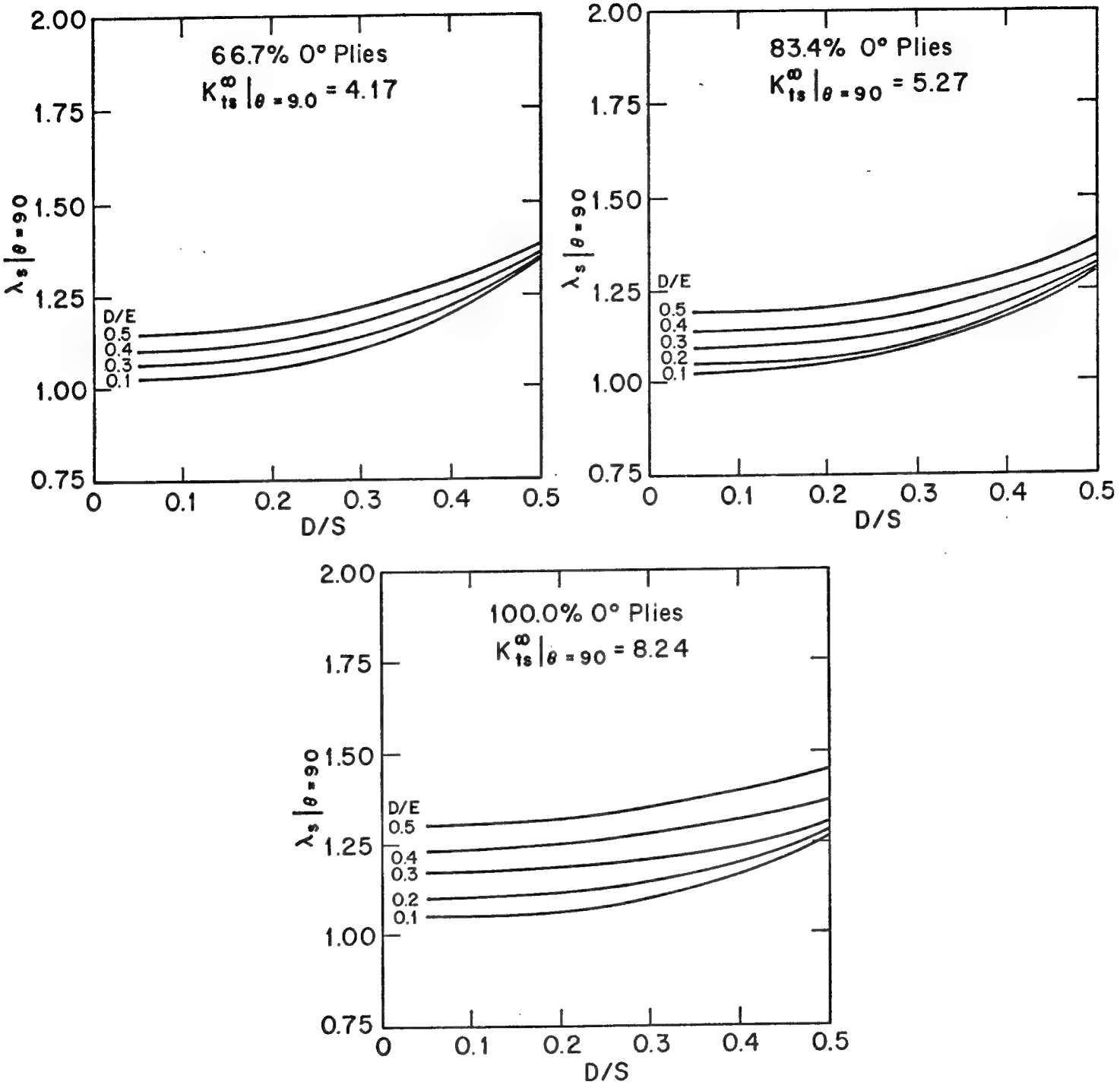

Figure 19 (Cont'd). Open Hole Finite Size Correction Factors, $\lambda_{s|\theta=90}$, for [0/±45] Boron-Epoxy Laminates

3.3.6 Correction Data for a Series of Holes in a Tension Field

By modeling the skin load on the finite size coupons as a uniform stress, Figure 13b, the induced stress concentrations along the circular boundary are higher than they really would be for the actual skin stress distribution, Figure 13a. The values of $\lambda_{h|\theta}$ developed in this section are intended to correct for this modeling error. Since the calculated stresses are all too large, the values of $\lambda_{h|\theta}$ will all be less than 1.0. By solving a series of problems involving three equally spaced, collinear fasteners subjected to a tensile loading and by calculating the hoop stress concentrations along the boundary of the inner hole, the correction factors of interest can be calculated. The applied skin stress seen by the inner hole in the vicinity of the two outer holes has the desired distribution. The capability of the BIE method for solving infinite plate problems is again utilized. Since the plates are infinite only the ratio of hole diameter to hole spacing, D/E, need be considered. As a result only five geometries per laminate are analyzed.

Although values for $\lambda_{h|\theta}$ were generated for θ=0°, 45° and 90°, only the hoop stresses at θ=90° are corrected for the effects of adjacent fasteners. The justification for not correcting for the effects of adjacent fasteners at θ=0 and 45° is that the stresses at these points are often near zero and that the magnitude of these $\lambda_{h|\theta}$ values are almost all within 10% of 1.0. The error involved in interpolating $\lambda_{h|\theta}$ values for near zero stresses can be of the same magnitude as the correction itself. Table 12 lists the anisotropic data for $\lambda_{h|\theta=90}$.

Table 12. Correction Factors, $\lambda_{h|\theta=90}$, for a Series of Three Holes in [0/±45] Boron-Epoxy Laminates

E/D	100% 0	83.4% 0	66.7% 0	50% 0	33.3% 0	16.6% 0	0% 0
2.0	0.64	0.70	0.74	0.78	0.82	0.87	0.93
2.5	0.67	0.74	0.78	0.83	0.86	0.91	0.96
3.33	0.71	0.79	0.85	0.89	0.92	0.95	0.98
5.0	0.79	0.88	0.92	0.95	0.97	0.98	0.99
10.0	0.92	0.97	0.99	1.00	1.00	1.00	1.00

The isotropic data for $\lambda_{h|\theta=90}$ plotted in Figure 20 along with data from Peterson [17] for an infinite row of fasteners in an infinite isotropic plate subject to a tensile loading. It is reasonable to expect the results for an infinite row of cut-outs to be lower than the data generated here since the stress field which the inner cut-out in a row of three sees is not fully developed. The stress concentrations for the inner cut-out would therefore be closer to the infinite plate stress concentration for a single cut-out, denoted by $\lambda_{h|\theta=90} = 1.0$ in Figure 20. If the values of $\lambda_{h|\theta=90}$ presented here for three holes in a row are used in the analysis of designs having four or more holes, the resulting stress concentration factor estimates will be conservative.

All the data in Table 12 shows that as the hole separation distance to diameter ratio becomes large the values of $\lambda_{h|\theta=90}$ approach 1.0. This is correct since the solution for a single cut-out in an infinite plate is being approached. Also, as more angle plies are used in the laminate the stress field at the inner row is affected less by the presence of adjacent cut-outs. The angle-ply fibers again act as efficient load carriers and enable the stress field to return more rapidly to a uniform distribution between the cut-outs, which in turn increases the stress concentration on the inner cut-out.

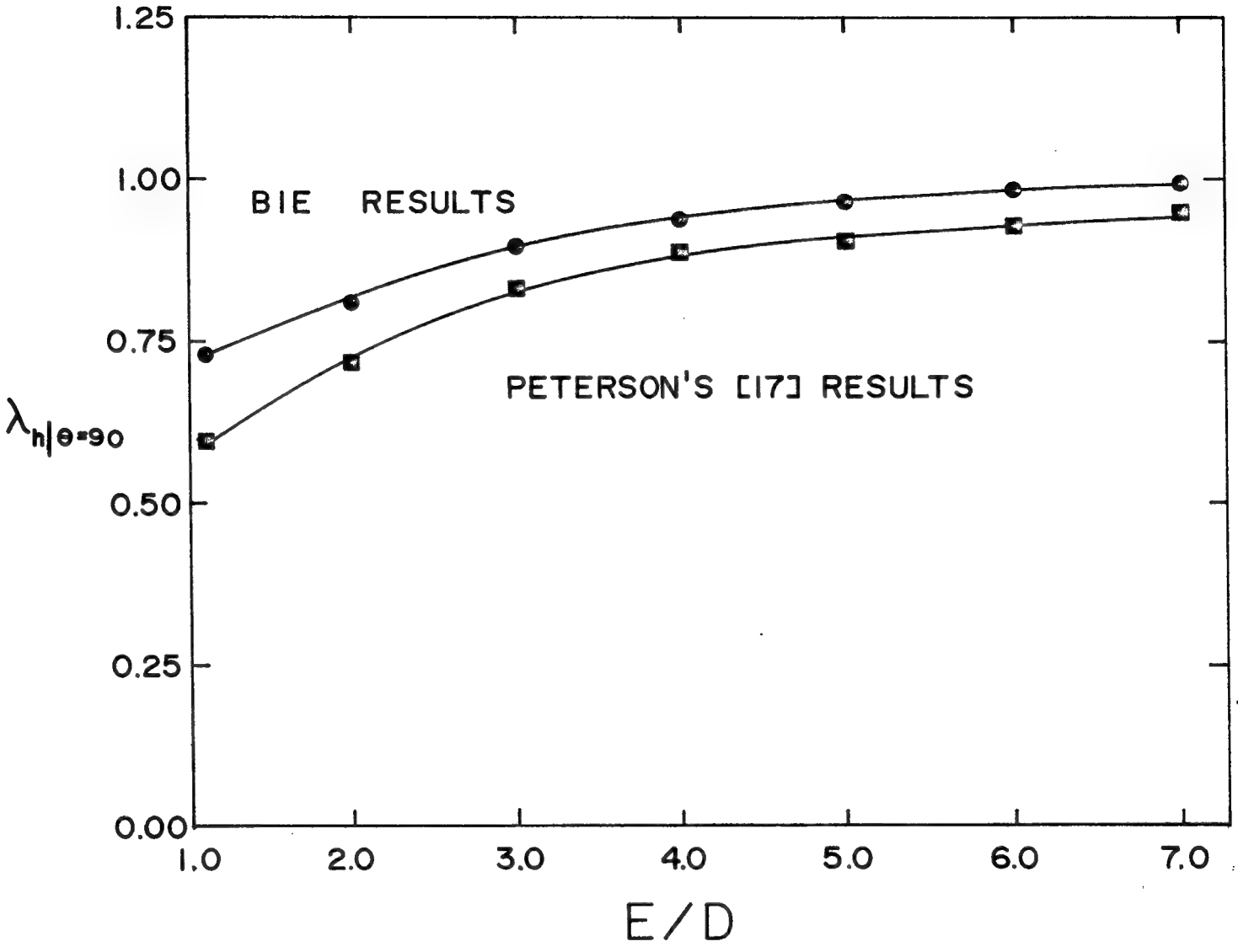

Figure 20. Correction Factors, $\lambda_{h|\theta=90}$, for a Series of Holes in an Infinite Isotropic Plate

The laminate correction factors which most closely resemble the isotropic material results here are those for the laminate containing 67% 0° plies. The laminate containing 40% 0° plies, which most closely resembled the isotropic results in the previous two cases, is within about 10% of the isotropic results.

3.3.7 Discussion of the Numerical Results

The correction factors developed herein for the [0/±45] family of boron-epoxy laminates are in many cases quite different from similar isotropic correction factors presented in the literature. The use of such isotropic data in the analysis of composite structures can lead to significant errors. For a small range of [0/±45] laminates containing approximately 40% 0° plies the isotropic correction factors give very good results; for others conservative errors up to 40% can occur.

In estimating the stress concentration for a given finite size laminate attempts were made to start with infinite plate results and to correct them to the finite coupon results of interest using material and geometric correction factors. All such attempts were unsuccessful, however. As a result it was necessary to interpolate between the existing data to estimate the required correction factors in the synthesis procedure. Rather than develop data for the entire [0/±α/90] family of boron-epoxy laminates, data was generated for the much smaller [0/±45] family. The assumption was then made that

the data generated was applicable to [0/±α/90] laminates based on the percentage of 0° plies present. This practice was restricted to these [0/±α/90] laminates containing less than 25% 90° plies and having a value of α within 15° of 45°. The results indicate that these assumptions were realistic. While the data reported is for boron-epoxy, it has been further assumed that the data can be used in the analysis of graphite-epoxy laminates. It has often been observed that normalized stress concentrations induced in angle-ply graphite-epoxy laminates are nearly equal (to within just a few percent) to those induced in boron-epoxy for the same lamination.

One problem was encountered in using the correction data. At some locations on the circular boundary of an infinite plate the hoop stresses passed through zero for the bolt loading and come very close to zero for the tension loading. In such cases the values of $\lambda_{b|\theta}$ and $\lambda_{s|\theta}$ can become quite large. When an interpolation of λ's involves one of these very large values, the larger value dominates and often results in estimated hoop stresses outside the range of original values. To eliminate the possibility of such errors the interpolations are all done in terms of σ_θ in the synthesis. When the interpolations of σ_θ are completed a value of λ can then be defined in terms of σ_θ and an interpolated value of the infinite plate stress concentration factor for that laminate at the location of interest.

3.4 Accuracy of the Approximate Stress Analysis Package

An efficient approximate analysis procedure for metal-to-composite multiple fastener joints has been developed. Combining the analysis procedure with the proposed joint strength criterion allows for rapid and conservative predictions of the failure characteristics of a given joint design.

One problem with this analysis procedure has been identified, however. The approximate stress analysis does not strictly satisfy equilibrium requirements in the joint. To determine the effects of this solution deficiency stress analysis results using the approximate method are compared to finite element results in Table 13. The problem analyzed was the graphite-epoxy multiple fastener joint analyzed in Appendix B. Results are presented for the first and last coupons for that joint. The last coupon was subjected only to a bolt load since there was no applied skin load to the leading edge of the main plate. The first coupon was subjected to both a bolt load and a skin load; the skin load accounting for 84% of the total load carried by the coupon.

The results show that the approximate model is in good agreement with the finite element method (in most cases overpredicting the finite element stresses) except at θ=45°. At θ=45° the approximate

Table 13. Comparison of Approximate Solution and Finite Element Stress Analysis Results on Experimentally Failed Multiple Fastener Joint: Specimen 6

Failure Location and Stress Component	First Coupon		Last Coupon	
	FE Solution	Approx. Sol.	FE Solution	Approx. Sol.
$\theta=90°$ σ_1/σ_{1ut}	0.96	0.99	1.38	1.45
$\theta=45°$ σ_1/σ_{1ut}	0.24	0.37	0.71	0.97
$\theta=45°$ σ_2/σ_{2ut}	0.28	0.48	0.82	1.22
$\theta=0°$ σ_1/σ_{1uc}	-0.16	-0.14	-1.18	-1.02
$\theta=0°$ σ_2/σ_{2ut}	-0.04	-0.08	1.55	1.75

method overpredicts the stresses by anywhere from 30 to 70%. During the development of the approximate stress analysis package a number of assumptions were made which have been identified as being conservative. These various contributions seem to be most significant at θ=45°.

All the results thus far indicate that the degree of conservatism in predicting net tension failures in multiple fastener joints is much less that that for the other possible modes. All the synthesis results presented later indicate that multiple fastener joints are usually critical in net tension all along the joint except at the leading edge fastener, which is usually critical in bearing or splitting. Therefore, excessive conservatism at θ=45° will at most result in an excessive build up of the material ahead of the leading edge fastener to inhibit a splitting failure at θ=45°. An overly conservative design at just the leading edge of the main plate in a mlltiple fastener joint will not result in a significant weight penalty. In fact, an overly conservative design in this area may be desirable in light of the premature splitting failures ahead of the last row of fasteners reported in Appendix B. Therefore, the fact that the approximate stress analysis does not strictly satisfy equilibrium does not seem to be a very serious problem. The resulting errors in the stress analysis are small and usually conservative at the most important locations in the material.

Presently we are in a position of being able to very efficiently perform a conservative strength analysis for a proposed joint design. The next major objective is to build this efficient stress analysis package and joint failure criterion into an automated design procedure. One of the key items required for such a synthesis procedure has yet to be discussed; the selection of a minimization algorithm which will make use of this efficient analysis package in seeking minimum weight designs. In the next chapter the selection of a minimization algorithm is made and the details of the joint synthesis procedure are discussed.

CHAPTER IV

SYNTHESIS PROGRAM DETAILS

4.1 Discussion of Minimization Techniques

The selection of a minimization algorithm is a very important decision. Many factors influence this decision and each must be carefully considered. The most fundamental consideration is whether the problem is to be a linear programming or a nonlinear programming problem.

The minimization problem in the current study can be stated as follows: Minimize the total weight of a metal-to-composite multiple fastener joint subject to a given design ultimate load, a specified joint failure criterion and various other geometric side constraints. The problem as stated is a constrained, nonlinear minimization problem. Both the objective function, total joint weight, and the behavioral design constraints, all of which are stress related quantities, are nonlinear functions of the design variables. While the total joint weight can be expressed in terms of the various geometric design variables, an expression relating the various stresses in the joint to the design variables cannot be written explicitly. Since this nonlinear problem is not readily amenable to linearization, nonlinear programming techniques are required.

Two general methods are available for solving nonlinear minimization problems: Constrained and unconstrained minimization algorithms. In

an unconstrained minimization an objective function is minimized with no restrictions at all imposed on the values which the design variables may assume. Local slope and curvature information can be used to select a preferred direction of travel in the design space along which the value of the objective function decreases. A linear minimization is then performed along that direction to locate a local minimum value of the objective function. Once the linear minimization converges, a new preferred direction of travel is selected based again on local slope and curvature information and the process is repeated. The iterative solution procedes until convergence to a local minimum for the nonlinear problem is achieved in the design space.

When trying to minimize the weight of a structural design (such as a bolted joint) which must carry a given load, a constrained minimization problem is involved. The minimum weight of a structure is zero. A finite design ultimate load implies that certain lower bounds on the geometric design variables exist. These lower bounds are, in fact, behavioral design constraints. That design which can most efficiently carry the load has a finite, positive weight and is located on one or more constraint surfaces.

The same general procedures used for solving unconstrained minimization problems can be adapted for constrained minimizations as a preferred direction of travel is still to be based on local slope and curvature information. Each time a small move is made in the feasible (acceptable) region, checks are made to see if any of the design

constraints have been violated. When constraint surfaces are approached the direction of travel must be modified to insure that the next step is made to a point which is not only in the feasible region but which also results in a lower weight design. Constrained minimization algorithms can be reasonably efficient for small problems involving just a few design variables and design constraints.

When complicated structural problems are encountered, however, it is computationally more efficient to convert the constrained minimization problem to an unconstrained minimization problem using an interior penalty function. Interior penalty functions are used to define a new objective function which has its minimum value inside the feasible region. By moving through the feasible region a local minimum for the *revised* objective function can be achieved using an unconstrained minimization algorithm. By successively reducing the magnitude of the penalty associated with moving closer to a constraint surface the actual minimum value of the original objective function, which is located on one or more constraint surfaces, is approached, from within the feasible design space.

The selection of a particular algorithm to solve a given constrained, nonlinear minimization problem is based on several factors: The number of design variables, the number of design constraints and the methods available for calculating the gradient of the objective function are the most important factors to be considered.

Consider again the joint illustrated in Figure 1. The maximum number of possible active design variables is seventeen; sixteen geometric design variables and the applied load. In a $[0/\pm\alpha/90]$ laminate there are a maximum of eleven possible behavioral constraints based on stress quantities which must be satisfied at each bolt hole along the joint. Seven are required to check for possible failures around the hole in the composite, three in the metal splice plates and one in the bolt. A typical joint design contains six fasteners per column which results in a possible total of 66 behavioral constraints alone. The number of side constraints presently required by the program is 25, which results in a possible total of 91 design constraints.

Due to the complexity of the problem it was decided that an interior penalty function would be used to convert the program to an unconstrained minimization. To calculate either slope or curvature information for the new objective function numerical methods are required. Such methods are relatively time consuming since up to seventeen function evaluations, each of which requires a complete joint stress analysis, must be performed if a forward difference technique is used to calculate the gradient of the new objective function. Using a central difference technique would require twice as many function evaluations. Generating curvature information (i.e., a matrix of second derivatives) is even more expensive.

4.2 The Variable Metric Method

For problems containing from ten to fifty design variables which require numerical evaluation of the gradient the variable metric method of Davidon [18] as modified by Fletcher and Powell [19] has been recommended [20, 21]. The function to be minimized is the total weight of the joint

$$W = W_M + W_S + W_B \tag{79}$$

where W_M is the weight of the composite main plate, W_S is the total weight of the two metal splice plates and W_B is the total weight of all the bolts. To create an unconstrained minimization problem the constraint equations, C(I), are combined with the total joint weight, W, using an interior penalty function. The new objective function, F, is given by

$$F = W + D_F \sum_{I=1}^{NC} 1/C(I) \tag{80}$$

where D_F, referred to here as the draw-down factor, is a positive constant which controls the magnitude of the penalty assigned to F. The draw-down factor will be made successively smaller during the optimization such that the constrained minimum of W is approached.

The constraint equations, C(I), are mathematical representations of the joint failure criterion, and are written such that $0 < C(I) \leq 1$ if the I^{th} constraint is satisfied. As an example suppose that the I^{th} constraint checks for fiber tension failures at some specified

location. Then

$$C(I) = 1.0 - \sigma_1/\sigma_{1_{ut}} \tag{81}$$

where σ_1 is the magnitude of the existing fiber tension stress and $\sigma_{1_{ut}}$ is the fiber's ultimate tension stress.

Note that the objective function, F, is defined in terms of the constraint equations such that large penalties are imposed as designs are selected which try to force the constraint equations to zero; in the case of (81), $C(I) \to 0$ as $\sigma_1 \to \sigma_{1_{ut}}$ or as fiber failure becomes imminent. As noted, the actual magnitude of the penalty depends on the value which we assign to the draw-down factor.

Methods which utilize interior penalty functions have one inherent limitation. The initial design specified by the designer *must* satisfy all the design constraints. If the initial design violates the I^{th} constraint, then $C(I) < 0$, and the algorithm, if permitted to operate according to (80), would attempt to minimize F by driving $F \to -\infty$. A method for accepting initial designs which are outside the feasible region is discussed at the end of this section.

The optimization method can best be illustrated by considering a design which is a function of only two variables (e.g., the weight of a right circular cylinder is given by $W = \rho\pi R^2 L$) subject to two design constraints. The constraints could represent a buckling stability and and strength criteria. Figure 21a illustrates a number of possible constant weight contours and the two design constraints. The minimum

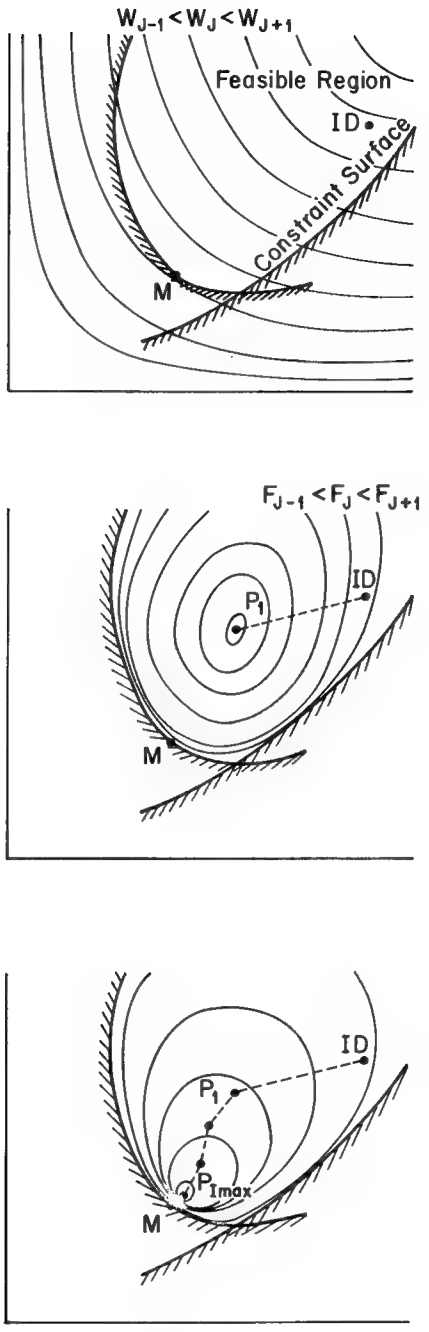

Figure 21. Variations in Objective Function Contours During the Optimization

weight design subject to no constraints is located at the origin. The minimum weight design subject to the imposed constraints is at M. The task is to systematically move through the feasible region from an initial feasible design, ID, to M. For an initial value of D_F, contours of F as defined by (80) are illustrated in Figure 21b. A convenient way of defining the initial value of D_F, which works well for a variety of different problems, is

$$D_F = W \Big/ \sum_{I=1}^{NC} 1/C(I) \tag{82}$$

where W and C(I) are evaluated for the initial design.

The minimum of F for the initial value of D_F is P_1. The move from ID to P_1 is made by a series of linear minimizations as outlined in the flow diagram, Figure 2. Once the process has converged to P_1, the value of D_F is reduced by some specified amount (in the present study by 80%) and the process is repeated. At the conclusion of a prespecified number of iterations, Imax, $P_{Imax} \rightarrow M$ as shown in Figure 21c.

The direction along which a given linear minimization is performed is given by

$$\mathbf{S} = -\alpha \, [\mathbf{H}] \quad \nabla F \tag{83}$$

where ∇F is the local gradient of F and $[\mathbf{H}]$ is an approximation of the local matrix of second derivatives of F. The linear minimization seeks that value of α, called α', which results in a minimum value of

F along the vector direction $\mathbf{S}$. For an initial approximation to $[\mathbf{H}]$ the identity matrix, $[\mathbf{I}]$, is used. The approximation to $[\mathbf{H}]$ is updated after the convergence of each linear minimization using the current approximation and gradient information at both the new and old designs. The direction of travel is seen to take into consideration both slope and curvature information which usually results in better convergence characteristics than exhibited by simple gradient methods (e.g., the steepest descent method). A detailed description of the variable metric method and a proof that the method does result in convergence to a local minimum are presented in [20].

As mentioned above, the procedure works well as long as the proposed initial design can safely carry the design ultimate load, P_{ULT}. However, for a given design ultimate load and a specified number of geometric constraints, the designer may find it difficult and often times impossible to propose an initial design which is in the feasible region. This task becomes more difficult as the number of variables increases.

The synthesis procedure in this study has been modified to accept initial designs which cannot carry the design ultimate load. A method similar to that discussed in [22] is used. Assume that the proposed initial design can carry some reduced load, P, which is less than P_{ULT} as implied by

$$P = (1-\lambda) \; P_{ULT} \quad , \quad 0 < \lambda \leq 1 \tag{84}$$

Since a linear stress analysis is being used the maximum value of P can be calculated from P_{ULT} using the value of the constraint which has been exceeded by the largest amount. In this study the maximum value of P is reduced further by ten percent to move the initial design away from the critical constraint surface. This added reduction is required since the convergence characteristics for a given problem are usually far better for initial designs near the center of the feasible region than they are for initial designs which are close to one or more constraint surfaces [21].

By redefining the objective function as

$$F = W + D_F \sum_{I=1}^{NC} 1/C(I) + W_F\lambda \tag{85}$$

and treating λ as an additional design variable, the program attempts to drive $\lambda \rightarrow 0$ to minimize F for a sufficiently large weighting function, W_F. Two additional constraints must be added to the penalty function summation to insure that λ remains in the range indicated in (84). If the imposed design constraints (e.g., maximum laminate thickness) prohibit all the feasible designs from carrying the design ultimate load, an optimum design for the largest possible applied load would be obtained.

The optimization algorithm used herein has an additional very important feature allowing the program to recover in the event a design is accidentally selected which is outside the feasible region. In such

cases the program merely reverses its direction of travel and moves back toward the last feasible design.

4.3 Input Data

The following information is read into the computer program as input data. The number of fasteners used in the column, N*, is included as input data to bypass the problems associated with integer optimization. The program also requires the user to specify the diameter of the bolts, D, which are to be used in the joint to avoid problems with not being able to use standard size bolts. Given an effective shear allowable for the bolt material, F_{SU}^{B}, and the design ultimate load for the column of fasteners, P_{ULT}, one can estimate the minimum number of bolts of a given diameter needed to carry the design ultimate load. It may be desirable to carefully select several different combinations of D and N and perform several syntheses to achieve greater weight savings.

Decisions may or may not have to be made concerning material selection. Either boron-epoxy or graphite-epoxy can be specified as the main plate material. The material properties and ultimate allowables must be input for the material system selected. Selection of the splice plate material will be application dependent. The values of F_{TU}^{S}, F_{SU}^{S} and F_{BRU}^{S} for the metal splice plate must be input so that constraint relationships may be defined to insure against net tension, shear-out

*Underlined symbols and phrases denote required input information.

and bearing failures in the splice plate. The splice plate modulus, E_S, is also required in the load partitioning calculations.

In summary the required input data is:

D	Bolt diameters
F_{SU}^{B}	Effective shear strength of bolt material
P_{ULT}	Design ultimate load for the column of bolts
N	Number of bolts per column
F_{TU}^{S}	Effective tension strength of splice plate material
F_{SU}^{S}	Effective shear-out strength of splice plate material
F_{BRU}^{S}	Effective bearing strength of splice plate material
E_S	Splice plate modulus
E_{11}, E_{22}, G_{12}, ν_{12}	Composite material ply properties
σ_{1ut}, σ_{2ut}, σ_{1uc}, σ_{2uc}	Composite material ply ultimate stress allowables

4.4 Design Variables

Sixteen geometric parameters are now identified which, in conjunction with the specified input data, completely define a multiple fastener joint design. If restrictions are not imposed on the design once the input data is determined, the sixteen geometric parameters would represent sixteen active design variables. If restrictions are imposed on some

of the geometric parameters, the number of active design variables is less than sixteen. "On-off" flags are read in at the beginning of the program to indicate which of the sixteen geometric parameters are to be predefined and which are to be active variables. The values of these predefined parameters are read in as part of the proposed initial design and are not permitted to vary throughout the synthesis. The remaining parameters represent the active design variables.

An allowable range of values for a number of the design variables has been defined for two basic reasons. The anisotropic correction data was generated for a specified range of possible finite size coupons. As a result proposed joint designs are not permitted to exceed this range of values. It is also necessary to formally state that the total thickness of each angle orientation be greater than or equal to zero at both ends of the main plate.

As mentioned the synthesis has been restricted to the $[0/\pm\alpha/90]$ class of laminates; α being a design variable. The value of α is restricted to the range $30° \leq \alpha \leq 60°$ since the correction data was generated for $\alpha = 45°$ and since it has been assumed that the correction data developed for $\alpha=45°$ can be applied to other laminates which exhibit small variations about $\alpha=45°$.

Consider the joint design shown in Figure 1. Independent linear variations in plate widths and thicknesses and individual ply thicknesses are permitted. Each of the sixteen geometric parameters are labeled

in the figure and are listed below, along with their respective ranges of permissible values where applicable.

Parameters	*Description*	*Range*
α	Angle ply orientation	$30° \rightarrow 60°$
$W_s(0)$, $W_s(L)$	Width of splice plate at x=0, L	
$t_s(0)$, $t_s(L)$	Thickness of splice plate at x=0, L	$0 \rightarrow \infty$
$W_m(0)$, $W_m(L)$	Width of main plate at x=0, L	$2D \rightarrow 20D$
L	Joint length	
$t_0(0)$, $t_0(L)$	Thickness of 0° plies at x=0, L	$0 \rightarrow \infty$
$t_{90}(0)$, $t_{90}(L)$	Thickness of 90° plies at x=0, L	$0 \rightarrow \infty$
$t_{\pm\alpha}(0)$, $t_{\pm\alpha}(L)$	Thickness of $\pm\alpha$ plies at x=0, L	$0 \rightarrow \infty$
$(E/D)_m$	Main plate leading edge distance to diameter ratio	$2 \rightarrow 10$
$(E/D)_s$	Splice plate leading edge distance to diameter ratio	$1 \rightarrow \infty$

4.5 Design Constraints

Two different types of design constraints must be considered: Behavioral constraints and side constraints. Behavioral constraints eliminate various regions of the design space from consideration because those designs do not behave in an acceptable manner. Designs which violate failure criteria make up this category. Limitations on the range of values which a certain design variable may take on are called side constraints. Constraint equations denoted by C(I) are mathematical representations of these design constraints. They are written such that $0 < C(I) \leq 1$ if the I^{th} constraint is satisfied and $C(I) \rightarrow 0$ as a

constraint is about to be violated.

Consider the possible failures which could occur at each hole along the joint. They are: (1) bolt failure in shear, (2) splice plate failures in bearing, shear-out and net tension and (3) localized ply failures due to matrix splitting, fiber tensile failures and fiber compressive failures ahead of the bolt. A constraint equation must be written for each of these possible failure mechanisms.

As an example consider the test for a bolt failure in shear: The maximum shear stress, τ, acting on the bolt cross sectional area is compared to the effective shear strength of the bolt material, F_{SU}^{B}. Since

$$\tau = 0.5\ P_B/(\pi R^2) \tag{86}$$

a valid constraint equation to insure against a bolt failure in shear is given by

$$C(1) = 1.0 - (P_B/2\pi R^2)\ /\ F_{SU}^{B} \tag{87}$$

Similarly, to insure against splice plate failures at a given hole in bearing, shear-out and net tension we have respectively

$$C(2) = 1.0 - (P_B/Dt)\ /\ F_{BRU}^{S} \tag{88}$$

$$C(3) = 1.0 - (P_B/2tE)\ /\ F_{SU}^{S} \tag{89}$$

$$C(4) = 1.0 - \frac{(P_B+P_S)\ /\ t(S-D)}{F_{TU}^{S}} \tag{90}$$

The bolt load on the coupon being analyzed, P_B, and the skin load, P_S, are known from the bolt load partitioning analysis.

Next consider the possible composite main plate failures. Checks for possible matrix failure initiation must be made at three locations: In the 0° plies at θ=0°, in the α plies at θ=α and in the 90° plies at θ=90°. These three constraints are all written as

$$C(I) = 1.0 - \sigma_2/\sigma_{2_{ut}} \quad , \quad I = 5,7 \tag{91}$$

Checks for possible fiber tensile failures are also made at three locations; in the 0° plies at θ=90°, in the -α plies at θ=90°-α and in the 90° plies at θ=0°. These constraints are all written as

$$C(I) = 1.0 - \sigma_1/\sigma_{1_{ut}} \quad , \quad I = 8,10 \tag{92}$$

The last ply failure checks for a fiber compressive failure in the 0° plies directly ahead of the bolt, θ=0°.

$$C(11) = 1.0 - \sigma_1/\sigma_{1_{uc}} \tag{93}$$

Thus a maximum of eleven possible behavioral constraint equations are required to represent the joint failure criterion at each cut-out in a [0/±α/90] laminate.

The various side constraints can be expressed mathematically in a similar manner. For example, to insure that α remains in the range $30° \leq \alpha \leq 60°$ two constraint equations are required.

$$C(J) = 1.0 - 30°/\alpha \tag{94}$$

$$C(J+1) = 1.0 - \alpha/60° \tag{95}$$

For values of α between 30° and 60° the values of both constraint equations are seen to be between zero and one as required

4.6 Time Saving Techniques

The most significant time saving technique employed in the synthesis was the use of a series stress analysis to replace the very time consuming finite element analysis method. As discussed above, run times were improved by a factor of more than 600.

The most promising area for achieving additional significant time savings involves methods for changing the convergence characteristics of the synthesis procedure. A number of critical factors which affect convergence characteristics are discussed below.

The method selected for calculating an initial value for the draw-down factor, D_F, and the size of successive reductions in its value can greatly influence run time. Experience shows [21] that defining the initial value of D_F in such a way as to make the size of the initial penalty the same order of magnitude as the initial weight of the design improves convergence significantly. Also, the magnitude of the reduction in size of D_F for successive global optimizations can vary from 50% to 90%, depending on the accuracy with which the stress and strength analyses are performed. For consistently accurate

analyses reductions on the order of 80 to 90% are recommended. A reduction of 80% was used in this study. Reducing D_F too quickly can trap the design against a constraint surface; reducing it too slowly results in very poor convergence characteristics.

The decision made early in this study to use the forward difference method rather than the central difference method to calculate local gradient information definitely affected the program's convergence characteristics and resulting computer run times. The question here is whether the additional cost associated with calculating the gradient using central differences would be offset by an increased speed of convergence of the synthesis. The data available is really not sufficient to answer this question, although it is felt that the forward difference method is the more efficient of the two for this particular problem. The fact that the magnitudes of the partial derivatives of F with respect to the various design variables were usually small would tend to imply that the slight improvement in convergence charactertics due to a more accurate representation of ∇F would not compensate for doubling the time required to calculate ∇F using central differences.

Probably the most proven time saving technique involves the criterion used to define convergence of the series stress analysis. Four different convergence schemes were considered. They all involved careful adjustment of the convergence criterion in accordance with how

far along the optimization program had progressed. A schematic plot showing the value of γ as a function of location in the optimization procedure is shown in Figure 22. The first method is by far the most time consuming but it has the most consistent convergence characteristics. The average time required to perform a single coupon stress analysis using method 1 is 0.17 seconds. The average time required by both methods 3 and 4 was only 0.06 seconds per fastener. Method 4 is preferred over 3 in this study since it had one major advantage over method 3. Problems which involved initial designs which were close to one or more constraint boundaries often ran into convergence problems using method 3 but did not using method 4. Method 2 involved performing refined analyses at certain critical points in the analysis with a much less refined analyses performed the remainder of the time. This method did not work at all. Designs which were predicted capable of carrying the applied load using the rather crude convergence criterion were often found to be outside the feasible region when the refined convergence criterion was applied. This resulted in the program getting trapped outside the feasible region and forced execution to terminate. The use of methods 3 and 4 in place of method 1 cut run times by a factor of three.

Two other factors should be mentioned. Results show that run times decrease and convergence characteristics improve as initial designs are selected which are more efficient load carriers. Finally,

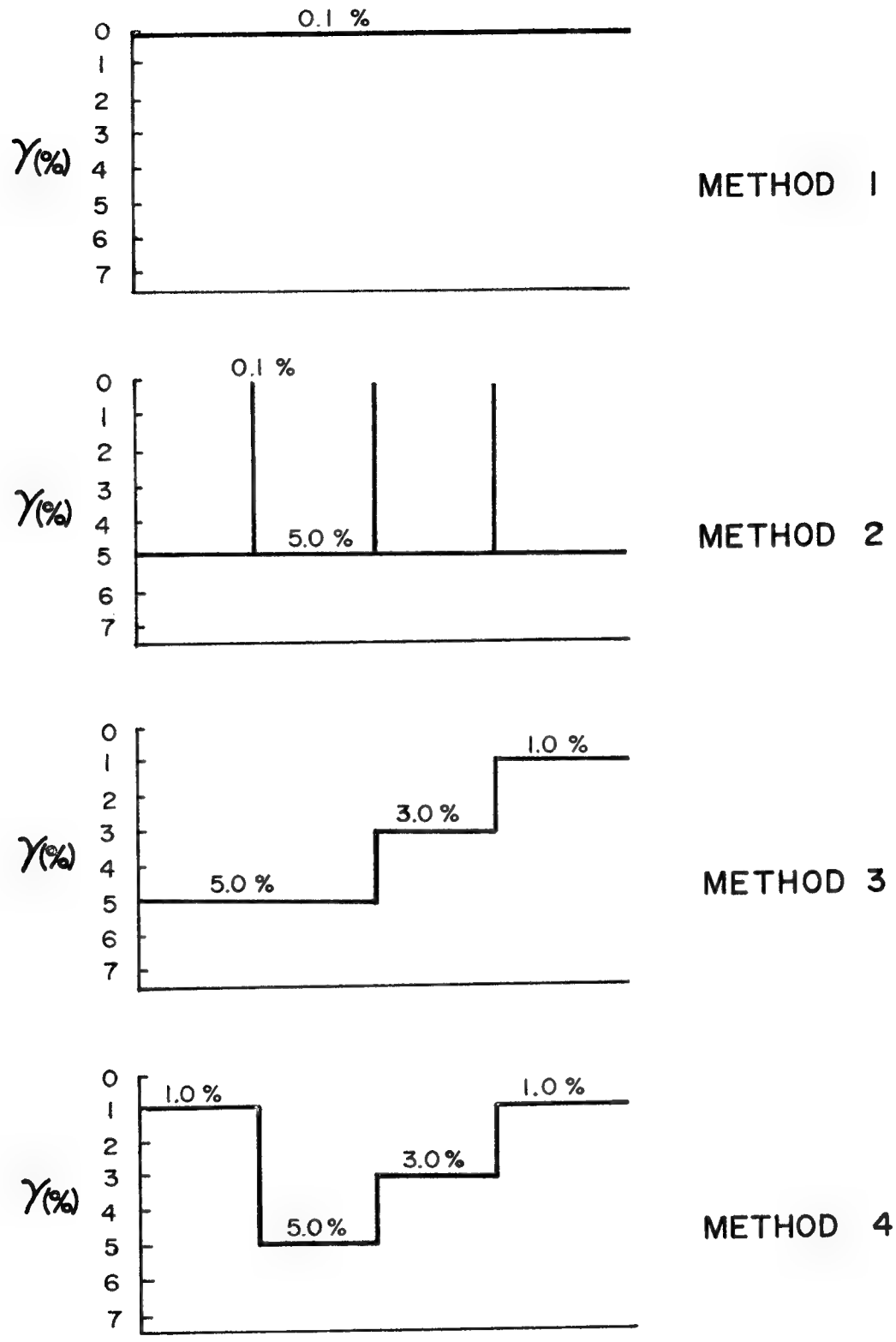

Figure 22. Methods for Converging the Series Solution Stress Analysis

when using interior penalty functions it is recommended [21] that initial designs be selected as close to the center of the feasible region as possible. The user, therefore, should make a serious effort to select an efficient initial design which is not near any of the constraint surfaces, preferably an equal distance away from several surfaces simultaneously.

CHAPTER V

SYNTHESIS RESULTS AND OBSERVATIONS

5.1 Introduction

The original goals of the synthesis were two-fold. The first was to develop an automated preliminary design procedure for multiple fastener joints. The second was to identify, if possible, common characteristics of minimum weight designs. Two sets of related problems were selected for analysis. The specific goal was to determine the effects of imposing different constraint combinations on the same design problem and to generate detailed information regarding the effects of material tailorability.

The results of these example problems are summarized in Table 14. In all cases the main plate material system is graphite-epoxy, the splice plates are made of 6Al-4V titanium and the bolts are made of steel, having an effective shear strength of 130,000 psi. The desired design ultimate load in each case is 18,700 pounds. A joint containing only three fasteners was selected to save computer time. In the optimization procedure an integer, I_{MAX}, must be specified to limit the number of times the program will reduce the draw-down factor and seek global minimums. A value of $I_{MAX} = 6$ was used for each of the problems. It was found, however, that some problems were not able to fully converge in only six passes through the optimization procedure. Since the convergence problems encountered did not adversely affect the program's ability to

Table 14. Summary of Synthesis Results

PROB	DESCRIPTION PREASSIGNED VARIABLES LISTED	BOLT ROW	LAMINATION % 0° PLIES	BOLT LOAD DISTRIBUTION % P_{ULT}	FAILURE MODES	COMPONENT WEIGHTS W_M, W_S, W_B, W	PREDICTED FAILURE LOAD	$\frac{LOAD(LB_F)}{WEIGHT(LB_F)}$
1	ANALYSIS OF PROPOSED INITIAL DESIGN (ID)	1 2 3	50 50 50	50 0 50	MP-S_P	0.672 1.600 0.115 2.387	22,200	9,300
2	USES 1 AS ID, ALPHA=45, $T_{90}(0)=T_{90}(L)=0$ No MP-SP COMPATIBILITY REQ'T	1 2 3	67 47 36	12 9 79	MP-T MP-T SP-T,B	0.098 0.051 0.081 0.230	18,900	82,000
3	USES 1 AS ID, ALPHA=45, $T_{90}(0)=T_{90}(L)=0$	1 2 3	48 45 42	16 6 78	MP-T SP-B	0.104 0.058 0.088 0.250	18,700	75,000
4	USES 1 AS ID, ALPHA=45, $T_{90}(0)=T_{90}(L)=0$ BOLT SHEAR STRENGTH + 50%	1 2 3	40 38 36	33 15 52	MP-T, SP-SO MP-T BOLT-S_H	0.081 0.127 0.072 0.280	18,700	67,000
5	USES 1 AS ID, ALPHA=45, $T_{90}(0)=T_{90}(L)=0$ NO TAPER IN PLATE WIDTHS	1 2 3	53 49 45	23 3 74	MP-T MP-T,S_P SP-T	0.269 0.206 0.110 0.585	20,300	34,500
6	ID, 0/±45/90 QI	1 2 3	57 52 45	11 7 82	SP-T	0.182 0.101 0.119 0.402	18,900	47,000
7	USES 1 AS ID, $T_{90}(0)=T_{90}(L)=0$	1 2 3	40 41 42	18 4 78	MP-T,SP SP-T,B	0.159 0.095 0.093 0.347	19,300	55,500
8	ID, $0_2/\pm35$, $T_{90}(0)=T_{90}(L)=0$	1 2 3	34 30 25	19 3 78	MP-T BOLT-S_H	0.212 0.116 0.104 0.432	23,100	53,500
9	ID, $0_2/\pm55$, $T_{90}(0)=T_{90}(L)=0$	1 2 3	59 56 53	16 3 81	MP-T SP-T	0.309 0.174 0.098 0.581	18,900	32,500

MP	Main plate	ID	Initial design
SP	Splice plate	QI	Quasi-isotropic
T	Tension	W_M	Weight of main plate
B	Bearing	W_S	Total weight of splice plates
SO	Shear-out	W_B	Total weight of bolts
S_p	Splitting	W	Total weight of joint
S_H	Shear		

to provide sufficient data to answer the important questions asked above, the problems affected were not rerun to full convergence.

A proposed initial design was selected which was able to carry the desired design ultimate load and is listed as problem 1 in the table. The entire length of the main plate is a $(0_2/\pm45)$ laminate. The main plate and splice plates are of the same constant width and they are both of constant thickness. The program's analysis package was used to analyze the proposed initial design. Although the predicted failure load of the design is only 20% greater than the desired design ultimate load, the design is a poor one. No attempt was made to taper the joint, minimize its width or decrease its length to increase its efficiency. The measure of joint efficiency used here is load carried per pound of joint material. The initial design is critical in a splitting mode ahead of the third bolt.

5.2 Effects of Geometric Constraints

Using problem 1 as an initial design, four problems (problem 2 through problem 5) were run to investigate the effects of various design constraint combinations on joint efficiency. As additional constraints are imposed (i.e., moving from problem 2 to problem 5) the efficiency of the individual minimum weight designs decreases drastically. A direct comparison of the various minimum design weights is not really possible since all the designs did not converge according to the same

convergence criterion. Several runs terminated prematurely due to problems involving the program's inability to recover from accidentally stepping out of the feasible region; others converged very slowly and terminated after completing the prespecified number of cycles through the optimization loop.

In problem 2 an unrealistic design was achieved and is illustrated in Figure 23. The synthesis procedure built up the main plate thickness at the end to enable the third bolt to carry 79% of the design ultimate load in bearing. The local laminate consists of nearly two-thirds ±45° plies to prevent a matrix failure in the 0° plies ahead of the bolt. The remainder of joint acts as a tension coupon, carrying the load back into the composite structure. Since the bearing loads on bolts 1 and 2 are small, a laminate consisting of two-thirds 0° plies is used to carry the load efficiently around the cut-outs, although the presence of these two unloaded holes makes the overall design appear to be an inefficient one. A single fastener joint design having the same characteristics as the leading edge fastener would appear to be preferred over this proposed minimum weight multiple fastener design.

Another problem with this design is that the main plate and splice plates are physically incompatible. Bending the splice plates to fit the main plate would induce undesirable bending effects. As a result an additional constraint was then imposed which requires geometric compatibility between the plates; the thickness of the main

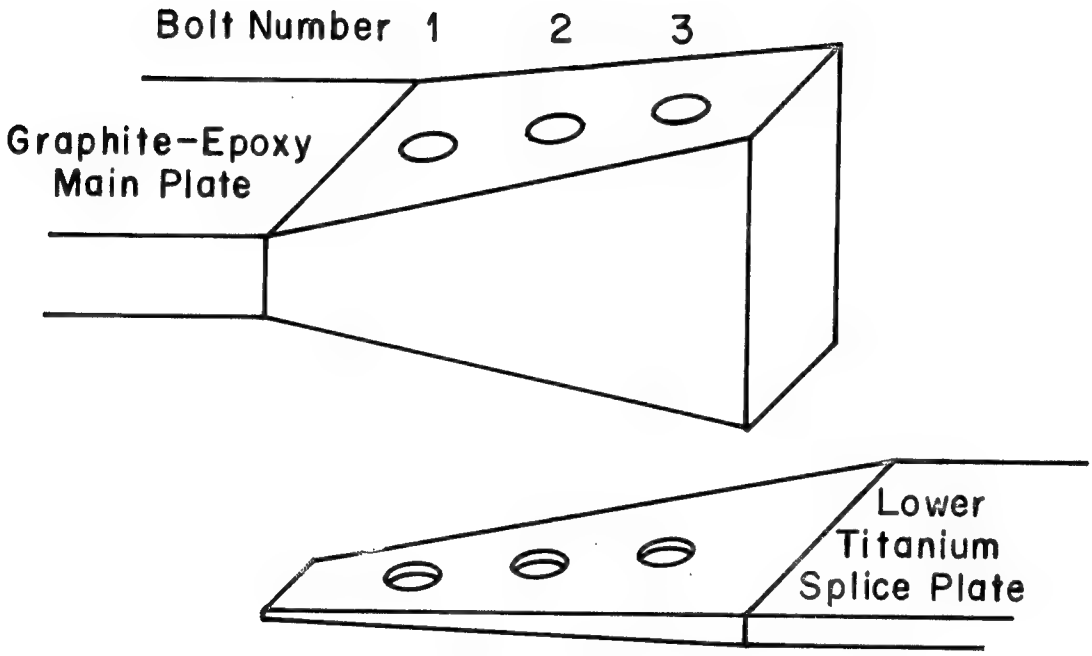

Figure 23. An Unrealistic, Incompatible Joint Design

plate at x = L was forced to be less than that at x = 0. Problem 3 represents a rerun of problem 2 subject to this additional compatibility requirement. The new minimum weight design has a nearly constant thickness main plate. The weight penalty and the resulting loss in efficiency due to the additional constraint, however, are small. As a result this compatibility constraint was incorporated in the synthesis program for all later analyses.

In problem 4 the bolt shear strength has been reduced by 50%. This will limit the load which the third bolt can carry since the third bolt was nearly critical in shear in problems 2 and 3. The bolt load distribution for problem 4 is much more uniform than for the previous two problems, as expected. Again a small weight penalty is paid as a result of the additional constraint. It is interesting to note that a single fastener joint design cannot be used here due to the reduced shear strength of these bolts. The leading edge fastener is critical in shear in this design which strongly influences the design's configuration.

In problem 5 an additional constraint was imposed: The main plate and splice plate widths were not permitted to taper and were required to remain equal to one another, although the actual joint width was permitted to vary. This constraint proved to be a very severe one, in that the joint efficiency was nearly cut in half.

5.3 Effects of Material Tailorability

The last four problems analyzed focus on the effects of material tailorability. In problem 6 a (0/±45/90) quasi-isotropic laminate was used as an initial design. During the optimization the 90° plies were completely eliminated, first at x = 0 then at x = L. The minimum weight design should have converged to the same design as did problem 3, but it did not, as can be seen by the predicted failure load.

In problems 7-9 the value of α was also permitted to vary. The program was unable to significantly change the value of α in any of the three cases. In problem 7 α increased from 45.0° to 45.1°, in problem 8 it increased from 35.0° to 36.8° and in problem 9 it decreased from 55.0° to 54.7°. Throughout all three runs the magnitude of $\partial F/\partial\alpha$, the partial derivative of the objective function with respect to α, was much smaller than that of the partial derivatives with respect to the other active design variables. As a result the program was biased toward changing the other variables and did very little to α. A very significant difference in the results was apparent, however. The value of $\partial F/\partial\alpha$ for $\alpha \tilde{=} 45°$ fluctuated about zero throughout the synthesis for problem 7. In problem 8 the value of $\partial F/\partial\alpha$ was always negative which indicates that F could be reduced by increasing the value of α from 35°. In problem 9 the value of $\partial F/\partial\alpha$ was always positive which indicates that F could be reduced by decreasing the value of α from 55°. The results, therefore, tend to indicate that α=45° is not only preferred

to α=35° and 55°, but that α=45° is close to an optimum value.

5.4 Convergence Problems

The relative efficiencies of problems 7-9 are somewhat misleading since they all converged very slowly. The extremely low efficiency for the [0/±55] laminate, problem 9, is due to a convergence problem involving one particular design variable, the leading edge distance of the main plate, $(E/D)_m$. The convergence problem here is very similar to that discussed above for α. As the synthesis proceeds the magnitude of $\partial F/\partial[(E/D)_m]$ remains small compared to the other partial derivatives and, as a result, significant changes in $(E/D)_m$ are not made for a considerable period of time. This same problem was observed in the early stages of several of the other example problems but in those cases the program was able to make significant changes in the value of $(E/D)_m$ during the last few iterations. Experience with the convergence problem indicates that if problem 9 were permitted to cycle through the optimization loop several more times it would converge to a much more efficient design having a shorter overall length.

Several possible causes for these convergence problems have been suggested [21]. The most probable source of difficulty involves the draw-down factor, D_F. It is recommended [21,23] that the initial value of D_F be selected such that the value of the penalty term be nearly equal to the initial joint weight. The manner of calculating

the initial value of D_F in this study, equation (82), does just that. The recommended reduction in size of D_F from one loop to the next is between 50 and 90%; the more accurate the stress and strength analyses, the larger the reduction. A value of 80% was used in this study. If the initial value of D_F is too large and/or the successive reductions in D_F too small, the synthesis will converge very slowly. This appears to be the case in this study. Two possible courses of action could be taken to alleviate this problem: Either appropriately modify the program's method of calculating initial values of D_F and also modify the method for successively reducing its magnitude, or simply allow for several additional passes through the optimization loop. The simplest and probably the best solution is the latter. Run times are presently short enough that permitting several additional passes through the optimization loop would not result in excessively long run times. A comparison of solution run times is presented in Table 15 which also indicates the type of convergence problem encountered in each case. Modifying the optimization procedure to solve problem 9 more efficiently would likely have an adverse effect on the convergence characteristics of some of the other example problems. As a result it was felt that additional modifications to the synthesis procedure were unwarranted.

Table 15. Comparison of Synthesis Run Times

Problem Number	Synthesis Run Time[1] (sec.)	Total Number of Joint Analyses Performed	Run Time Per Single Fastener (sec.)	Stress Anal. Conv. Criterion, γ(%)	Convergence Problems Encountered
1	N/A	1	N/A	0.1	N/A
2	177	1067	0.055	5 - 3 - 1	None
3	179	1051	0.056	5 - 3 - 1	None
4	162	961	0.056	5 - 3 - 1	None
5	184	365	0.168	0.1	2
6	149	563	0.088	1.0	3
7	156	718	0.073	1.0	3
8	373	825	0.151	0.1	2
9	288	542	0.177	0.1	3

[1] Times are for a UNIVAC 1108.

[2] Accidentally stepped outside the feasible region and was unable to recover.

[3] $\partial F/\partial[\ (E/D)_m\ ]$ too small after six loops through the optimization procedure to warrant reducing $(E/D)_m$.

5.5 Summary

The results of the reported syntheses show that joint efficiencies decrease significantly as designs become more highly constrained. For designs with little or no constraints imposed on them by the designer, single fastener joints appear to be preferred over multiple fastener designs. A common characteristic of efficient bolted joint designs, for a variety of different constraint combinations is exhibited, and involves a specific failure mode combination. The main plate and splice plates are critical in net tension at most fastener locations while the main plate is critical in splitting at the outermost fastener. The splice plate exhibits either bearing or shear-out at the outermost fastener. A related result is that uniform bolt load distributions in metal-to-composite joints are not necessary to induce such failure mode combinations.

Several interesting observations were made concerning the effect of material tailorability on joint efficiency. When a quasi-isotropic, (0/±45/90), laminate was used as an initial design, the optimization routine quickly elminated the 90° plies throughout the joint. The advantages of using 90° plies to prevent splitting failures of the 0° plies ahead of the bolts is far outweighed by the problem of preventing matrix failures of the 90° plies themselves. Hence they are eliminated. The limited data also tends to favor the use of ±45° plies as the most

efficient cross ply angles, $\pm\alpha$, for the laminate class considered, $[0/\pm\alpha/90]$.

For the convenience of the user the program has been setup such that a proposed design which cannot carry the desired design ultimate load will be accepted as an initial design. The program automatically resizes the design, if possible, to enable it to carry the desired load before any attempts are made to minimize the weight of the joint. The disadvantage of proposing a poor initial design is that the synthesis convergence characteristics are degraded. However, the task of picking an initially valid design is enormous in most cases involving geometric constraints. Thus, the penalty of slower convergence when using the ultimate load as a variable is clearly acceptable.

CHAPTER VI

CONCLUSIONS

Experience [24,25,26] has shown that the potential weight savings available through the use of composite materials are severely penalized due to an inability to design efficient bolted joints in composites. Conventional design techniques used in conjunction with existing design data are insufficient to predict the failure characteristics of these joints. Premature failures of composite joints are often observed in unexpected failure modes [26]. The existence of unique failure modes attributable to the anisotropy of the material makes it very difficult to correlate failure data with nominal strength based design procedures [27, 28]. The need to consider the detailed stress field in the vicinity of a bolted hole in a composite joint to predict failure was apparent at the outset of the current study.

The development of a conservative strength analysis capability for such joints was the first real success achieved in this investigation. A successive failure analysis based on a simple maximum ply stress failure criterion was found capable of conservatively predicting the failure characteristics (i.e., failure load and mode) of a number of single fastener coupons using finite element results. This simple strength analysis, used in conjunction with the joint modeling procedure and bolt load partitioning analysis described herein, was found capable of conservatively predicting the failure characteristics (i.e., failure loads, modes and locations) of several multiple fastener joints.

The development of an analysis capability alone for joint designs is not, however, the tool which a designer really needs to design efficient joints in composites. The large number of design variables which must be considered in formulating an efficient (i.e., minimum weight) design is too large for the designer to handle in a conventional analysis-resizing iterative solution. An extremely efficient stress analysis package, which proved to be some 600 times faster than a comparably accurate finite element solution, was developed and substituted in place of the finite element method in the joint stress analysis. The ability to rapidly perform a conservative strength analysis of an entire proposed joint design enabled automation of the tedious analysis-resizing cycle.

While an efficient, automated preliminary design tool should be a real aid to the designer, the identification of common characteristics of minimum weight designs may prove even more useful to the designer in his everyday calculations. The results of a number of carefully selected example problems run using the synthesis procedure provide some important conclusions for the basic design philosophy of bolted joints.

A combination of failure modes has been identified which is common to all the minimum weight designs achieved in the limited number of problems considered. The failure pattern is independent of constraint combinations although significant weight penalties are paid as designs become more highly constrained. In the case of designs which are not

highly constrained it appears that single fastener coupons are preferred over multiple fastener joints. The effects of material tailorability are somewhat surprising. The results indicate that the [0/±45] family of laminates is preferred over all possible families belonging to the [0/±α/90] class. The use of the correction factor data generated for the [0/±45] family of laminates in the synthesis procedure may have biased the program toward this family. As a result of this limited study it is questionable whether this conclusion is generally applicable to all joint problems.

In using the synthesis procedure the user need not specify a design which can carry the desired design ultimate load. The program treats the applied load as a variable, initially resizes the specimen to carry the desired design ultimate load and then seeks a minimum weight design which satisfies all the constraints imposed on it by the user. Since an approximate stress analysis is utilized in the synthesis, the proposed minimum weight design should be reanalyzed using more refined analysis procedures (e.g., the finite element or boundary-integral equation method). If modifications to the design are necessary, sensitivity information from the synthesis regarding the various geometric design variables (e.g., gradient information) can be used to aid in minor resizing.

The conclusions discussed above may be valid only for the particular problem analyzed herein. That is, a metal-to-composite multiple fastener joint consisting of a single column of fasteners

loaded in simple tension. It is felt that more complicated problems, involving joints consisting of a series of columns of adjacent fasteners, under more complex loading situations (i.e., combinations of tension or compression with shear, torsion or bending) could be handled in a very similar manner. Additional anisotropic correction factor data for these more complex loading situations would be required to facilitate the use of infinite plate solutions based on the theory of anisotropic elasticity.

To justify further efforts in developing synthesis procedures for such joints, however, it is felt that two prerequisite studies must be completed. The first involves utilizing the synthesis procedure developed herein to solve a number of design problems, accompanied with experimental verification, to really demonstrate the method's capabilities. The second study involves gaining a better understanding of the actual failure mechanism which governs the strength of a composite laminate in the vicinity of a stress concentration. Experimental programs similar to those discussed above [10,11] will be required to gain additional insight into this area, particularly for combined states of loading.

It is clear that the computerized analysis tool developed herein cannot be treated as a "black box"; extensive user interaction is required. Through careful application the results of this work should prove to be of great value in the preliminary design stages of multiple fastener joints in composites.

REFERENCES

1. Ashton, J. E., Halpin, J. C., and Petit, P. H., *Primer on Composite Materials: Analysis*, Technomic Publishing Co., Inc. (1969).
2. *Strength of Metal Aircraft Elements*, Military Handbook MIL-HDBK-5, March 1961.
3. Waszczak, J. P. and Cruse, T. A., "Failure Mode and Strength Predictions of Anisotropic Bolt Bearing Specimens", *Journal of Composite Materials*, 421 (July 1971).
4. Pipes, R. B. and Pagano, N. J., "Interlaminar Stresses in Composite Laminates Under Axial Extension", *Journal of Composite Materials*, Vol. 4 (1970) 538.
5. Puppo, A. H. and Evensen, H. A., "Interlaminar Shear in Laminated Composites under Generalized Plane Stress", *Journal of Composite Materials*, Vol. 4 (1970) 204.
6. Lekhnitskii, S. G., *Theory of Elasticity of an Anisotropic Elastic Body*, Holden-Day, Inc. (1963).
7. Zienkiewicz, O. C., *The Finite Element Method*, McGraw-Hill Publishing Company, 38 (1967).
8. Cruse, T. A., "Boundary-Integral Equation Solution Methods", in *Interactive Program for Analysis and Design Problems in Advanced Composites Technology*, T. A. Cruse and J. L. Swedlow, Eds., AFML-TR-71-268, December 1971.
9. Advanced Composite Technology, Fuselage Program - Phase I, Second Quarterly Progress Report, General Dynamics, 90-110 (February 1970).

10. Waddoups, M. E., Eisenmann, J. R., and Kaminski, B. E., "Macroscopic Fracture Mechanics of Advanced Composite Materials", Convair Aerospace Division of General Dynamics, FZM-5670, (February 1971).

11. Eisenmann, J. R., Convair Aerospace Division of General Dynamics Corporation, Fort Worth, Texas, Private Communication (1971).

12. Bickley, W., "The Distribution of Stress Round a Circular Hole in a Plate", *Phil. Trans. Roy. Soc., A.* (London), 227, 383 (1928).

13. Peterson, R. E., *Stress Concentration Design Factors*, John Wiley and Sons, Inc., 99 (1966).

14. Timoshenko, S. and Goodier, J. N., *Theory of Elasticity*, Second Edition, McGraw-Hill Book Company, 80 (1951).

15. Peterson, R. E., *Stress Concentration Design Factors*, John Wiley and Sons, Inc., 84 (1966).

16. Howland, R. C. J., "Stresses in a Plate Containing an Infinite Row of Holes", *Proc. Roy. Soc.* A (London), Vol. 148 (1935) 471.

17. Peterson, R. E., *Stress Concentration Design Factors*, John Wiley and Sons, Inc., 91 & 94 (1966).

18. Davidon, W. C., *Variable Metric Method for Minimization*, AEC Research Development Report ANL-5990, (Rev.), 1959.

19. Fletcher, R. and Powell, M. J. D., "A Rapidly Convergent Descent Method for Minimization", *The Computer Journal* 6 (1963) 163-168.

20. Fox, R. L., *Optimization Methods for Engineering Design*, Addison-Wesley Publishing Co., Inc. (1971).

21. Schmit, L. A., University of California, Los Angeles, Los Angeles, California, Private Communication (1973).

22. Tocher, J. L. and Karnes, R. N., "The Impact of Automated Structural Optimization on Actual Design", Proc. AIAA/ASME 12th Structures, Structural Dynamics, and Materials Conference, Anaheim, California, April 1971.

23. McCullers, L. A., Convair Aerospace Division of General Dynamics Corporation, Fort Worth, Texas, Private Communication (1972).

24. Advanced Composite Wing Structures - Volume I, Engineering, Grumman Aerospace Corporation, Technical Report AFML-TR-70-231, 150-166 (December 1970).

25. Boron/Epoxy Wing Skins, F-100D Aircraft Structural Design and Analysis - Volume I, Los Angeles Division of North American Rockwell Corporation, Technical Report AFML-TR-71-29, 155 (August 1971).

26. Advanced Development of Boron Composite Wing Structural Components, Convair Aerospace Division of General Dynamics, AFML-TR-70-261, 66 (December 1970).

27. Advanced Composite Wing Structures Boron-Epoxy Design Data - Vol. II, Grumman Aerospace Corporation, 177-191 (November 1969).

28. Advanced Composite Technology, Fuselage Program - Phase I, Third Quarterly Progress Report, General Dynamics, 107-122, (1 February 1970).

29. Advanced Composite Technology, Fuselage Program - Phase I, Second Quarterly Progress Report, General Dynamics, 164-172, (1 November 1969).

30. Coker, E. G. and Filon, L. N. G., *Photo-Elasticity*, Cambridge, 524-530 (1957).

31. Investigation of Joints in Advanced Fibrous Composites for Aircraft Structures, Air Force Flight Dynamics Laboratory, 13, (June 1969).

32. Daniels, I. M., IIT Research Institute, Chicago, Illinois, Private communication (1971).

33. Peterson, R. E., *Stress Concentration Design Factors*, John Wiley and Sons, Inc., 92 & 95 (1966).

34. Roberts, R. H., Convair Aerospace Division of General Dynamics Corporation, Fort Worth, Texas, Private communication, Drawing Number FW7006048 (June 1971).

APPENDIX A

FINITE ELEMENT ANALYSES OF SINGLE FASTENER COUPONS

Introduction

This study investigates the stress concentrations induced in anisotropic plates loaded by means of a single fastener hole. The study is an attempt to further understand the failure characteristics of such bolted joints. The development of a prediction capability for both failure mode and ultimate load is the major goal of this work. An implied goal is an evaluation of three proposed anisotropic failure criteria; the maximum ply stress, maximum ply strain and Tsai-Hill criteria.

Finite Element Model

A constant strain, finite element computer program using triangular elements was modified to handle anisotropic composite materials using lamination theory as presented in [1]. The experimental work done on bolt bearing specimens, from which this study draws heavily, only considered specially orthotropic laminates. That is, laminates which are mid-plane symmetric and are angle-plied. As a result, this numerical study is also limited to this class of laminates. It is important to remember that the use of lamination theory ignores interlaminar shear; consequently it is expected that the degree of error in the results will

vary with specimen anisotropy.

The design of a finite element grid representation to simulate bolt bearing test specimens was subject to two major considerations. First, the grid had to be sufficiently detailed around the bolt hole to pick up the large stress gradients which are induced in this area. Secondly, the number of elements and nodes was restricted by the storage capacity of the computer. Taking advantage of the two lines of specimen symmetry shown in Figure A-1 only one-fourth of the specimen was included in the finite element simulation. Figure A-2 shows a computer plot of the specimen section for E/D = 5.0, S/D = 10.0, and HL/D = 20.0. The grid representation used contains 480 elements and 279 nodes. The condition of specimen symmetry is met by forcing the x-displacement of the vertical line of symmetry and the y-displacement of the horizontal line of symmetry to be zero in each computer run. Typical run time for an analysis using this grid on a UNIVAC 1108 is 40 seconds. A computer subroutine was also developed which transforms the co-ordinates of the grid shown in Figure A-2 to any desired specimen geometry, i.e., E/D, S/D, HL/D.

To check whether or not the grid was sufficiently detailed around the hole an isotropic test case was run. A uniform tension stress was applied to the ends of the specimen. Comparison with results presented in [14] (See Figures A-3a and A-3b) indicated that further refinement of the finite element mesh around the hole was not necessary. The

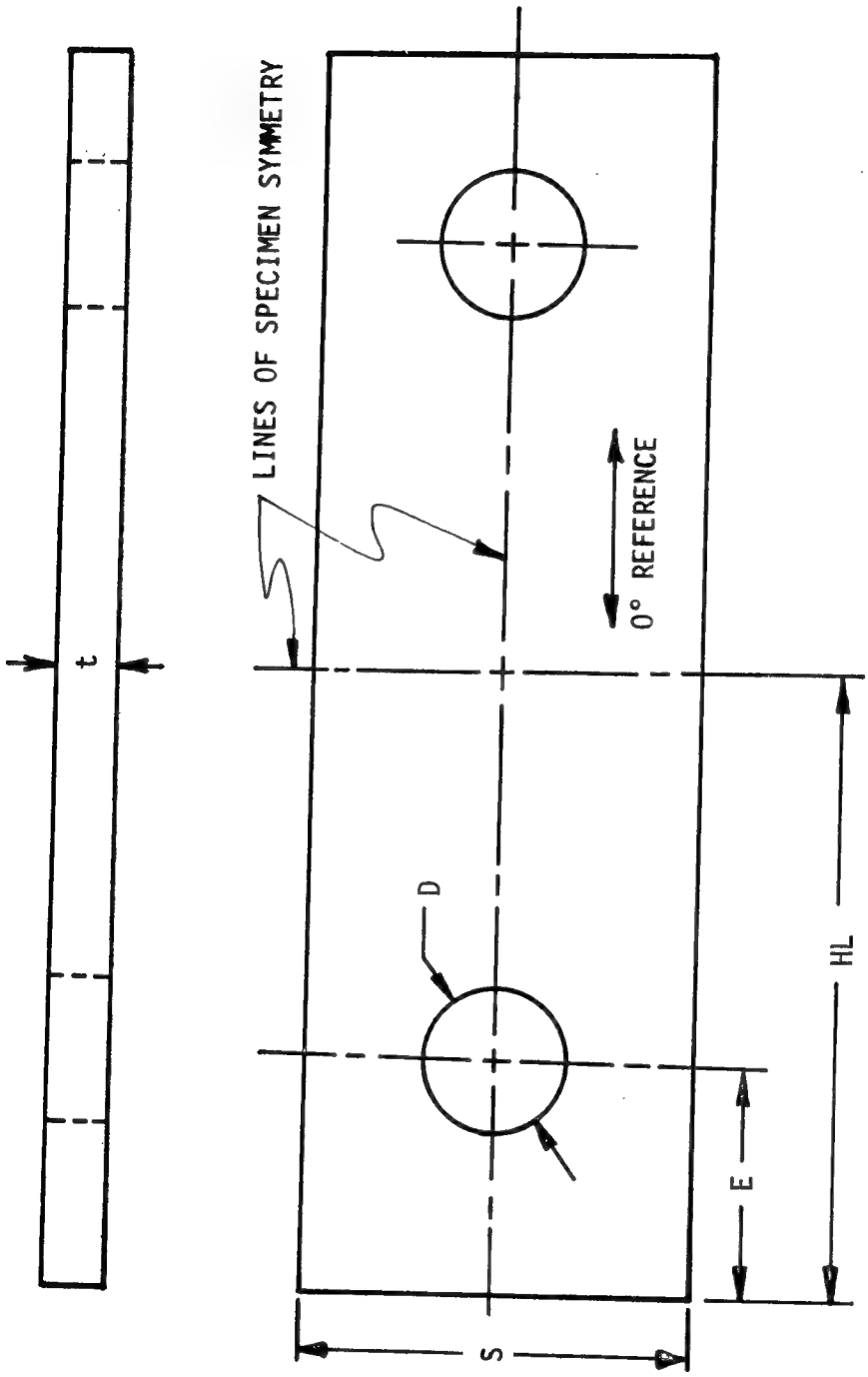

Figure A-1. Bolt Bearing Test Specimen

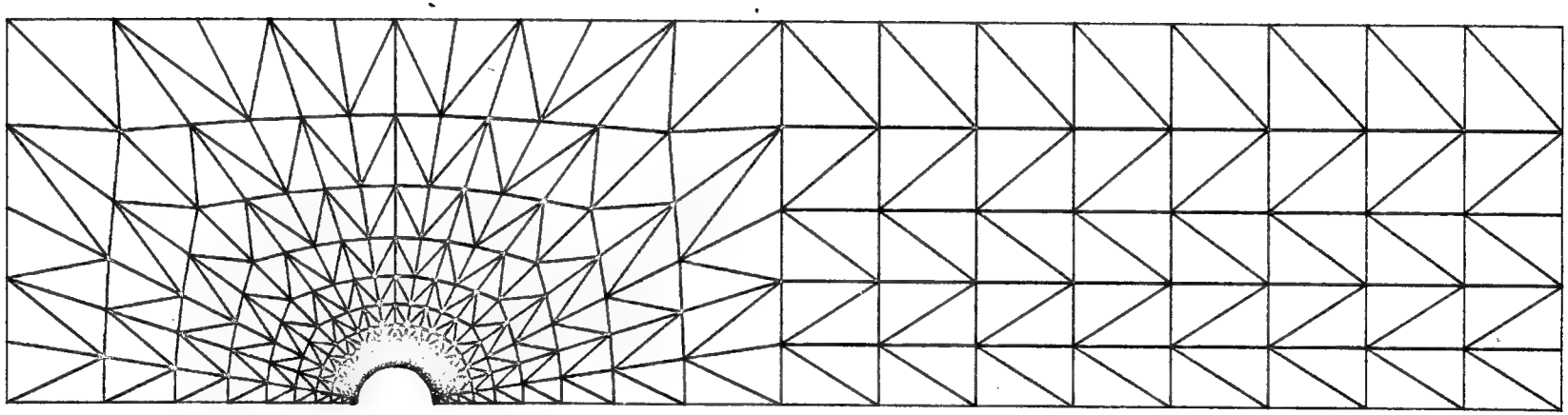

Figure A-2. Finite Element Grid Representation for a Bolt Bearing Specimen

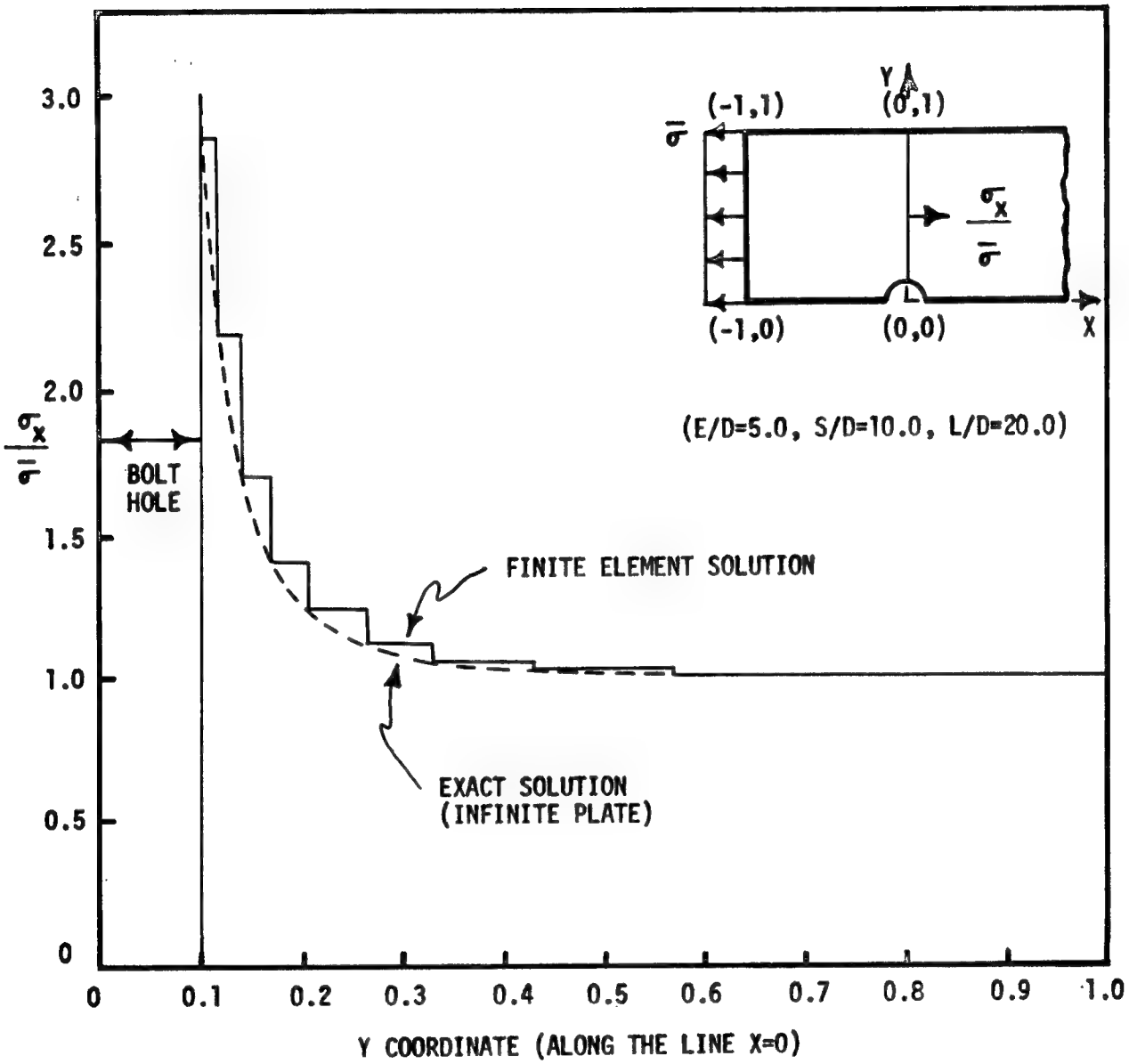

Figure A-3a. Isotropic Bolt Bearing Verification: $\sigma_x/\bar{\sigma}$ vs Y

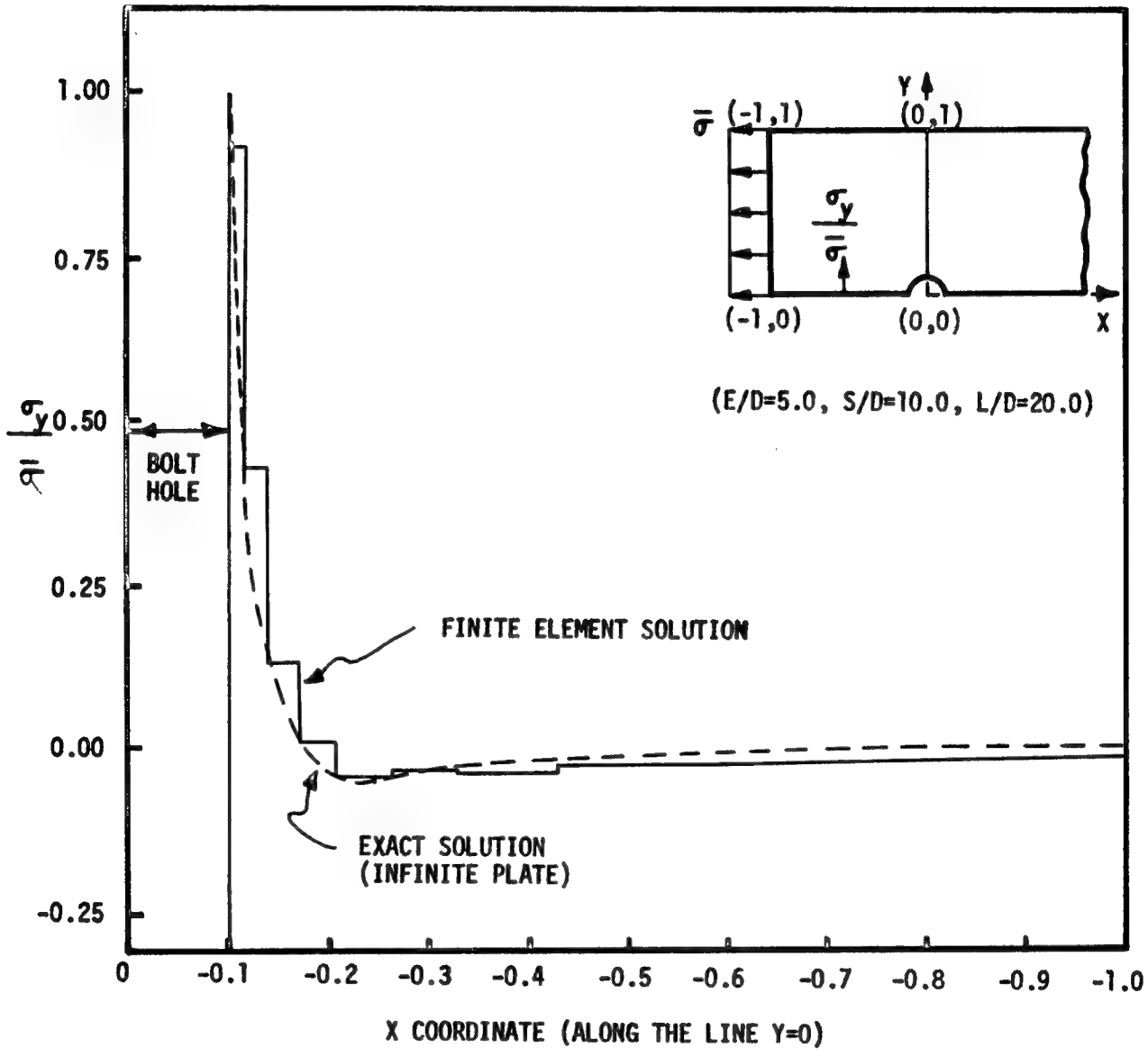

Figure A-3b. Isotropic Bolt Bearing Verification: $\sigma_y/\bar{\sigma}$ vs X

observation that the computed finite element values of stress are higher than the exact values agrees well with the results illustrated in [7].

A cosine distribution of normal stress acting over the upper half of the hole surface was used to simulate the resulting stress distribution caused by the bolt. The interaction was, therefore, assumed to be frictionless. Bickley [12] shows this to be an excellent approximation for isotropic bolt bearing specimens. A finite element analysis of the bolt-specimen interaction in certain composite laminates was performed at General Dynamics [29]. The cosine distribution of normal stress was again shown to be a realistic approximation of the interaction stresses.

Further confidence was gained in both the cosine distribution and the grid mesh by running an isotropic bolt bearing test program and observing the qualitative agreement of the computed stress field around the hole surface (See Figure A-4) with work by Coker and Filon [30]. The specimen used in their study had significantly larger values of E/D and S/D and thus a quantitative comparison was not performed.

Finally, two other normal distributions of stress, which were significantly different from the cosine distribution (See Figure A-5), were used as the bolt-specimen interface stress boundary condition for one of the composite material specimen runs. The net force in the load direction in each case was the same. It was observed that significant variance about the cosine distribution resulted in

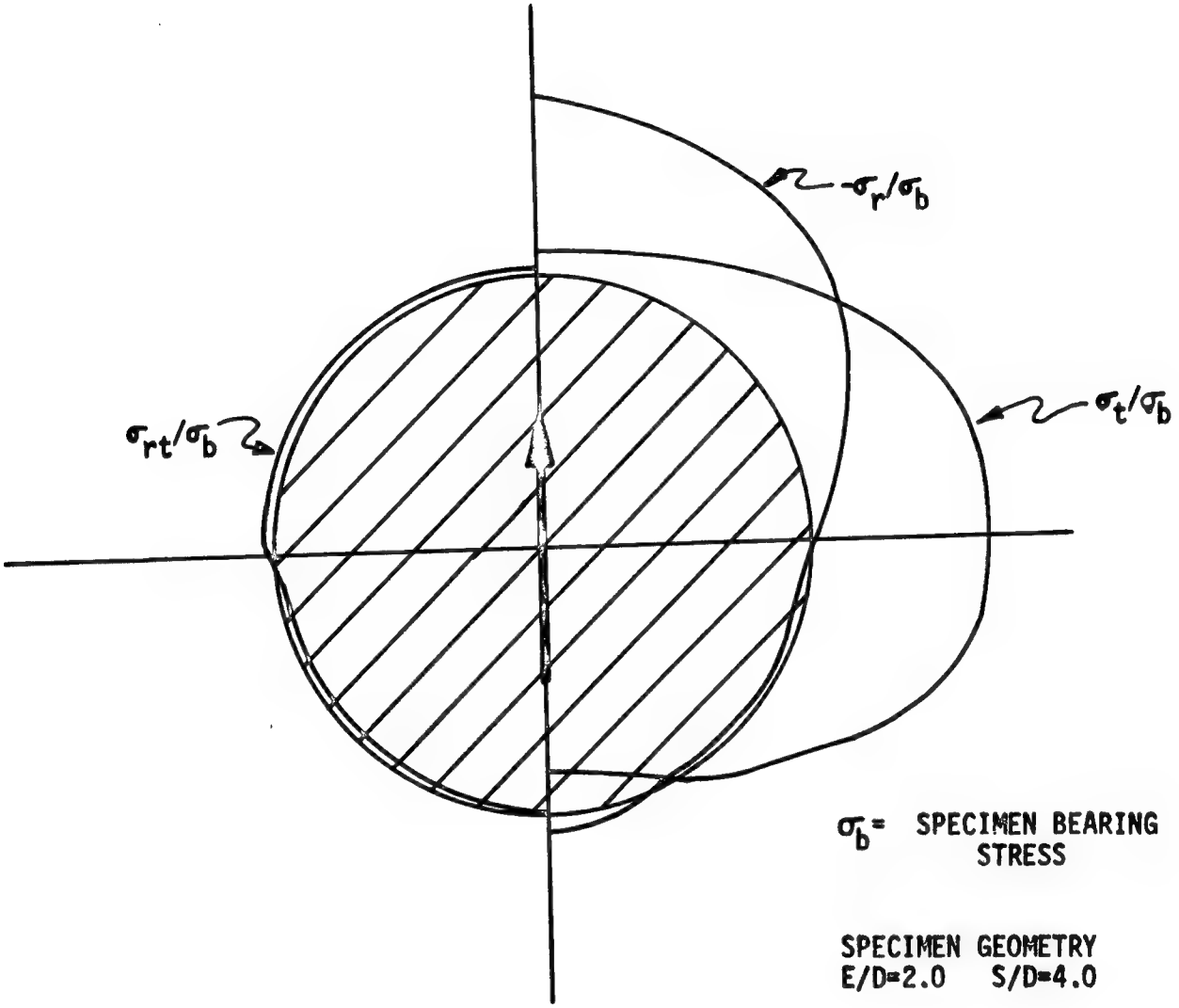

Figure A-4. Polar Plot of Edge Stresses for an Isotropic Test Run

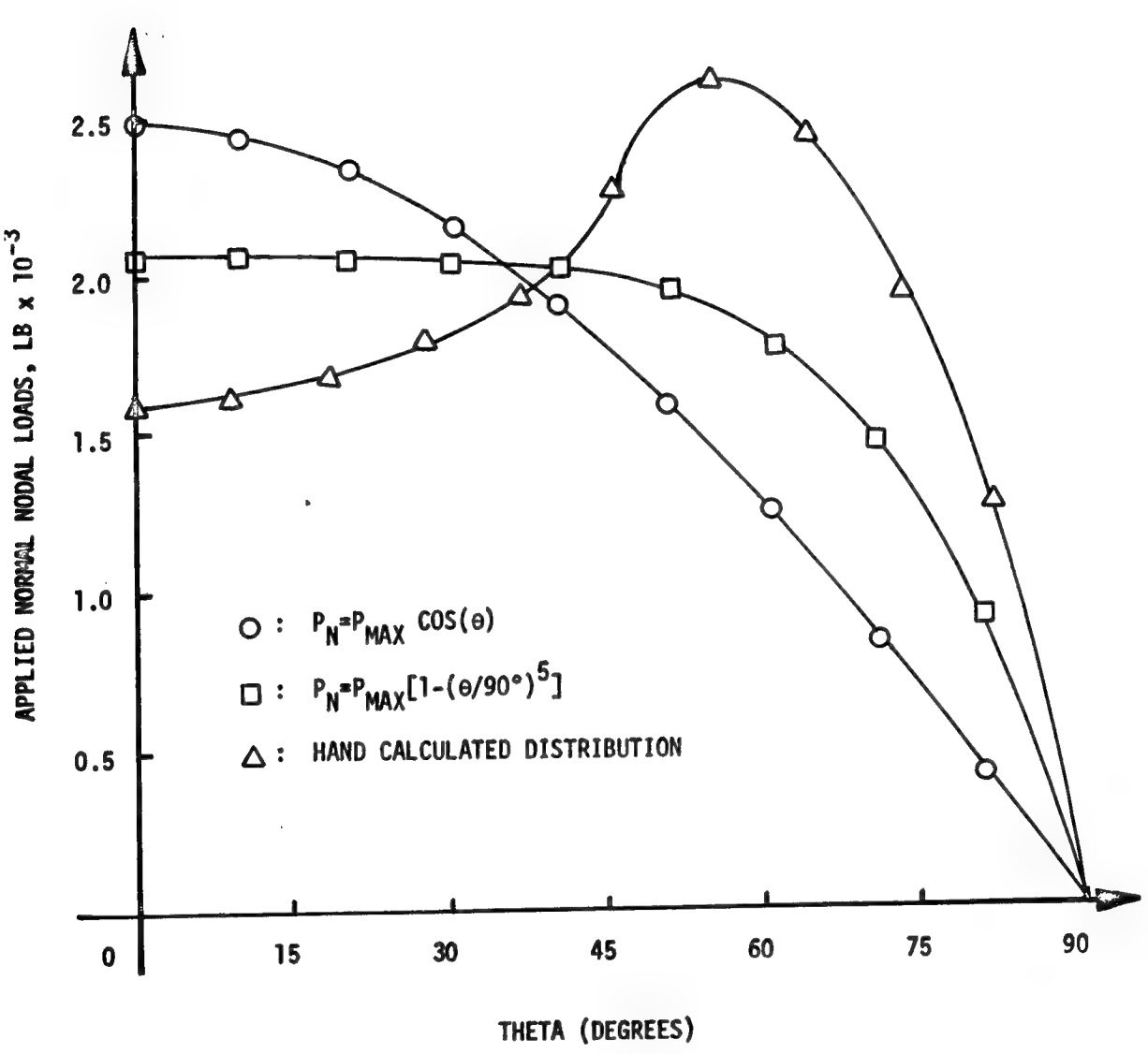

Figure A-5. Variations about the Cosine Distribution of Normal Stress

insignificant alterations of the calculated stress fields for the specimen considered.

Analysis Results For Bolt-Bearing Specimens

The selection of specimen geometries for this investigation was made from data which has been published by General Dynamics [28,29] and Grumman Aerospace [27]. Included were two net-tension failure specimens, two shear-out failure specimens, one bearing failure specimen and one specimen which exhibited failures in a transition region between a net tension and a combination failure mode. See Figure A-6 for illustrations of these various failure modes.

A strength analysis of a fibrous laminated composite material may be based on the strengths of its individual plies. The strength of a single orthotropic ply can, in theory, first be determined experimentally, producing an ultimate strength envelope for that material. This three dimensional surface (in terms of principal ply stresses) could then be used to analytically predict the ultimate strength of the total laminate. The state of the art has yet to reach this level of sophistication, however, The present three dimensional ultimate strength envelope is constructed using only five points on the stress axes due to the, as yet, unsolved problems encountered in off-axis testing.

The Tsai-Hill failure criterion is a widely accepted representation of this three dimensional envelope; it has been found in this study to be a reliable means of predicting bolt bearing specimen failure modes.

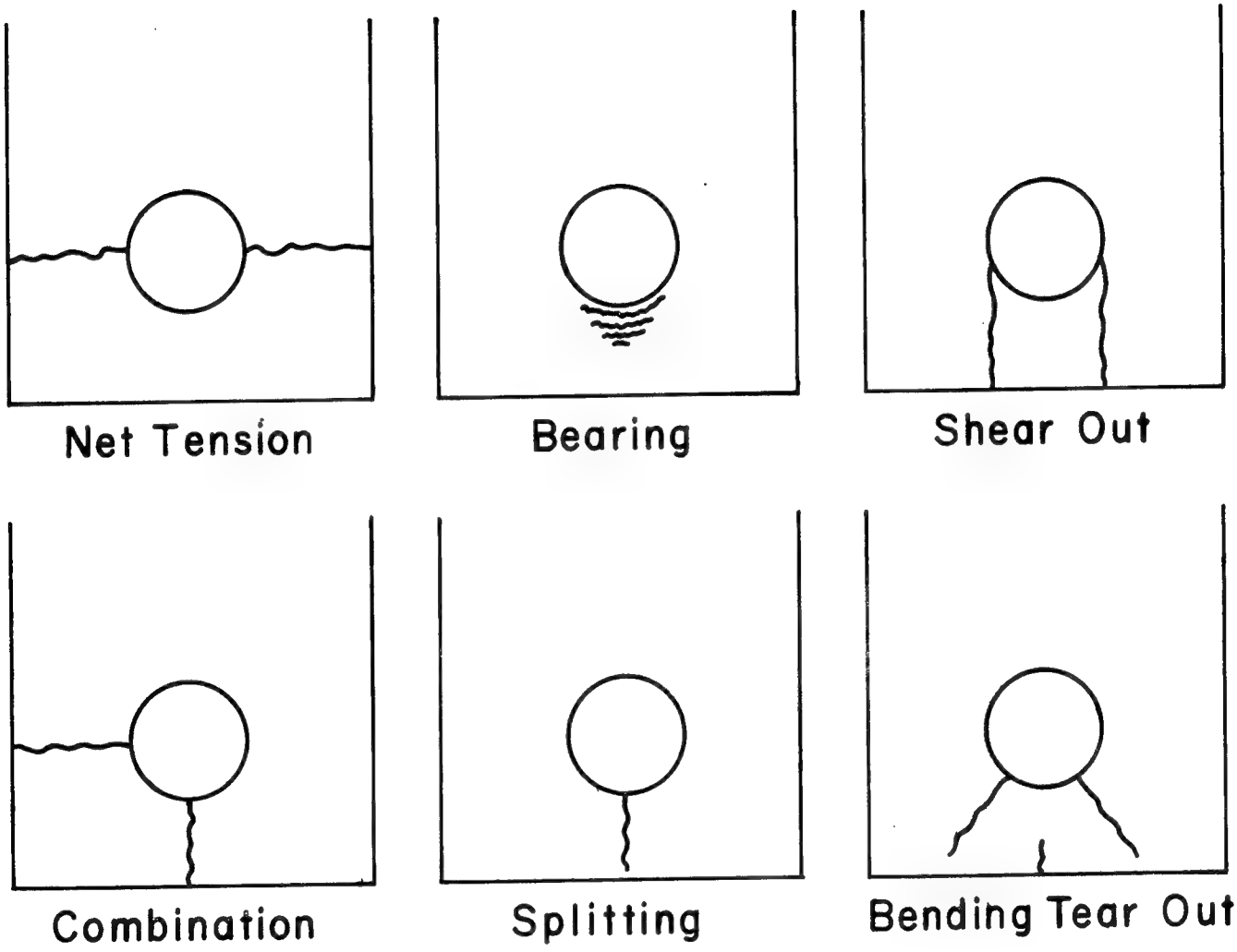

Figure A-6. Bolt Bearing Test Specimen Failure Modes

Interpretation of principal stress and strain ratio data in an attempt to predict specimen failure modes has been very unsuccessful. The difficulty results from the directionality of the composite material. As shown in [1] ply failure is predicted to occur by the Tsai-Hill criterion when the following set of principal stress ratios (normalized on their respective ultimate stresses) add to a number greater than or equal to one.

$$THC = \left(\frac{\sigma_1}{\sigma_{1u}}\right)^2 + \left(\frac{\sigma_2}{\sigma_{2u}}\right)^2 + \left(\frac{\tau_{12}}{\tau_{12u}}\right)^2 - \left(\frac{\sigma_{2u}}{\sigma_{1u}}\right)\left(\frac{\sigma_1}{\sigma_{1u}}\right)\left(\frac{\sigma_2}{\sigma_{2u}}\right) \tag{1A}$$

The maximum stress (or strain) failure criterion, on the other hand, requires that the ratio of principal stresses (or strains) to their respective ultimate stresses (or strains) be greater than or equal to 1.0 for failure to occur. Figures A-7 through A-10 show contour plots of THC for typical net tension, shear-out, bearing, and combination failure modes.* An initial application of the experimentally determined failure load was applied in each case. The contour plots were sufficient to enable the prediction of failure modes in all but the shear-out cases.

*Figures A-7a through A-7d represent the contour plots of four plies which compose a net tension failure specimen. A single plot of the major load carrying ply for each of the other three failure modes is included to illustrate the pattern of the contours for these various modes.

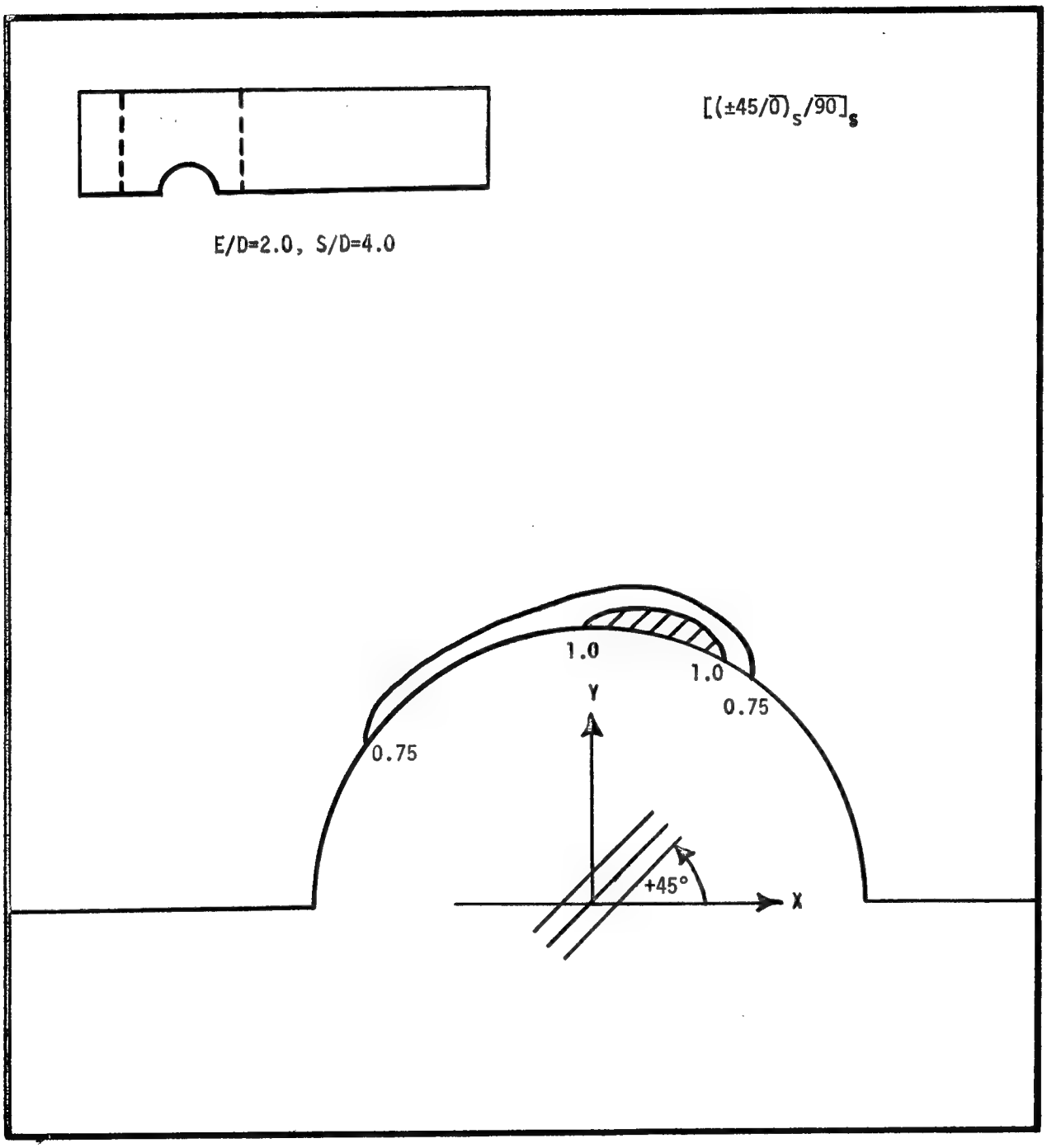

Figure A-7a. Net Tension Failure: THC Contour Plot, +45° Plies

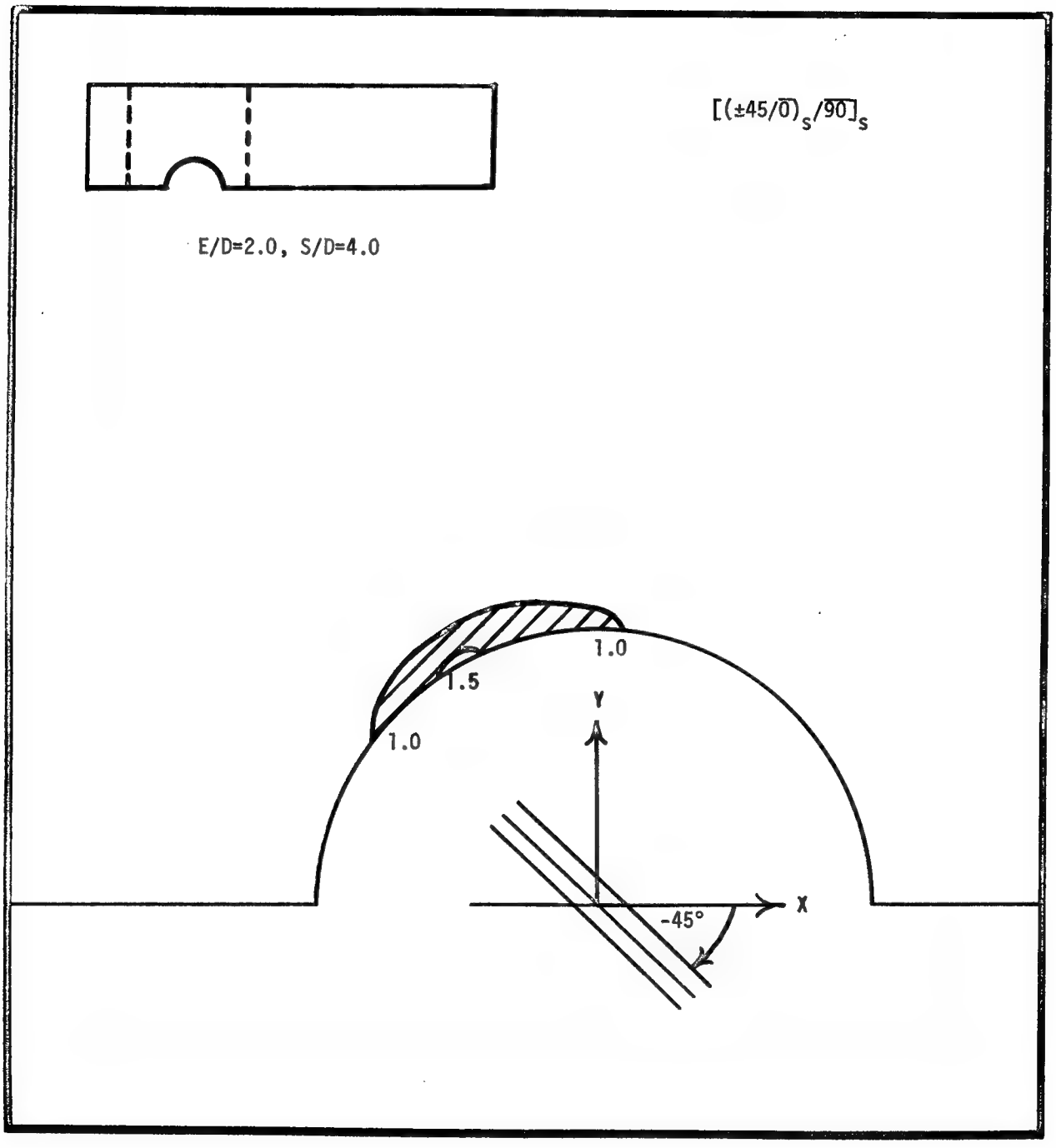

Figure A-7b. Net Tension Failure: THC Contour Plot, -45° Plies

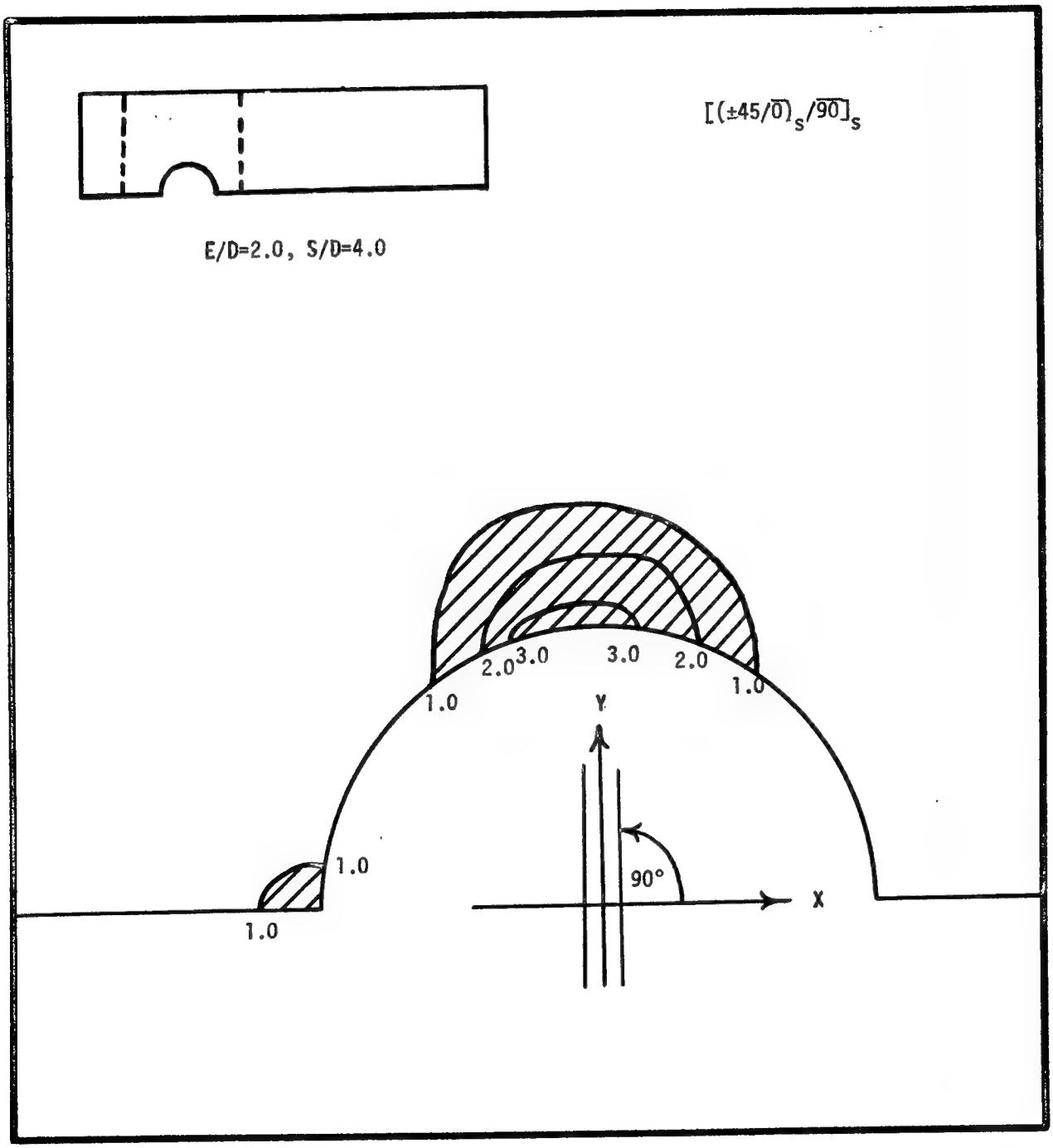

Figure A-7c. Net Tension Failure: THC Contour Plot, 90° Plies

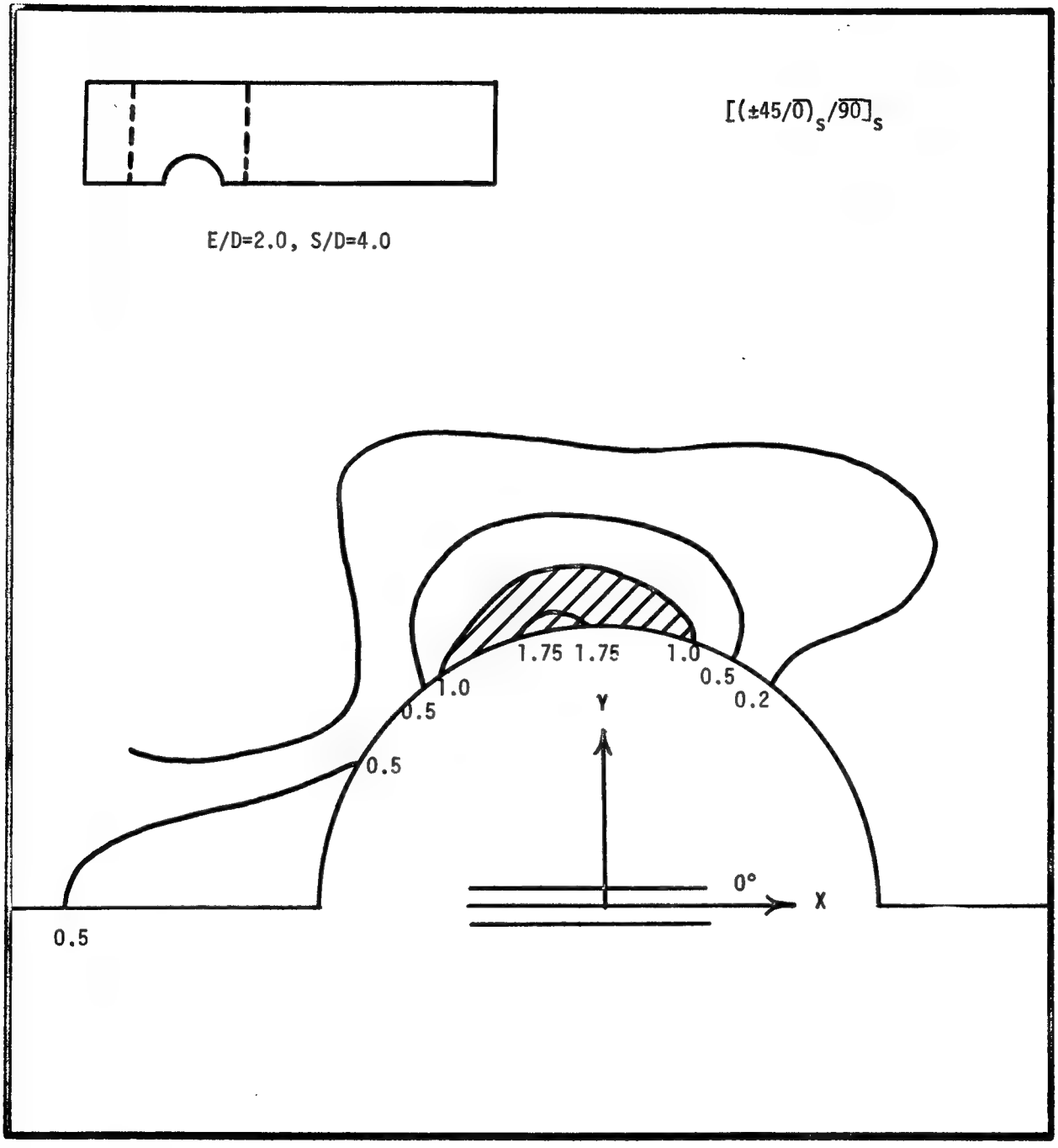

Figure A-7d. Net Tension Failure: THC Contour Plot, 0° Plies

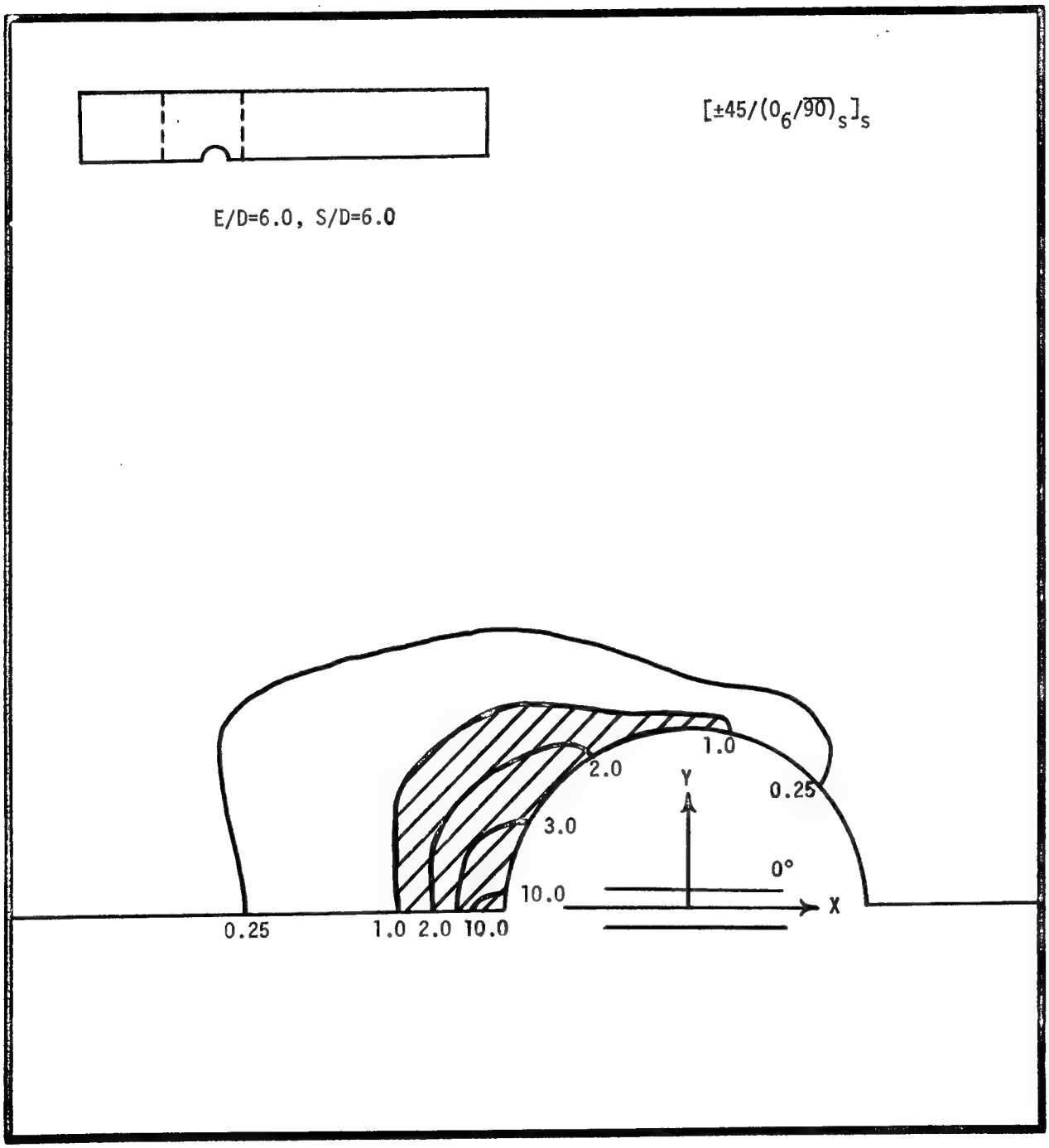

Figure A-8. Slug Type Shear-Out Failure: THC Contour Plot, 0° Plies

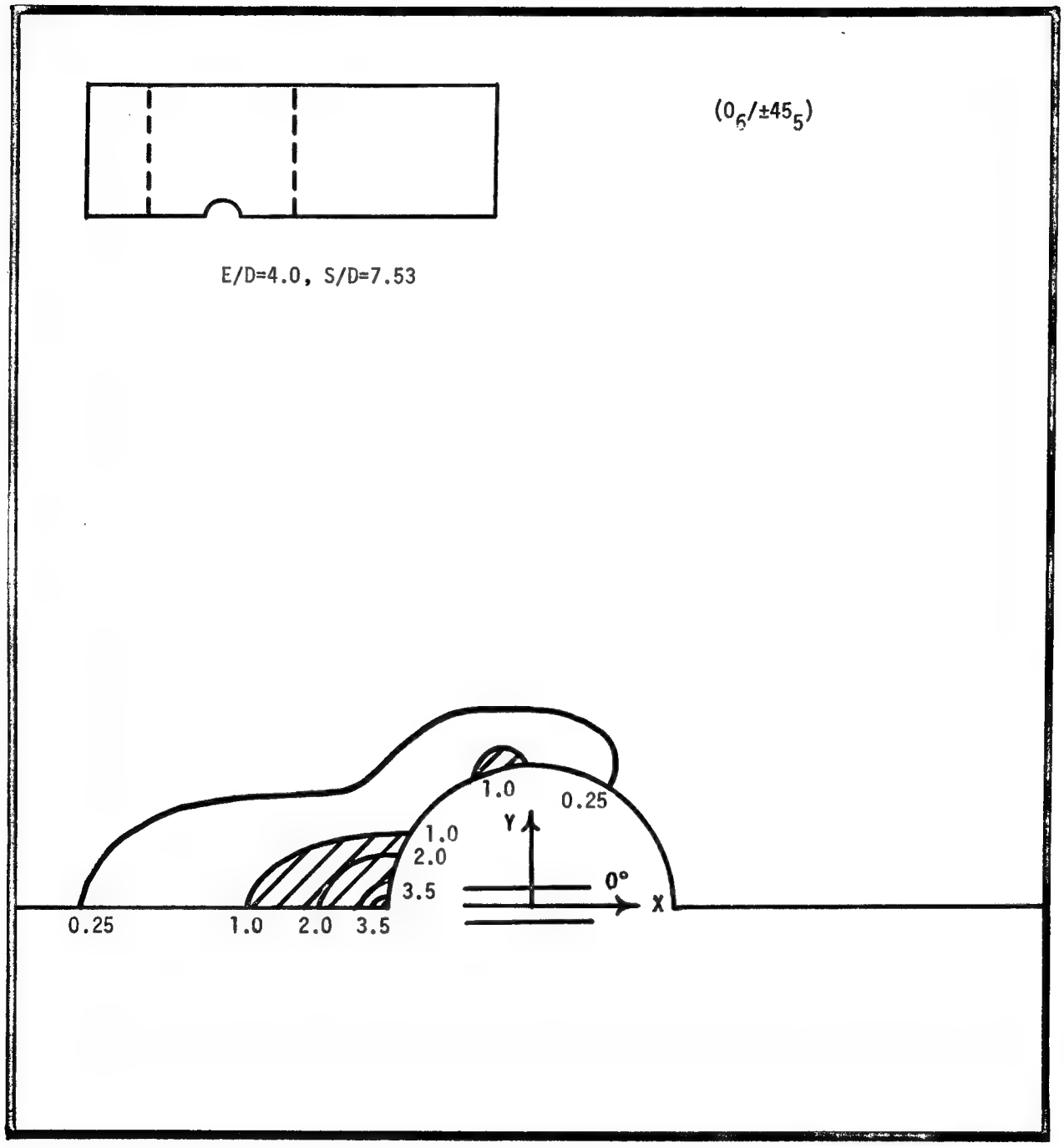

Figure A-9. Bearing Failure: THC Contour Plot, 0° Plies

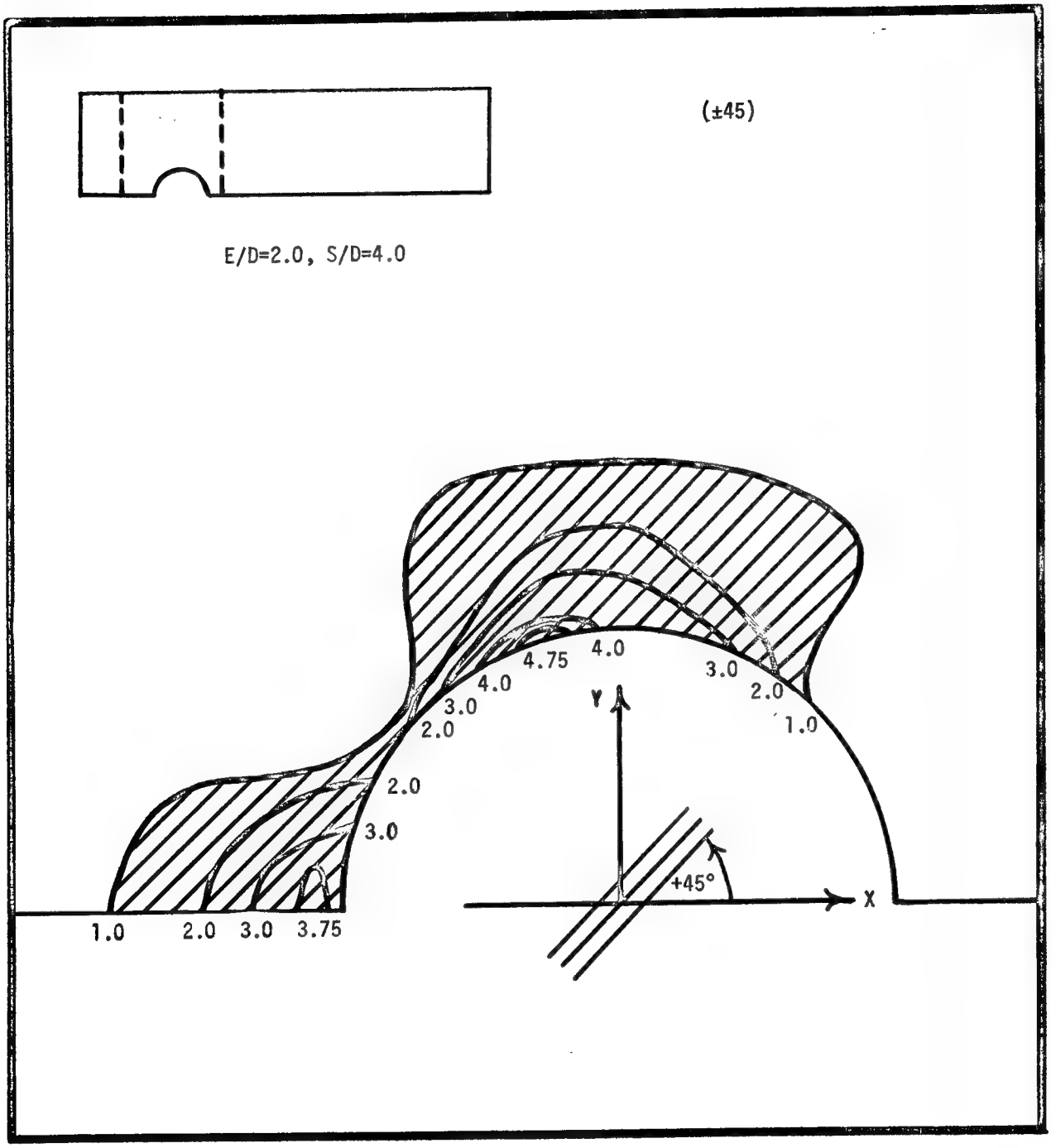

Figure A-10. Combination and Net Tension Failure: THC Contour Plot, +45° Plies

For these specimens it was necessary to consider the ratios of principal stresses to their respective ultimate stresses in the highly stressed regions to more clearly identify the mechanism which led to the failure of these specimens. For example, two slug type shear-out failures were reported and analyzed. One involved a laminate which contained 80% 0° plies; the other only 37.5% 0° plies. In both cases the contour plots indicated failure initation would occur near the point where the +45° plies were tangent to the hole. In the specimen with 80% 0° plies, after the +45° and -45° plies failed by fiber breaking and matrix splitting respectively, the dominant stress in the 0° plies was the matrix shear stress, τ_{12}. In the other specimen the dominant stress in the 0° plies was the matrix splitting stress, σ_2. With almost all 0° plies in a laminate it is expected that the failure mode would be one of shear-out. With a lot of angle-plies present a splitting mode makes more sense. In both cases, however, failure initiation involved the breaking of fibers which were tangent to the hole and the splitting of fibers perpendicular to the boundary. This is the real information of value since the ability to predict failure initiation is of major importance to a strength criterion, not the ability to predict the exact mechanism or path of failure propagation.

Prediction of failure load was also based on the Tsai-Hill criterion. The values of THC in the first row of circumferential elements around the hole were considered for each ply. A successive failure analysis

similar to that discussed in [31] was used to predict ultimate load. As soon as an element in any given ply achieved a value of THC equal to 1.0 that ply was assumed to have failed and was removed from the laminate. The load was then redistributed among the remaining plies and all values of THC were recalculated. If all recalculated values of THC were less than 1.0 more load was applied until another ply reached failure. This process was repeated until total laminate failure occurred.

The resulting predictions of failure load based on the Tsai-Hill criterion were always conservative. The degree of conservatism varied with failure mode, but more importantly it appeared to be a function of specimen anisotropy. To date only [0/±45/90] specimens have been considered. The predicted failure loads for the net tension specimens improve greatly as the percentage of ±45° plies decreases (See Table A-1). For example, for a (±45) laminate the predicted failure load is about one-half the experimental failure load. For a $(\pm 45_5/90_6)$ laminate the predicted failure load is about nine-tenths the experimental failure load. This same type of behavior was reported by Grumman Aerospace [27] in a study they performed on laminate tension data.

The maximum stress and maximum strain failure criteria were also applied using a successive failure analysis at the points of failure initiation. The results of these predictions are also listed in

Table A-1. Summary of Bolt Bearing Specimen Data

Failure Mode	Laminate	Material	% ±45°	% 0°	% 90°	$\frac{E}{D} : \frac{S}{D}$	Predicted Failure Load / Experimental Failure Load		
							THC	Maximum Stress	Maximum Strain
T,T,C	(± 45)	G/E	100	-0-	-0-	2:4	0.47	0.47	0.62
T	$[(\pm 45/\overline{0})_s/\overline{90}]_s$	B/E	72.7	18.2	9.1	2:4	0.76	0.58	0.49
T	$(\pm 45_5/90_6)$	B/E	62.5	-0-	37.5	3:4	0.93	0.94	1.00
S	$[\pm 45/(0_6/\overline{90})_s]_s$	B/E	13.3	80.0	6.7	6:6	0.58	0.61	1.89
S	$(0_6/\pm 45_5)$	B/E	62.5	37.5	-0-	2.5:7.53	0.98	1.10	0.95
B	$(0_6/\pm 45_5)$	B/E	62.5	37.5	-0-	4:7.53	~0.65	0.58	0.49

Nomenclature:

T	Tension	G/E	Graphite-Epoxy
C	Combination	B/E	Boron-Epoxy
S	Shear-Out		
B	Bearing		

Table A-1 for comparison. The Tsai-Hill criterion was the only criterion of the three which was conservative in predicting failure load for each specimen investigated. Both the maximum stress failure criterion and the maximum strain failure criterion underpredicted one specimen ultimate load. That is, even when the experimentally determined failure load was used as the applied load in the computer program, the ratio of principal stresses (or strains) to their respective ultimate stresses (or strains) did not exceed 1.0 in any of the plies. The ratios of predicted failure load to experimental failure load shown in Table A-1, as a result, are in excess of 1.0 for these two nonconservative failure load predictions. Note, however, that failure load predictions made using the maximum stress failure criterion are always in agreement with those of the Tsai-Hill failure criterion to within about ten percent. The major disadvantage of the maximum stress criterion is its inability to clearly indicate failure modes. Its major advantage is its simplicity.

A final interesting observation can be made regarding the prediction of the bearing failure for the last specimen. The local stresses ahead of the bolt for the applied experimental failure load show matrix splitting in the 0° plies at a load equal to 58% the load at which the bearing failure was observed in the lab. A successive failure analysis shows that the remaining plies ahead of the bolt were capable of carrying the hoop load transferred to them from the failed 0° plies.

The excessive conservatism implied by the maximum stress criterion therefore resulted from assuming that a bearing failure initiated when the ratio $\sigma_2/\sigma_{2_{ut}}$ in the 0° plies exceeded the value of 1.0. This criterion was used to predict bearing failures at the time due to a lack of a better criterion. Recently data has been presented [32] which indicates that a stress ratio of $\sigma_1/\sigma_{1_{uc}} \tilde{=} 0.65$ is sufficient to induce a bearing failure in a 0° laminate which has already failed by matrix splitting. The value of $\sigma_1/\sigma_{1_{uc}}$ for the 0° plies for the applied failure was 0.65. The exact agreement is coincidental but the idea that unbonded fibers fail in bearing at much lower loads than do fibers which are bonded tightly together makes sense. Therefore, in all future successive failure analyses this is the criterion which will be used to predict bearing failures.

APPENDIX B

FINITE ELEMENT ANALYSES OF MULTIPLE FASTENER JOINTS

The purpose of this study was to finalize the selection of a joint failure criterion for the composite laminate which could be automated and included in the synthesis program. The proposed criterion must be able to consistently predict both joint failure location and failure mode. It should also be conservative in predicting failure loads and as operationally simple as possible.

Analyzing a complete joint in a single finite element run with any degree of accuracy is impossible due to computer storage limitations. It is, in fact, only possible to analyze one hole at a time, as was done in Appendix A, to achieve suitable accuracy. Thus the following analysis procedure was used in this study to analyze multiple fastener joints. Each of the joints consisted of a number of identical columns of bolts as ilustrated in Figure B-1. It was assumed that each column could be analyzed separately and that each carried an equal share of the total joint load which was present at failure. The joint geometries of the six specimens selected for investigation were such that if the joints were made of an isotropic material the effects of adjacent columns of bolts would be negligible [33]. Experience in analyzing both loaded and open holes in anisotropic plates has shown that the

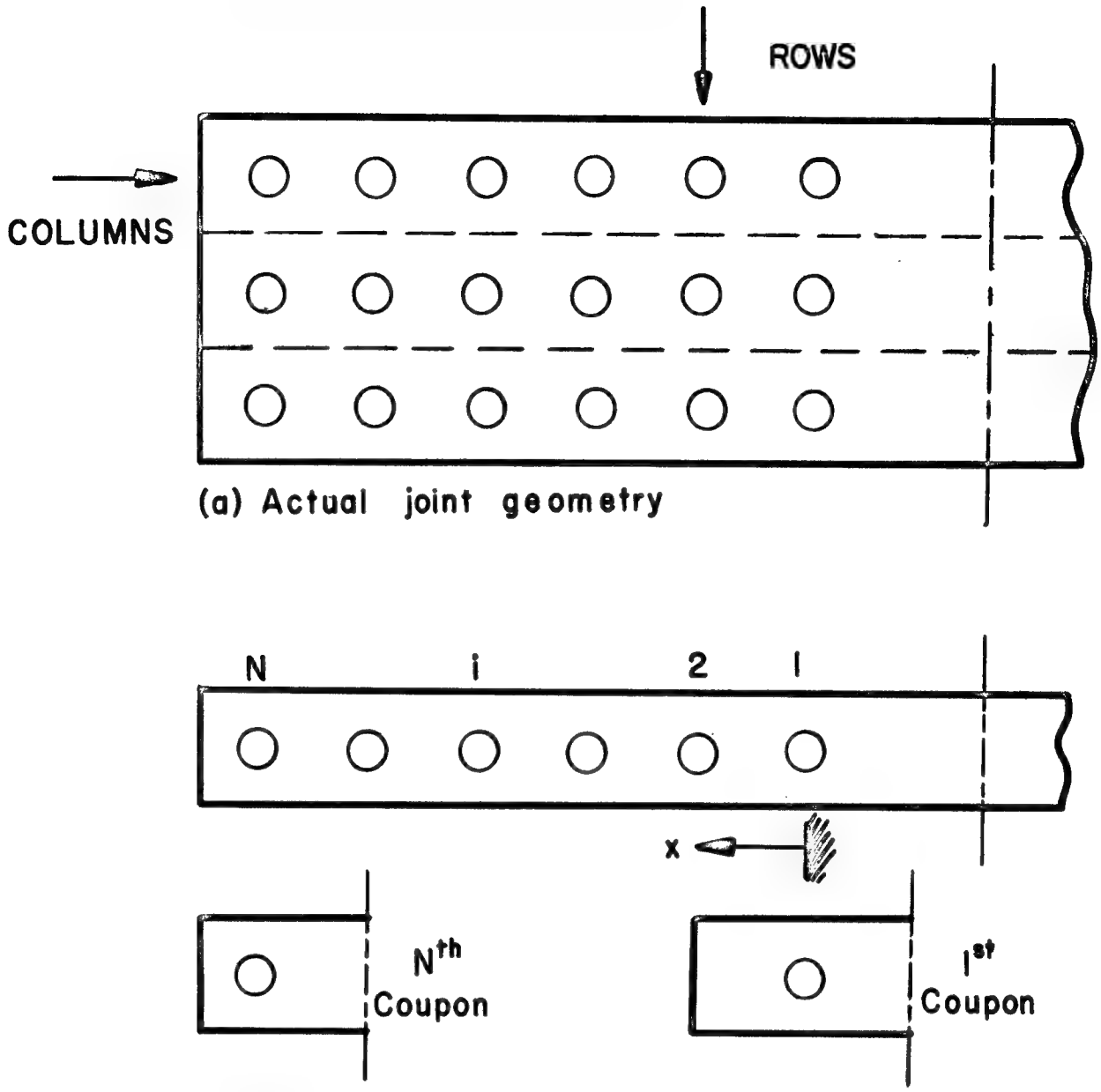

Figure B-1. Modeling Procedure for Multiple Fastener Joints Containing Several Columns of Fasteners

stress concentration factors which result in anisotropic coupons are always greater than the stress concentration factors which result in geometrically similar isotropic coupons, with the exception of the (±45) laminate. Thus the assumption was made that the effects of adjacent columns of bolts were negligible in the actual composite joints since for the same applied load a greater stress concentration factor implies a more rapid stress field decay between adjacent columns. This must be true if equilibrium is to be satisfied.

A series of single fastener coupons was used to model the multiple fastener joints analyzed in this study. It was assumed that the pins were rigid and that the effects of plate bending were negligible. Two different methods were proposed for determining the bolt load distribution in each joint. The first, referred to as the point strain matching technique, equated the longitudinal strains in the main plate to those in the splice plate at the mid-points between adjacent fasteners. The second, referred to as the elongation matching technique, equated the total elongation of the main plate to that of the splice plates between adjacent fasteners. By requiring that overall joint equilibrium be satisfied, each of these two techniques resulted in N equations in terms of the N unknown bolt loads. The point strain matching technique has one definite advantage over the elongation matching technique; computationally it is much simpler to use. The properties and cross-sectional areas of the plates need only

be specified at the mid-points between adjacent fasteners. The elongation matching technique, on the other hand, requires that these properties and areas along the joint be represented by quadratic functions in x. The equations which result for the bolt loads contain some rather involved integrations which make hand calculations very tedious.

The equations expressing the various bolt loads in terms of the total applied load per column, F, for the point strain matching technique are much simpler and are given by

$$\sum_{k=1}^{i} P_k = \frac{F}{1 + \frac{1}{2}\frac{E_{xm}}{E_{xs}}\frac{A_m}{A_s}} \quad , \quad i = 1, N-1 \qquad (1B)$$

The material properties and plate cross-sectional areas are evaluated at the mid-point between the bolts labeled i and i+1. Equation (1B) in conjunction with the overall joint equilibrium equation

$$F = \sum_{k=1}^{N} P_k \qquad (2B)$$

result in N equations in terms of the N unknown bolt loads which can be solved directly.

Six joints designed and tested at General Dynamics were selected for analysis from [26,34]. Each is described in detail in Table B-1. The bolt load distributions for the various joints shown in Figure B-2 were determined using the point strain matching technique. The elongation matching technique was also used to predict the bolt load

Table B-1. Description of the Six Specimens Selected for Analysis

Spec. No.	Lamination	Splice Plate Material	Loading	Rows of Bolts	Bolts per Row	Failure Mode	Ultimate Load(lb)	P(Pred)/P(Exp)
1	B/E,$(0_4/\pm45)$	D6-AC Steel	SS	6	4	SP	94,200	0.67
2	B/E,$(0_4/\pm45)$	D6-AC Steel	SS	5	4	SP	115,500	0.77
3	B/E,$(0_4/\pm45)$	6-4 Ti	SS	5	4	SP	110,400	0.70
4	B/E,$(0_4/\pm45)$	D6-AC Steel	SS	4	4	SP	125,400	0.65
5	B/E,$(0_2/\pm45)$	D6-AC Steel	DS	4	4	T	189,000	0.78
6	G/E,$[0/\pm45]^1$	6-4 Ti	SS	6	2	T	74,800	0.97

Nomenclature:

SS	Single Shear
DS	Double Shear
B/E	Boron-Epoxy
G/E	Graphite-Epoxy
SP	Splitting
T	Tension

Notes:

(1) Lamina thicknesses vary linearly along the specimen length from $(0_2/\pm45)$ at the first row of bolts to $(0_2/\pm45_3)$ at the last row of bolts.

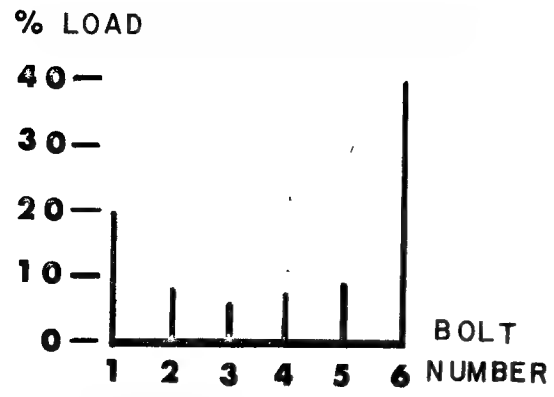

(a) Specimen 1

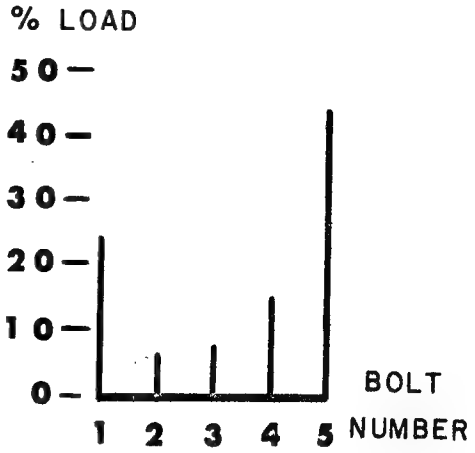

(b) Specimen 2

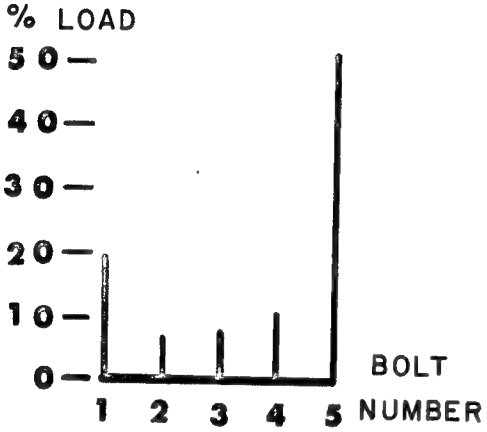

(c) Specimen 3

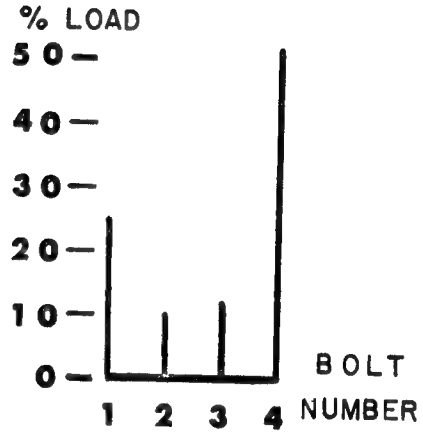

(d) Specimen 4

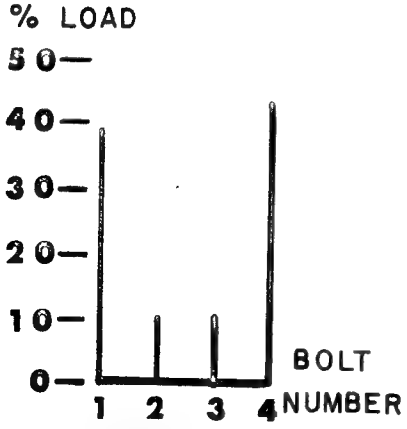

(e) Specimen 5

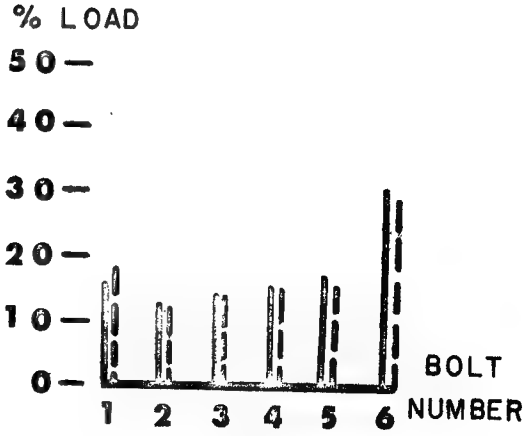

(f) Specimen 6

Figure B-2. Bolt Load Distributions for Specimens 1 thru 6

distribution for specimen 6 for reasons of comparison. These results are included in Figure B-2f and are denoted by the dashed lines. The difference between the two sets of results is considered negligible. While the point strain matching technique is used here the elongation matching technique is used in the synthesis since it is physically more satisfying to this investigator.

All of the single fastener coupons for each joint were not analyzed. Each coupon for specimen 6 was analyzed while only the first and last coupons for specimens 1 thru 5 were analyzed. Specimens 1 thru 5 were designed to fail in net tension at the first row of fasteners but four of them failed in a splitting type mode which appeared to originate ahead of the leading edge fasteners in each case. To save computer time it was decided to perform finite element analyses of only the two coupons of immediate interest to see if the premature splitting failures were predictable using the maximum stress and Tsai-Hill failure criteria.

Contour plots of THC, similar to those presented in Appendix A, for the six specimens analyzed are shown in Figure B-3 thru B-8. It was shown in Appendix A that such plots provide an extremely convenient method for quickly predicting failure modes. Table B-2 summarizes the important information contained in these figures, including the principal stress ratios which are dominant in the highly stressed regions. Figures B-3 thru B-7 are for the five

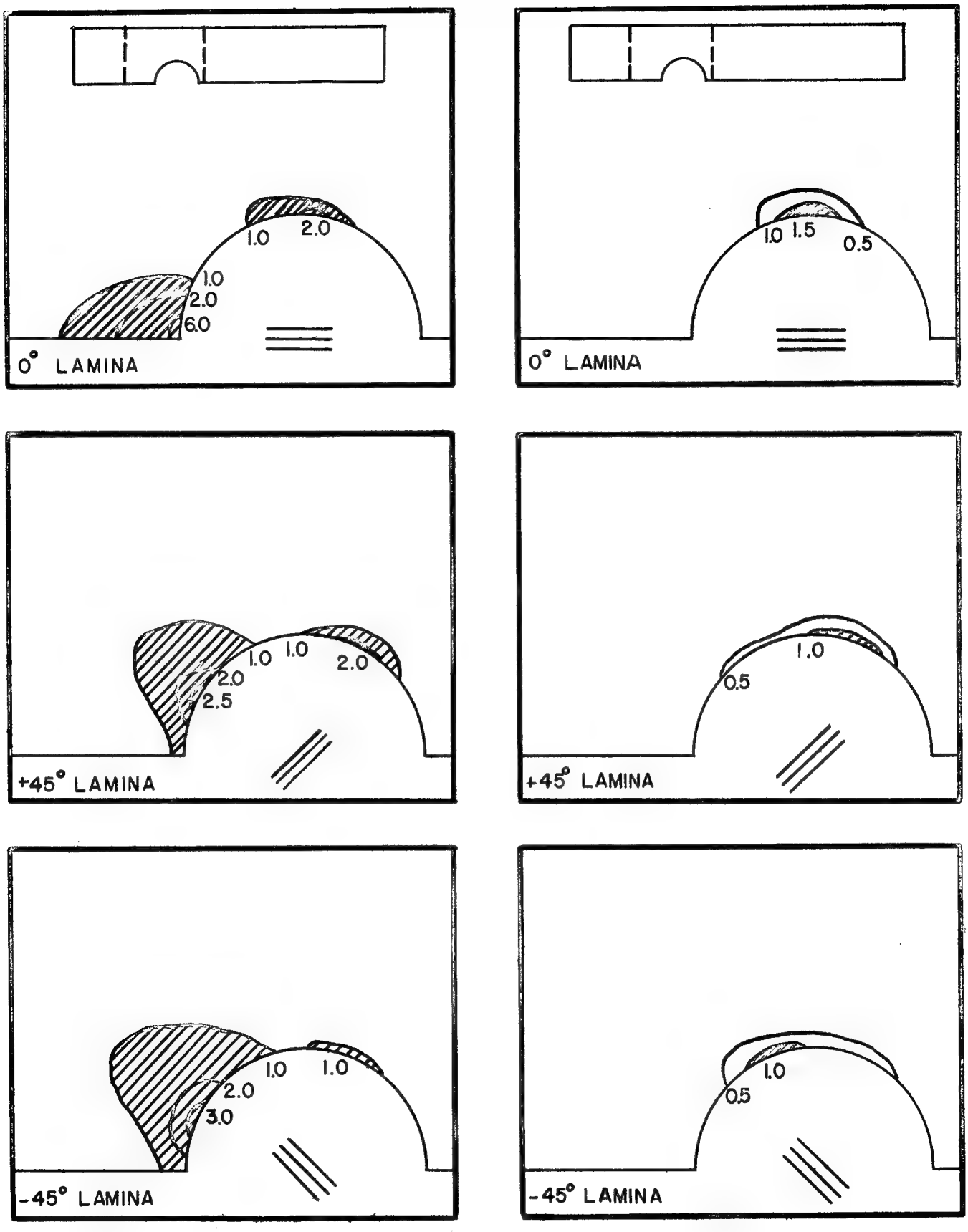

Figure B-3. THC Contour Plots for Specimen 1 at the Experimental Failure Load

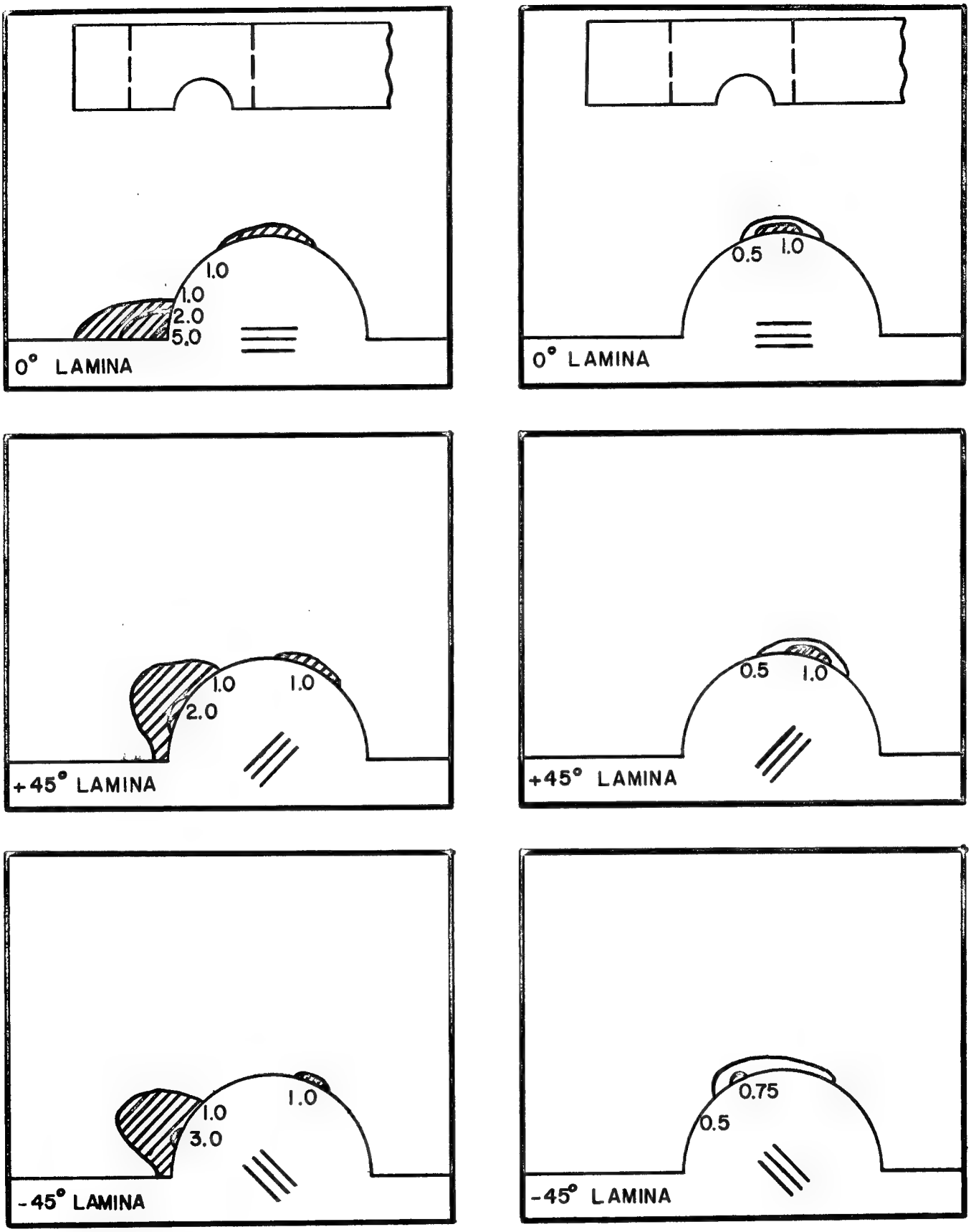

Figure B-4. THC Contour Plots for Specimen 2 at the Experimental Failure Load

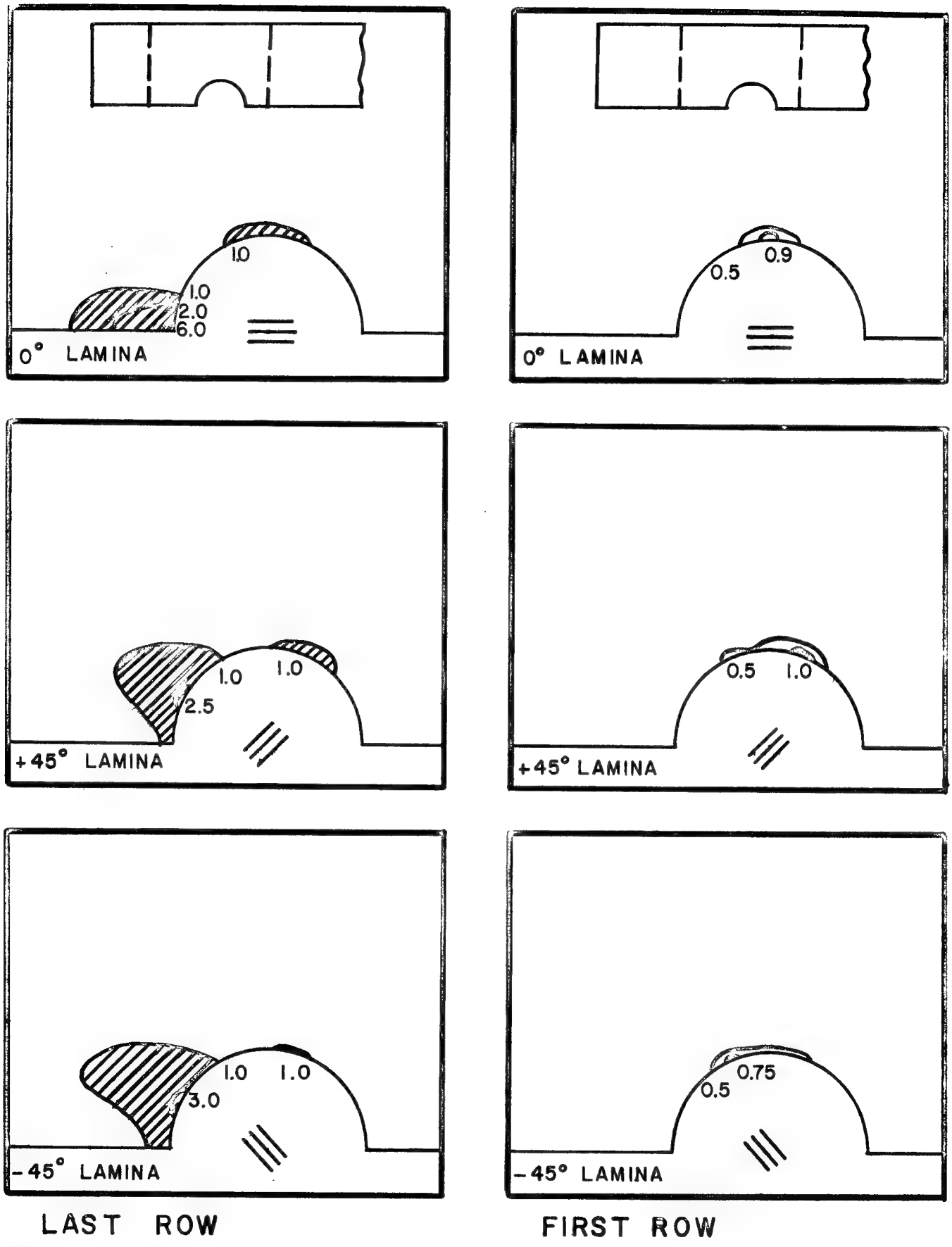

Figure B-5. THC Contour Plots for Specimen 3 at the Experimental Failure Load

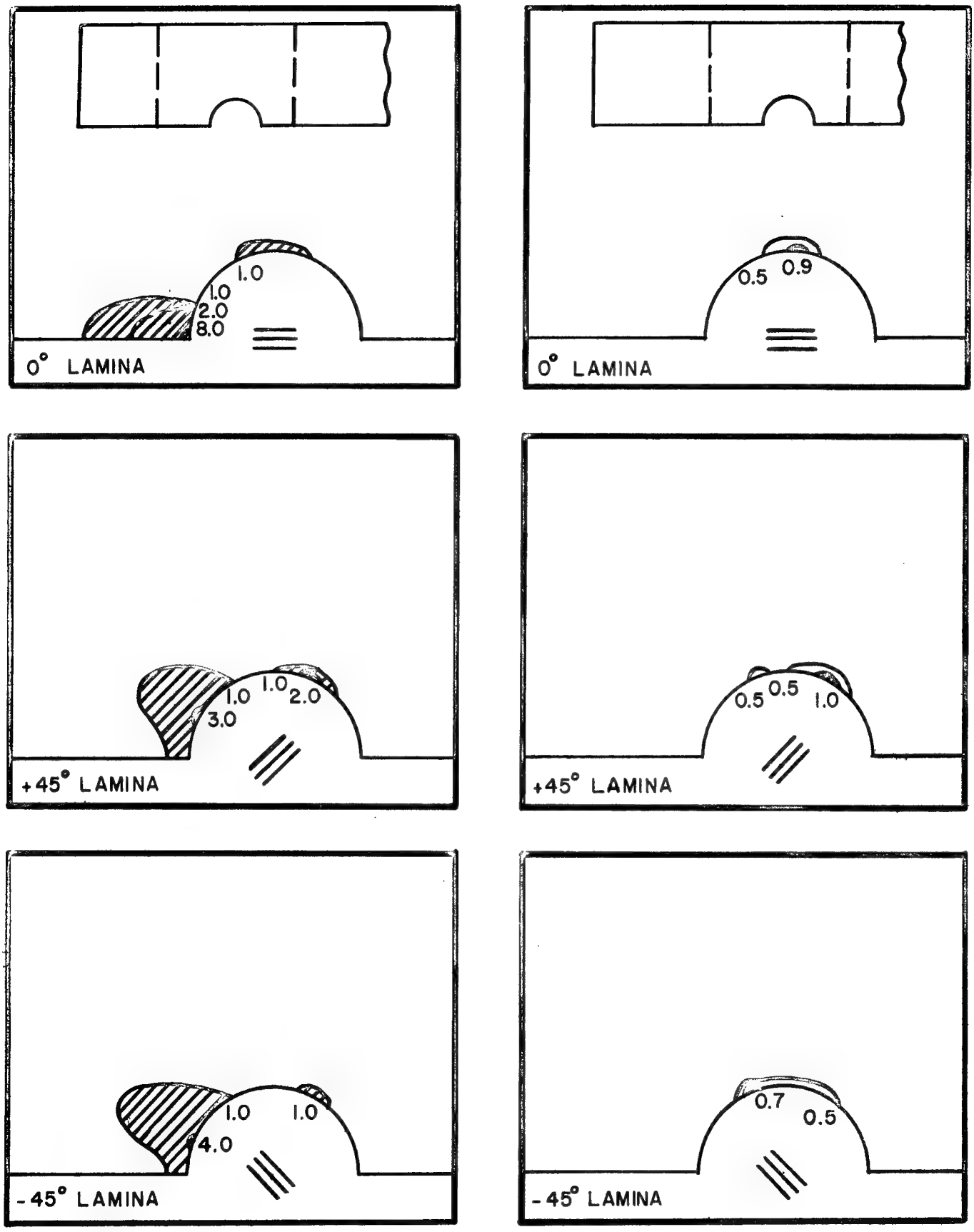

Figure B-6. THC Contour Plots for Specimen 4 at the Experimental Failure Load

Figure B-7. THC Contour Plots for Specimen 5 at the Experimental Failure Load

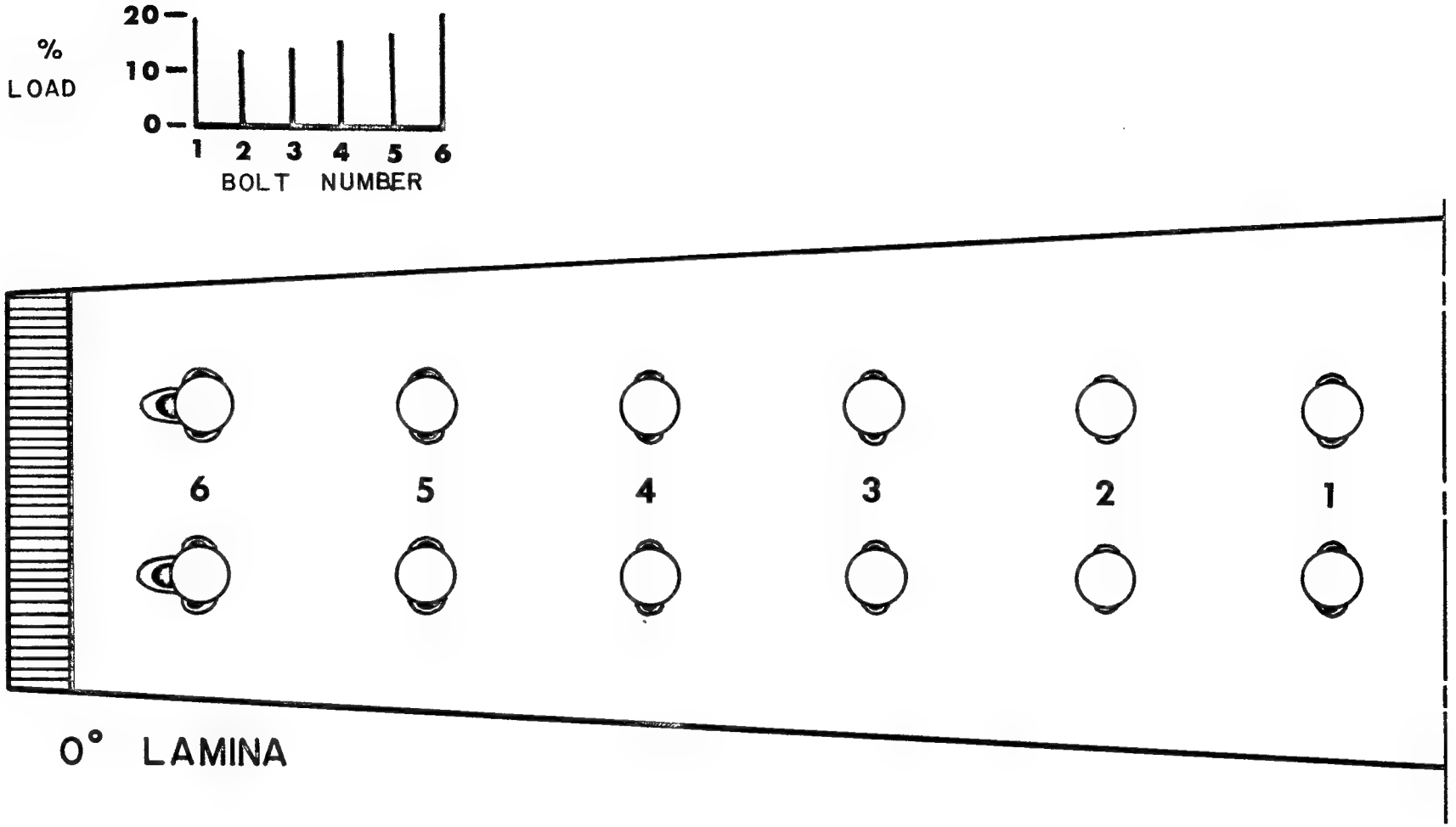

Figure B-8a. THC Contour Plots for Specimen 6 at the Experimental Failure Load, 0° Plies

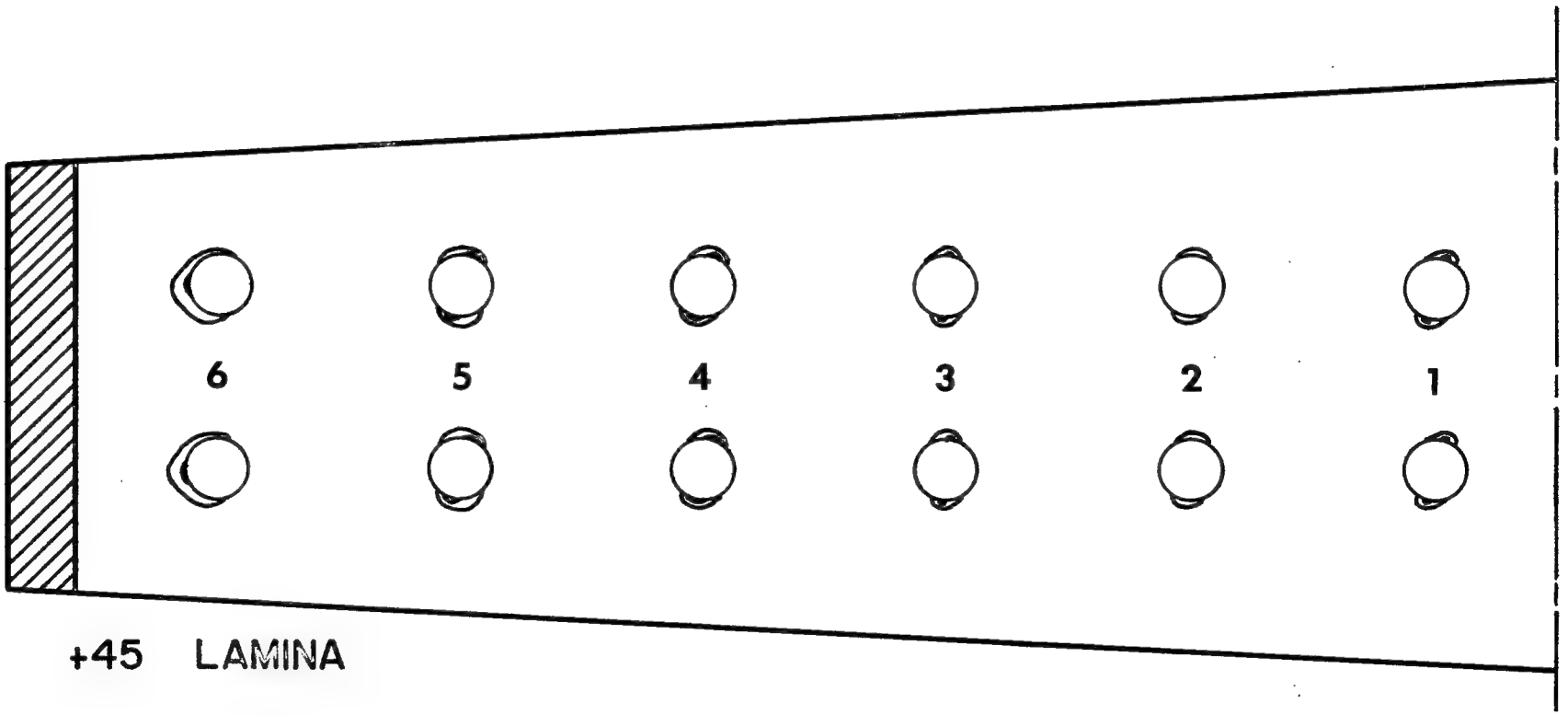

Figure B-8b. THC Contour Plots for Specimen 6 at the Experimental Failure Load, +45° Plies

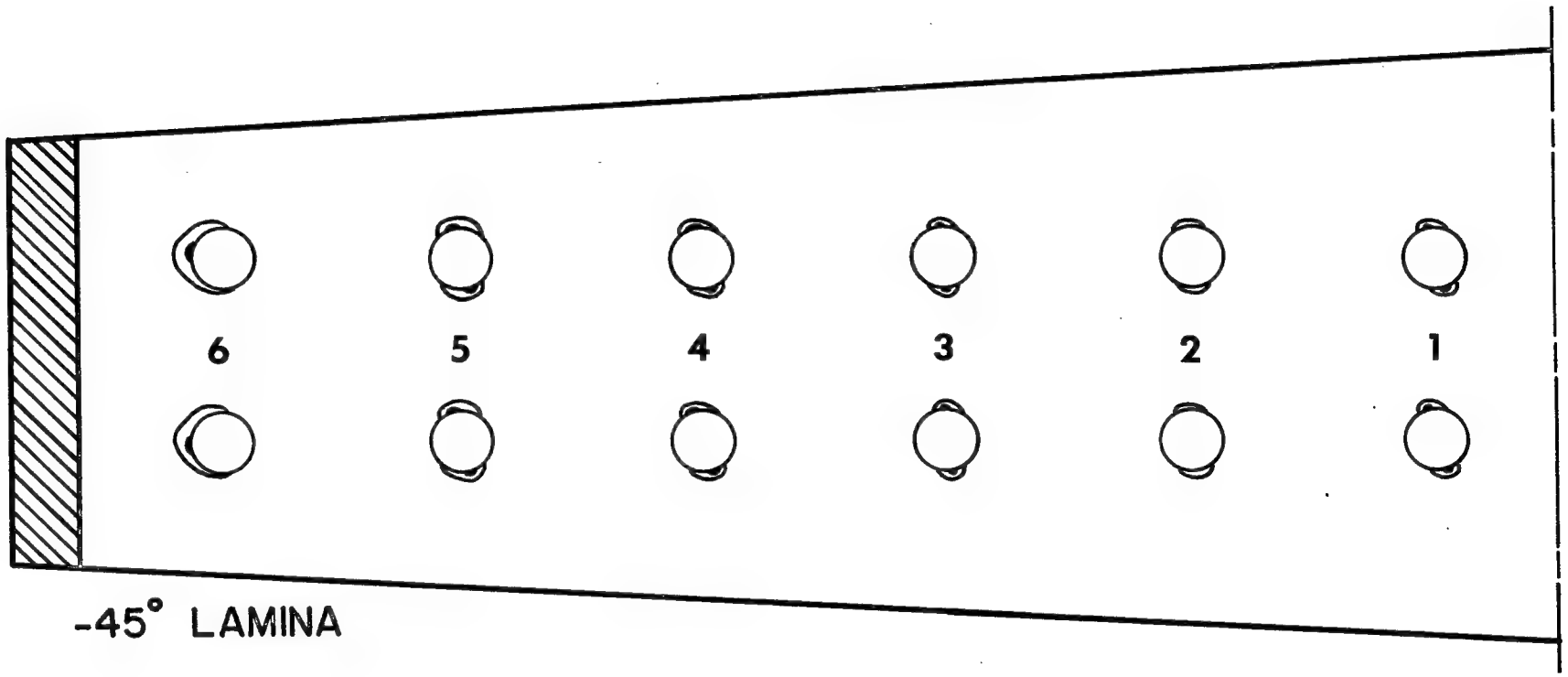

Figure B-8c. THC Contour Plots for Specimen 6 at the Experimental Failure Load, -45° Plies

Table B-2. Summary of Significant Data from Figures B-3 thru B-8

Spec. No.	Row No.	Bearing, θ=0°			Tension, θ=90°		Splitting, θ=+45°			
		0° Lamina			0° Lamina		+45° Lamina		-45° Lamina	
		$\frac{\sigma_1}{\sigma_{1uc}}$	$\frac{\sigma_2}{\sigma_{2ut}}$	THC	$\frac{\sigma_1}{\sigma_{1ut}}$	THC	$\frac{\sigma_1}{\sigma_{1ut}}$	THC	$\frac{\sigma_2}{\sigma_{2ut}}$	THC
1	First	0.07	C*	0.02	1.05	1.50	0.21	0.10	0.83	1.10
	Last	0.49	2.50	5.80	1.33	2.00	1.50	2.50	1.65	3.20
2	First	0.10	0.04	0.01	0.91	1.00	0.42	0.25	0.80	0.75
	Last	0.50	2.30	5.10	1.11	1.41	1.30	2.10	1.55	2.60
3	First	0.07	0.05	0.01	0.83	0.90	0.63	0.47	0.79	0.71
	Last	0.47	2.50	6.00	1.34	1.45	1.43	2.50	1.73	3.00
4	First	0.13	0.29	0.11	0.85	0.85	0.58	0.40	0.69	0.55
	Last	0.52	2.80	7.95	1.07	1.51	1.55	2.70	1.90	3.75
5	First	0.30	0.56	0.42	1.29	2.00	0.79	0.90	0.92	0.90
	Last	0.60	2.00	4.00	1.02	1.41	1.15	1.65	1.21	1.88
6	First	0.17	0.04	0.03	0.90	0.95	0.57	0.44	0.75	1.12
	Fifth	0.37	0.26	0.21	1.03	1.20	0.63	0.60	0.83	1.15
	Sixth	0.80	1.00	1.90	0.80	1.00	0.63	0.65	0.95	0.95

*C Compressive stress

specimens selected from the original testing program at General Dynamics [26]. The first four specimens failed experimentally in splitting modes; the fifth failed in net tension. Figure B-8 represents the single specimen tested in the second General Dynamics program [34]. It also failed in net tension at the first row of bolts. The experimental failure behavior of these specimens, in conjunction with the stress analysis results illustrated in the figures, was used in the development of the proposed joint failure criterion. A description of how the criterion evolved is presented below.

Consider Figures B-3 thru B-6. The contour plots show that the stress field distributions are the same; only the magnitudes of the individual stress components are different. The discussion which follows for Figure B-3 is also valid for Figures B-4 thru B-6. A region of highly stressed material occurs in the 0° plies directly ahead of the last bolt in the specimen column. The $\sigma_2/\sigma_{2_{ut}}$ ratio is dominant in this region, which implies local matrix failure (splitting). The maximum value of $\sigma_1/\sigma_{1_{uc}}$ in the region is 0.49. Results from [3,32] indicate that once the 0° plies split (i.e., $\sigma_2/\sigma_{2_{ut}} \geq 1.0$) a value of $\sigma_1/\sigma_{1_{uc}} \cong 0.65$ is sufficient to cause a bearing failure to occur. Thus, even though the 0° plies have split the values of $\sigma_1/\sigma_{1_{uc}}$ are not large enough to cause a bearing failure to occur.

It has been assumed here that matrix failure does not significantly degrade the laminate since the percentage of hoop load carried by the 0° plies directly ahead of the bolt was small. However, in specimens where a large percentage of the hoop load is carried by the matrix prior to failure a similar assumption is not possible. Consider a specimen consisting of almost all 0° plies and only a few ±45° plies. Matrix failures in the 0° plies would result in a significant load transfer to the ±45° plies. Even if laminate failure did not occur as a result of this load transfer the laminate would be significantly damaged.

High values of THC also result in the 0° plies at θ=90°, Figure B-3, at both the first and last row of bolts due to large values of $\sigma_1/\sigma_{1_{ut}}$ in these regions. The maximum value of THC at the last row of bolts, 2.0, is greater than the maximum value at the first row, 1.5. The same is true of the maximum values of $\sigma_1/\sigma_{1_{ut}}$ in these two regions. If the 0° plies were to fail, the ±45° plies would not be able to carry the additional load transferred to them from the 0° plies; as a result, laminate failure would occur. Thus a net tension failure at the last row of bolts is the most probable failure mode indicated from the results so far.

The assumption that matrix failure does not significantly degrade the laminate is valid throughout specimen 1. The highly stressed regions which result from large $\sigma_2/\sigma_{2_{ut}}$ ratios are therefore eliminated from consideration. The only remaining region of interest is the one in

the +45° plies which occurs at the last row of bolts where the fibers are tangent to the hole. Both the maximum THC value and maximum $\sigma_1/\sigma_{1_{ut}}$ value in this region are greater than the corresponding values which indicated a net tension failure at the same hole. Once the +45° fibers break in tension a successive failure analysis shows that the remainder of the laminate cannot carry the existing load. Therefore a complete laminate failure also occurs. Thus a splitting mode is favored over the net tension mode previously indicated for specimen 1. Since all the possible regions of failure initiation have been examined a splitting mode is predicted by the analysis. The actual specimen did indeed fail in a splitting mode. The predicted failure load is conservative. If P_F is the actual experimental failure load for specimen 1 the Tsai-Hill criterion predicts failure to occur at $P_F/\sqrt{2.5}$ or 0.64 P_F. The maximum stress failure criterion predicts failure to occur at $P_F/1.5$ or 0.67 P_F. Analyses of specimens 2 thru 4 yield very similar results.

Following the same procedure it can be deduced that a bearing failure does not occur in specimen 5, Figure B-7. Both the Tsai-Hill and maximum stress failure criteria conservatively predict a net tension failure to occur at the first row of bolts, which again agrees with the experimental failure mode.

Predicting failure for specimen 6 is slightly more complicated.

The finite element results, Figure B-8, indicate that $\sigma_1/\sigma_{1_{uc}}$ reaches 0.65 at the last row of bolts in the 0° plies prior to matrix failure, $\sigma_2/\sigma_{2_{ut}} = 1.0$. A bearing failure is predicted to occur in such a case at that load where either $\sigma_2/\sigma_{2_{ut}}$ reaches 1.0 or $\sigma_1/\sigma_{1_{uc}}$ reaches 1.0, whichever occurs first. The assumption is made at bearing failure initiation that the bolt causing the bearing failure to occur is unable to carry any additional load during subsequent specimen loading. The additional applied load is distributed among the remaining bolts in the column in proportion to the loads which they carried at bearing failure initiation. Figure B-8 is the revised representation of the state of stress present in specimen 6 when the experimental failure load was applied. Notice that $\sigma_2/\sigma_{2_{ut}} = 1.0$ and $\sigma_1/\sigma_{1_{uc}} = 0.80$ in the 0° plies directly ahead of the last row of bolts. The material ahead of the last row of bolts has failed in bearing and load redistribution, as described above, has taken place. The hoop load carried by the 0° plies was successfully transferred to the remaining ±45° plies. A load distribution plot for specimen 6 is also illustrated in Figure B-8. Note that the revised load distribution plot is much more uniform than that of Figure B-2f.

Observe that regions of high THC values do not occur in the vicinity θ=+45° at any of the bolt holes except at the last row of bolts in the -45° plies. Matrix failure is on the verge of occurring here. Net tension failures, however, are indicated at various locations along

the specimen which would occur prior to matrix failure in the -45° plies. A splitting mode is, therefore, definitely not indicated by the plots.

Regions of high THC values in the 0° plies at θ=90° are present at all but the second row of bolts. The maximum THC value, 1.2, occurs at the fifth row. The largest value of $\sigma_1/\sigma_{1_{ut}}$ in these four regions of interest is 1.03, which also occurs at the fifth row. Thus, both the Tsai-Hill and maximum stress failure criteria predict a net tension failure to occur in specimen 6 at the fifth row of bolts. The predicted failure load for this specimen using the maximum stress criterion is again conservative but only by about 3% as opposed to about 35% for specimens 1 thru 5. The failure mode was again predicted by both criteria but the location was not. Table 3 summarizes the prediction results for these analyses.

Thus a joint failure criterion has been proposed which has successfully satisfied the requirements imposed on it. The criterion was able to predict both failure location and failure mode in all but specimen 6 where it incorrectly predicted failure location. More importantly it was able to conservatively predict failure loads for each specimen. It was found that the maximum stress failure criterion agreed with the Tsai-Hill failure criterion to within just a few percent in predicting failure loads and was less conservative in each case. It was also found that failure was always initiated at locations around the hole where the fibers were tangent to the hole surface and were being broken in tension.

Table B-3. Summary of Maximum Stress and Tsai-Hill Criteria Failure Predictions

Problem Number	Predicted Failure Load / Experimental Failure Load		Failure Mode Prediction	Failure Location Prediction
	Tsai-Hill	Maximum Stress		
1	0.64	0.67	C	C
2	0.69	0.77	C	C
3	0.64	0.70	C	C
4	0.61	0.65	C	C
5	0.71	0.78	C	C
6	0.92	0.97	C	I

C Correct prediction.

I Incorrect prediction.

UNCLASSIFIED
Security Classification

DOCUMENT CONTROL DATA - R & D

(Security classification of title, body of abstract and indexing annotation must be entered when the overall report is classified)

1. ORIGINATING ACTIVITY *(Corporate author)*
Carnegie-Mellon University
Mechanical Engineering Department
Pittsburgh, Pennsylvania 15213

2a. REPORT SECURITY CLASSIFICATION
UNCLASSIFIED

2b. GROUP
N/A

3. REPORT TITLE

A SYNTHESIS PROCEDURE FOR MECHANICALLY FASTENED JOINTS IN ADVANCED COMPOSITE MATERIALS

4. DESCRIPTIVE NOTES *(Type of report and inclusive dates)*
Final Report (November 1971 - August 1973)

5. AUTHOR(S) *(First name, middle initial, last name)*
J. P. Waszczak and T. A. Cruse

6. REPORT DATE	7a. TOTAL NO. OF PAGES	7b. NO. OF REFS
September 1973	201	34

8a. CONTRACT OR GRANT NO.	9a. ORIGINATOR'S REPORT NUMBER(S)
F33615-72-C-1214	SM-73-11
b. PROJECT NO.	
c. 6169 CW	9b. OTHER REPORT NO(S) *(Any other numbers that may be assigned this report)*
d.	AFML-TR-73-145; Volume II

10. DISTRIBUTION STATEMENT
Approved for Public Release: Distribution Unlimited

11. SUPPLEMENTARY NOTES	12. SPONSORING MILITARY ACTIVITY
	Advanced Composites Division (AFML/LC) Air Force Materials Laboratory Wright-Patterson Air Force Base, Ohio

13. ABSTRACT

The purpose of this study is to provide the composites designer with an automated preliminary design capability for weight minimized mechanically fastened joints and to identify the common characteristics of such minimum weight designs. The problem of a single column of fasteners loaded in simple tension is considered. The main plate can be made of either graphite-epoxy or boron-epoxy and is loaded by double shear metal splice plates. Independent linear variations in plate widths and thicknesses, including individual ply orientation thicknesses, are permissible along the length of the joint.

An optimization algorithm based on the variable metric method is used to solve the unconstrained minimization problem which is formulated using an interior penalty function. The development of an extremely efficient approximate stress analysis package based on lamination theory and the theory of anisotropic elasticity made the development of the automated synthesis procedure possible.

A first failure analysis, based on the maximum ply stress failure criterion, used in conjunction with a simple joint modeling procedure and bolt load partitioning analysis is shown capable of conservatively predicting the failure characteristics of several multiple fastener joints. A combination of failure modes has been identified which is common to all the minimum weight designs achieved in this limited study.

DD FORM 1 NOV 65 1473

UNCLASSIFIED
Security Classification

14. KEY WORDS	LINK A		LINK B		LINK C	
	ROLE	WT	ROLE	WT	ROLE	WT
Composite Materials						
Education						
Manufacturing						
Statistics						
Stress Analysis						
Fracture Mechanics						
Optimization						
Synthesis						
Criteria						